COLLOIDAL HETEROSTRUCTURES OF SEMICONDUCTOR QUANTUM WELLS: SYNTHESIS, CHARACTERIZATION AND APPLICATIONS

A DISSERTATION SUBMITTED TO

THE GRADUATE SCHOOL OF ENGINEERING AND SCIENCE

OF BILKENT UNIVERSITY

IN PARTIAL FULFILLMENT OF THE REQUIREMENTS FOR

THE DEGREE OF

DOCTOR OF PHILOSOPHY

IN

MATERIALS SCIENCE AND NANOTECHNOLOGY

By

Yusuf Keleştemur

June 2017

COLLOIDAL HETEROSTRUCTURES OF SEMICONDUCTOR QUANTUM WELLS: SYNTHESIS, CHARACTERIZATION AND APPLICATIONS

By Yusuf Keleştemur

June 2017

We certify that we have read this dissertation and that in our opinion it is fully adequate, in scope and in quality, as a dissertation for the degree of Doctor of Philosophy.

_____
Hilmi Volkan Demir (Advisor)

_____
Evren Mutlugün

_____
Emine Yegân Erdem

_____
Oğuz Gülseren

_____
Ahmet Macit Özenbaş

Approved for the Graduate School of Engineering and Science:

_____
Ezhan Karaşan
Director of the Graduate School

ABSTRACT

COLLOIDAL HETEROSTRUCTURES OF SEMICONDUCTOR QUANTUM WELLS: SYNTHESIS, CHARACTERIZATION AND APPLICATIONS

Yusuf Keleştemur

Ph.D. in Materials Science and Nanotechnology
Advisor: Hilmi Volkan Demir
June 2017

Colloidal semiconductor quantum wells, also known as nanoplatelets (NPLs), have recently emerged as a new class of colloidal semiconductor nanocrystals enabling fascinating excitonic properties. With their quasi two-dimensional structure resembling epitaxially-grown quantum wells, these atomically-flat nanoplatelets exhibit narrow emission linewidths, giant linear and nonlinear absorption cross-sections, and ultrafast fluorescence lifetimes when compared to other classes of semiconductor nanocrystals. These appealing features have led to achievement of low lasing thresholds and high color purity by using simple heterostructures of these NPLs. To further exploit the benefits of these solution-processed NPLs and develop next-generation colloidal optoelectronic devices, novel heterostructures of NPLs with superior excitonic properties are in high demand. In this thesis, to address these needs, we proposed and demonstrated novel heterostructured NPLs. This thesis includes the rational design and systematic synthesis and characterization of these hetero-NPLs.

To overcome the lower photoluminescence quantum yield (PL-QY) and stability issues of core/shell NPLs, we successfully synthesized CdSe/CdS/CdS core/crown/shell NPLs resembling platelet-in-a-box. With this advanced architecture, we accomplished substantially enhanced PL-QY and absorption cross-section as well as stability, allowing for the achievement of low-threshold optical gain. However, due to the pure vertical confinement observed in these NPLs, these exciting excitonic features of NPLs suffered from the limited spectral tunability. By developing homogenously alloyed $CdSe_xS_{1-x}$ NPLs together with their alloyed core/crown and alloyed core/shell heterostructures, we succeeded in obtaining highly tunable excitonic features and further extending tunability of the optical gain from these NPLs. In addition to the NPLs having Type-I electronic structure, we demonstrated the highly uniform growth of CdSe/CdTe core/crown NPLs having Type-II electronic structure exhibiting unique excitonic properties.

Additionally, to realize the evolution of Type-II electronic structure, we synthesized $CdSe/CdSe_{1-x}Te_x$ core/crown NPLs by precisely tailoring the composition of the crown region. Without changing their vertical thicknesses, we achieved again highly tunable excitonic features and near-unity PL-QY from these hetero-NPLs. Based on the proposed architectures of these heteronanoplatelets, we believe the findings of this thesis provide important guidelines and inspiration for the synthesis of highly efficient and stable heterostructured NPLs to construct high-performance colloidal optoelectronic devices, possibly challenging their conventional epitaxially-grown counterparts.

ÖZET

KOLOİDAL YARIİLETKEN KUANTUM KUYULARININ HETEROYAPILARI: SENTEZLENMESİ, KARAKTERİZASYONU VE UYGULAMALARI

Yusuf Keleştemur

Malzeme Bilimi ve Nanoteknoloji, Doktora

Tez Danışmanı: Hilmi Volkan Demir

Haziran 2017

Son zamanlarda nanolevhalar olarak da bilinen koloidal yarıiletken kuantum kuyuları, büyüleyici eksitonik özellikleri ile kolloidal yarıiletken nanokristallerin yeni bir sınıfı olarak ortaya çıkmıştır. Epitaksiyal olarak büyütülmüş kuantum kuyularına benzeyen iki boyutlu yapısıyla, atomik düzeyde yassı olan bu nanolevhalar diğer kolloidal yarıiletken nanokristallerle karşılaştırıldıklarında dar ışıma aralıklarına, çok yüksek doğrusal ve doğrusal olmayan soğurma kesitlerine ve oldukça hızlı ışıma yaşam sürelerine sahiptirler. Bu dikkat çekici özellikler, bu nanolevhaların basit yapıları kullanılarak düşük eşik değerine sahip optik kazanç ve yüksek renk saflığı elde edilmesini sağlamıştır. Bu kolloidal nanolevhaların faydalarından daha fazla yararlanmak ve yeni nesil optoelektronik aygıtları geliştirmek için, üstün eksitonik özellik gösteren yenilikçi mimarilere sahip nanolevhalar büyük rağbet görmektedir. Bu tezde, bu ihtiyaçları karşılamak için, yenilikçi mimari yapılara sahip nanolevhaları önerdik ve gösterdik. Bu tez, bu heteroyapıların rasyonel tasarımı, sistematik sentezi ve karakterizasyonunu içermektedir.

Çekirdek/kabuk mimarisine sahip nanolevhaların düşük ışıma verimliliği ve dayanıklılık sorunlarını gidermek için, kutu içinde kuantum levha mimarisini andıran CdSe/CdS/CdS çekirdek/taç/kabuk nanolevhalarını başarıyla sentezledik. Bu gelişmiş yapıya sahip nanolevhaların, ışıma verimliliklerini, soğurma kesitlerini ve dayanıklılıklarını önemli ölçüde geliştirerek, düşük eşik değerine sahip optik kazanç elde edilmesini sağladık. Ancak, bu nanolevhalarda sadece dikey boyutta gözlemlenen kuantum sınırlamasından dolayı, koloidal nanolevhaların bu heyecan verici eksitonik özellikleri sınırlı bir spektral aralıkta elde edilebilmiştir. Tezde, alaşımlı çekirdek/taç ve alaşımlı çekirdek/kabuk yapıları ile birlikte homojen olarak alaşımlanmış $CdSe_xS_{1-x}$ nanolevhalarını

geliştirerek, çok geniş bir spektral aralıkta ayarlanabilir eksitonik özellikler elde etmeyi ve bu nanolevhalardan elde edilen optik kazancın spektral aralığını genişletmeyi başardık. Tip-I elektronik yapıya sahip nanolevhalara ek olarak, eşsiz eksitonik özellikler sergileyen Type-II elektronik yapıya sahip olan CdSe/CdTe çekirdek/taç nanolevhalarını çok düzgün bir şekilde sentezlenmesini de gösterdik. Ayrıca, Type-II elektronik yapısının oluşumunu detaylı bir şekilde incelemek için, taç bölgesinin kompozisyonunu kontrollu bir şekilde ayarlayarak, CdSe/CdSe$_{1-x}$Te$_x$ çekirdek/taç nanolevhalarını sentezledik. Nanolevhaların dikey kalınlıklarını değiştirmeden, geniş bir spektral aralıkta ayarlanabilen eksitonik özellikler elde ettik ve bu yapıya sahip nanolevhalarla yüzde yüze yakın ışıma verimliliğine ulaştık. Önerilen farklı mimarilere sahip nanolevhalar ile birlikte bu tezin bulgularının, yüksek performans gösterebilen kolloidal optoelektronik cihazlar inşa etmekte kullanılacak yüksek verimliliğe ve dayanıklılığa sahip nanolevhaların sentezi için önemli bir kılavuz ve ilham kaynağı olacağına inanıyoruz. Bu gelişmiş yapıya sahip olan koloidal nanolevhalar muhtemelen epitaksiyal olarak büyütülen ve yaygın bir şekilde kullanılan kuantum kuyularına karşı ileride çok güçlü bir rakip olacaktır.

Anahtar sözcükler: Koloidal yarıiletken nanokristaller, kuantum kuyuları, koloidal nanolevhalar, kuantum noktacıkları, heteroyapılar.

Acknowledgement

First, I would like to thank my supervisor Prof. Hilmi Volkan Demir. With his kind, positive, friendly, and warm personality and his invaluable guidance, motivation, immense knowledge and endless support, he has been more than a supervisor for me. During my graduate study, I learned a lot from him about both academic and social life, which was invaluable for me.

I would like to thank my thesis monitoring committee members Assoc. Prof. Evren Mutlugun and Asst. Prof. Emine Yegan Erdem for their valuable comments and discussion. I would like to sincerely thank my jury members Prof. Oguz Gulseren and Prof. Ahmet Macit Ozenbas for being on my PhD jury and for their remarks and suggestions.

This thesis would not be possible without the support and contribution from my close friends and colleagues. I am thankful to the past and present members of Demir Research Group. Especially, I would like to thank Dr. Evren Mutlugun, who always shares his knowledge and experience with me both research and life. I would also like to thank Ozgun Akyuz, Emre Unal, Dr. Burak Guzelturk, Dr. Talha Erdem, Kivanc Gungor, Dr. Sedat Nizamoglu, Dr. Emre Sari, Dr. Rohat Melik, Dr. Can Uran, Dr. Zeliha Soran Erdem, Dr. Aydan Yeltik, Ahmet Fatih Cihan, Shahab Akhavan, Onur Erdem, Didem Dede, Nima Taghipour, Dr. Urartu Ozgur Safak Seker, Dr. Nihan Kosku Perkgoz, Dr. Pedro Ludwig Hernandez-Martinez, Dr. Vijay Kumar Sharma, Dr. Manoj Sharma, Ashma Sharma, Dr. Murat Olutas, Dr. Savas Delikanli, Dr. Akbar Alipour, Mehmet Zafer Akgul, Berkay Bozok, Halil Akcali, Ibrahim Akcali, Cuneyt Eroglu, Onur Akin, Dr. Mustafa Akin Sefunc, Yasemin Coskun, Sayim Gokyar, Dr. Veli Tayfun Kilic, Refik Sina Toru, Hatice Ertugrul, Dr. Durmus Ugur Karatay, Ozan Yerli, Togay Amirahmadov, Birsen Bilgili, and Can Firat Usanmaz. I will never forget their friendship and great times that we had in our highly close-packed office. Also, I would like to thank all the professors, graduate students, technical and administrative staff at UNAM. I would like to also thank Mustafa Guler for his support and help in TEM imaging.

I must express my very profound gratitude to my dear-wife and love Emel. She has always made my life colorful. I would like to thank her for providing

Contents

List of Figures

List of Tables

Chapter 1

Introduction

One of the characteristic features of semiconductor materials is their energy gap between the fully-occupied valence band and unoccupied conduction band. With their relatively lower energy gap ($<$ 2-3 eV) enabling the harnessing of light, semiconductors have become indispensable for the field of optoelectronics. The strong interaction of semiconductors with light including its generation, detection and management has paved the way to utilize novel light-emitting and -harvesting optoelectronic devices for a broad range of applications spanning from the information technologies and life sciences to the lighting and displays technologies. For further exploiting the benefits of optoelectronics, a new class of materials have been strongly desired offering highly tunable excitonic properties together with the ability of fabricating low-cost, large-area and ultra-flexible devices. While the current semiconductor technology has shown great success in the fabrication of small-area and/or chip-scale devices under the ultra-high vacuum conditions, the fabrication of large-area and ultra-flexible devices would not be achievable in a cost-effective way by using the current technology. Also, the commonly used semiconductors have suffered from the limited tunability of their excitonic features.

At this point, colloidal semiconductor nanocrystals (NCs) stand out as a promising class of materials with their fascinating excitonic properties [1]–[3]. With the quantum

confinement effect observed in these tiny nanocrystals, they exhibit highly tunable optical properties and electronic structures, which can be controlled simply by tailoring their size, shape and compositions [4]. Also, the synthesis of free-standing semiconductor NCs using a relatively simple and robust colloidal approach has enabled the engineering of different heterostructures of NCs with desired excitonic properties for the development of the solution-processed optoelectronic devices [5]–[7]. With the considerable progress in the understanding of the physical chemistry of semiconductor NCs together with their excitonic properties, the first products of these tiny nanocrystals have been recently announced with the introduction of semiconductor NCs based displays offering dramatically improved color quality and efficiency [8], [9]. These pioneering products have proved the significant potential of colloidal semiconductor NCs to revolutionize optoelectronic technology and trigger the development of various colloidal NCs based light-emitting and light-harvesting optoelectronic devices including light-emitting diodes (LEDs) [10], lasers [11], photovoltaic cells [12], detectors [13] and luminescent solar concentrators (LSCs) [14]. Thus, to utilize the benefits of these optoelectronic devices, great efforts have been devoted to the development of colloidal semiconductor NCs with superior excitonic properties.

Recently, colloidal semiconductor quantum wells, also known as colloidal nanoplatelets (NPLs), have arisen as a novel class of colloidal semiconductor NCs and attracted a lot of attention with their remarkable excitonic properties [15], [16]. With their two-dimensional (2D) structure [17], resembling the epitaxially-grown quantum wells, these solution-processed NPLs exhibit the narrowest emission linewidths ($<$ 35-40 meV), giant oscillator strength, ultrafast radiative lifetime and extremely large absorption cross-section. Also, with the colloidal synthesis of core/crown [18] and

2

core/shell [19] NPLs, their excitonic properties have been further improved to achieve enhanced device performances. To date, record low lasing thresholds [20] and LEDs with high color quality [21] have been demonstrated by using these heterostructures of atomically-flat NPLs, surpassing the performance of other classes of colloidal semiconductor nanocrystals. These great successes achieved by using these primitive heterostructures of colloidal quantum wells has shown their great potential for the achievement of solution-processed optoelectronic devices and emphasized the necessity of the novel heterostructured NPLs.

To address these needs, in our thesis, we have focused on the design, synthesis and characterization of novel heterostructured colloidal NPLs to obtain superior excitonic properties, enabling the development of high-performance optoelectronic devices. We have proposed and synthesized solution-processed colloidal NPLs with novel heterostructures such as core/crown/shell NPLs by precisely controlling their size, shape and composition. We have verified the growth of highly uniform and crystalline NPLs with well-defined shape and compositions by using structural characterization tools employing transmission electron microscopy, X-Ray photoelectron spectroscopy and X-Ray diffraction. Their resulting excitonic properties have been also investigated with optical spectroscopy techniques including steady-state absorption and photoluminescence spectroscopy, photoluminescence excitation spectroscopy, and time-resolved fluorescence spectroscopy. Our findings have shown that that carefully heterostructured NPLs will play a critical role in the development of future high-performance colloidal optoelectronic devices, which may even possibly challenge their traditional epitaxially grown thin-film based counterparts.

1.1 Organization of the Thesis

In Chapter 2, we present the basic concepts about colloidal semiconductor nanocrystals including their size-dependent optical properties and electronic structures, their synthesis and different heterostructures. We also introduce the colloidal quantum wells, emerging as a new class of colloidal semiconductor nanocrystals.

In Chapter 3, we present the characterization techniques used for the detailed investigation of the structural and optical properties of the synthesized NPLs with unique heterostructures.

In Chapter 4, we report the synthesis of CdSe/CdS/CdS core/crown/shell NPLs having a novel three-dimensional heterostructure resembling platelet-in-box structure together with their optical and structural characterization. We also present their highly stable and low-threshold optical gain performance.

In Chapter 5, we describe the synthesis of alloyed $CdSe_xS_{1-x}$ core NPLs with their core/crown and core/shell heterostructures. These alloyed heterostructured NPLs exhibit highly tunable excitonic properties, enabling the achievement of amplified spontaneous emission at varied wavelengths.

In Chapter 6, we introduce the synthesis and characterization CdSe/CdTe core/crown heterostructured NPLs having Type-II electronic structure. Here, we present their unique excitonic properties significantly different than NPLs having Type-I electronic structures.

In Chapter 7, we present the synthesis and characterization of $CdSe/CdSe_xTe_{1-x}$ core/crown NPLs with precisely controlled crown composition. We report the highly tunable excitonic properties achieved in these heterostructured NPLs without changing their thicknesses.

In Chapter 8, we conclude our thesis with final remarks and future outlooks.

Chapter 2

Colloidal Semiconductor Nanocrystals

This thesis work involves the synthesis, characterization and applications of novel heterostructures of colloidal nanoplatelets, emerging as a new class of colloidal semiconductor nanocrystals. In this chapter, before presenting our findings and related discussion, we would like to provide background information about colloidal semiconductor nanocrystals for the ease of understanding subsequent chapters. We start with the basics concepts about the colloidal NCs including their size-dependent electronic structures and optical properties. Subsequently, we continue with the colloidal synthesis of these tiny crystalline semiconductors and their different heterostructures. Finally, we conclude this chapter with the colloidal nanoplatelets, showing exciting excitonic properties when compared to the other classes of semiconductor nanocrystals.

2.1 Basic Concepts of Semiconductor Nanocrystals

Colloidal semiconductor nanocrystals can be defined as tiny crystalline semiconductors consisting of hundreds to thousands of atoms with a typical diameter ranging from 2 to 20 nm [2], [3]. With the quantum confinement effects observed at this length scale, these tiny crystals exhibit unique size-dependent electronic structure and optical properties significantly different from their bulk counterparts [4], [22]. In the bulk semiconductors, a large density of covalently and/or ionically bonded atoms give rise the formation of continuous energy levels in the conduction and valence bands, which are separated with a fixed band gap energy depending on the composition and crystal structure of the semiconductor material (Figure 2.1) [1]. On the other hand, semiconductor NCs composed of finite number of atoms possess atomic-like discretized energy levels with a tunable effective band gap energy, which can be controlled by simply changing their size and shape [1]. The effective band gap energy of semiconductor nanocrystals can be increased by decreasing their size, enabling a wide coverage range of electromagnetic spectrum by using a single material system having the same chemical compositions.

BULK SEMICONDUCTORS

COLLOIDAL SEMICONDUCTOR NANOCRYSTALS
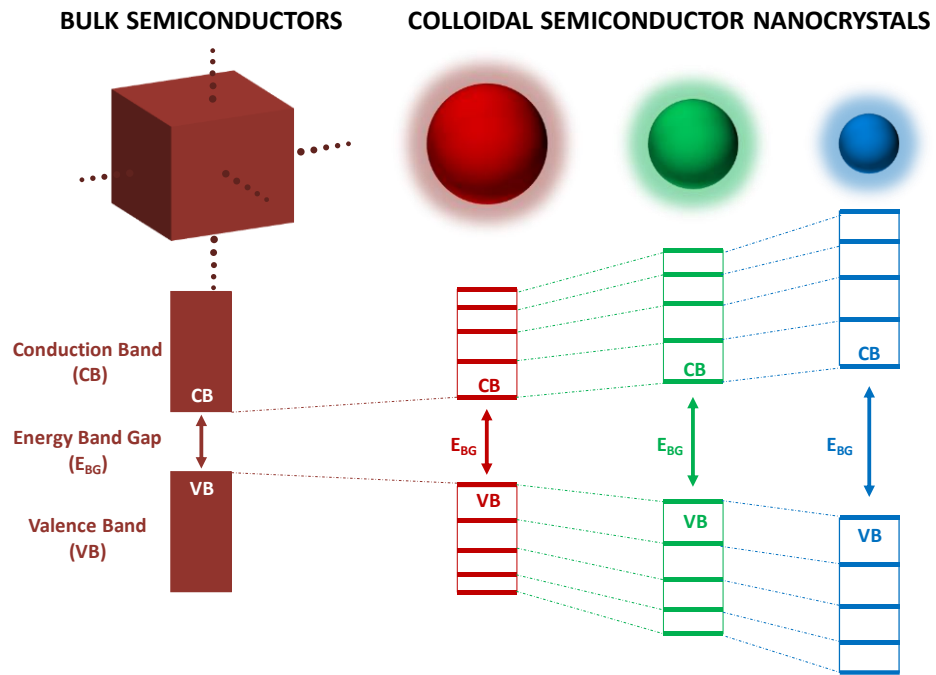
Figure 2.1. Schematic illustration of band diagrams in bulk semiconductors and colloidal semiconductor NCs. While continuous band diagrams are observed in the bulk semiconductors, colloidal semiconductor NCs exhibit quantized energy levels in their band structure. Also, with decreasing the size of the colloidal semiconductor NCs, their effective band gap energy is increased.

Upon the excitation of semiconductors with photons having higher energies than their band gap, electron and hole pairs are formed, which are known as excitons. However, owing to higher dielectric constant of the bulk semiconductors, generated electron and hole pairs feature small Columbic binding energy and they generally act as free carriers [6]. On the other hand, in the semiconductor NCs having a comparable and/or smaller size than the exciton Bohr radius, the quantum and dielectric confinement effects give rise to increased exciton binding energy and strongly modify their excitonic properties [3], [6]. With the increased exciton binding energy, semiconductor NCs exhibit strongly

enhanced excitonic absorption features with broad absorption spectrum (Figure 2.2). Thanks to their discrete energy levels, these NCs feature narrow emission linewidth with wide spectral tunability. Also, they possess improved photoluminescence quantum yield (PL-QY) together with faster fluorescence lifetime. Moreover, these tiny crystalline semiconductors composed of inorganic cores and organic ligands have excellent photostability and chemical stability when compared to their organic counterparts [23].
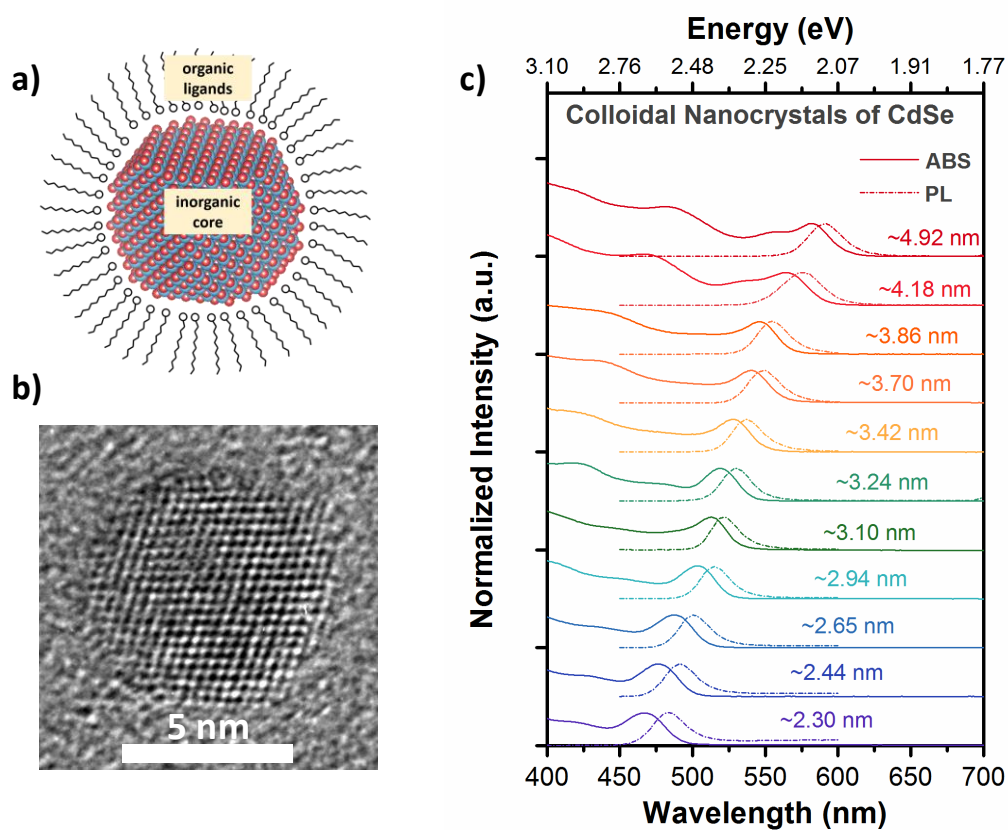
Figure 2.2. (a) Schematic drawing of a colloidal semiconductor NC composed of inorganic core and organic ligands together with (b) a representative high-resolution transmission electron microscopy image of a single colloidal semiconductor NC, synthesized at our laboratories. (c) Normalized absorption and photoluminescence

spectra of colloidal CdSe NCs having different diameters showing their strongly tunable excitonic properties, synthesized at our laboratories.

In addition to the these exciting excitonic properties of colloidal semiconductor NCs, their solution process-ability make them highly appealing for the development of the next-generation light-emitting and light-harvesting optoelectronic device applications. The colloidal dispersion of semiconductor NCs enables the development of low-cost, large-scale, ultra-flexible and functional optoelectronic devices with the solution-processed fabrication techniques [7], [24]. However, to utilize the great potential for the achievement of superior device performance, the synthesis of high-quality semiconductor NCs is the key.

2.2 Colloidal Synthesis of Semiconductor Nanocrystals

With the realization of quantum confinement effect in semiconductors enabling the size and shape tuning of the optical properties and electronic structures, synthesis of semiconductor NCs has attracted increasingly great attention and become one of the most promising research problems in the colloidal community within the last three decades. The first observation of quantum confinement effect in semiconductor crystals was reported by Ekimov [25]. This early work demonstrated that nano-sized semiconductor crystals grown in the glass medium exhibit size-dependent excitonic absorption behaviors. Also, with the synthesis of different sized nano-colloids, size-dependent electronic structures and optical properties were shown by Brus [26]. Although these pioneering studies successfully demonstrated the quantum confinement

effect in semiconductor crystals, a major challenge was to obtain highly crystalline, monodisperse and isolated semiconductor NCs for a full understanding of their unique excitonic properties and exploiting their potential in novel device architectures.

This goal was eventually achieved with the colloidal synthesis of highly monodisperse, uniform and crystalline CdSe, CdS and CdTe semiconductor NCs by the group of Bawendi [4]. With the co-injection of organometallic precursors into a hot coordinating solvent, sudden nucleation of semiconductor crystallites was achieved from its supersaturated solution. Subsequently, it was followed with the separate growth stage, leading to formation of highly monodisperse and uniform shaped colloidal semiconductor NCs in the presence of organic ligands in the reaction solution. This relatively simple and novel approach for the synthesis of semiconductor NCs has made a major breakthrough in the field of colloidal chemistry and inspired the community for the synthesis of different kinds of nanomaterials.

A typical colloidal synthesis of semiconductor NCs is composed of three basic components: molecular precursors, ligands and solvents [27]–[29]. Molecular precursors are decomposed into monomers at higher reaction temperatures and supply the required materials for the nucleation and growth of nanocrystals. Their reactivity can be also tuned by changing molecular side groups [30]. Another important component of the colloidal synthesis is the ligands, which are organic molecules commonly used to achieve uniformity and monodispersity [31]. They are dynamically attached to the surface of the nanocrystals and play a critical role for the determination of their final size and shape [32], [33]. Also, these organic molecules are responsible for the colloidal stability of nanoparticles to form a stable dispersion. Finally, solvents used in the

colloidal synthesis enable the complete dissolution of molecular precursors to form a homogenous reaction mixture. In addition, together with ligands, they are accounted for the colloidal stability of nanocrystals in the reaction mixture. With the appropriate selection of molecular precursors, ligands and solvents, highly crystalline semiconductor NCs can be synthesized by using colloidal approaches [28], [34].

In addition to the appropriate selection of chemicals, the understanding of the nucleation and growth kinetics in colloidal synthesis is highly crucial for the achievement of highly monodisperse and uniform semiconductor NCs. With the proposed nucleation and growth model by La Mer [35], it was shown that separation of nucleation and growth stages is highly required to achieve monodispersity in the colloidal synthesis (Figure 2.3). To obtain discrete nucleation and growth stages, supersaturated solution is formed with the fast injection of molecular precursor into the hot reaction solution. With the decomposition of the molecular precursors in the reaction solutions, the monomer concentrations exceed the critical limit for the homogenous nucleation and small size crystallites are nucleated rapidly. During the fast nucleation step, the monomer concentrations are consumed significantly and decreased below the critical limit for the homogenous nucleation, eliminating the formation probability of new nuclei. Then, it is followed by a separate growth stage of almost identical size seed nanocrystals, allowing the formation of uniform colloidal nanocrystals with a highly monodisperse size distribution.
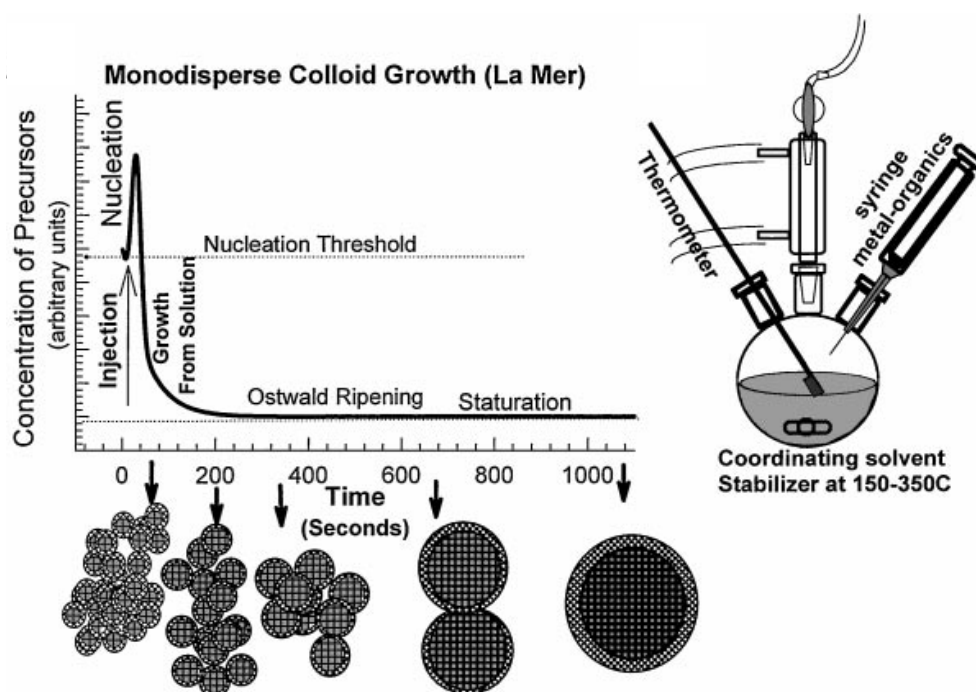
Figure 2.3. The nucleation and growth model describing colloidal synthesis of highly monodisperse NCs proposed by La Mer together with schematic drawing of a typical colloidal synthesis setup. Reprinted with permission from [27].

The growth stage in the colloidal synthesis can be also analyzed in two separate steps [36]. In the early stage of the growth, in the case of relatively higher monomer concentration in the reaction solution, smaller size nanocrystals grow at a faster rate with respect to the larger ones, leading to the decreased size distribution. On the other hand, with the depletion of monomer concentration in the final stage of the growth, smaller size nanocrystals start to dissolve due to their higher surface energy, while bigger size nanocrystals start to grow, resulting in the increased size distribution. This process is

called as Ostwald ripening and controlling the Ostwald ripening during the colloidal synthesis is highly critical to achieve highly monodisperse colloidal semiconductor NCs.

A better understanding of reaction kinetics together with the expanded chemical library by developing less toxic and highly stable molecular precursors have enabled colloidal synthesis to become highly robust, allowing for a simple approach for the synthesis of different kinds of semiconductor NCs. Starting with the successful synthesis of II–VI group compounds including CdSe, CdS and CdTe [37] nanocrystals, colloidal approach is further extended to the synthesis of III–V group compounds such as InP [38], [39] and InAs [39] nanocrystals and IV–VI group compounds including PbS [40], PbSe [41], and PbTe [42] nanocrystals. In addition to the core-only semiconductor nanocrystal having spherical shape, different kinds of semiconductor nanocrystals with mixed dimensionalities and various heterostructures have been also synthesized using colloidal approach for further engineering their excitonic properties [43]–[47].

2.3. Different Heterostructures of Semiconductor Nanocrystals

With decreasing the size of nanocrystals, the ratio of the surface-to-volume atoms reaches significantly higher levels and this dramatically affects the resulting optical properties of colloidal semiconductor NCs [2]. While the atoms residing inside the nanocrystals have complete numbers of bonding with surrounding atoms, the surface atoms seriously suffer from the incomplete numbers of bonding and/or dangling bonds, diminishing their performance. Although the surface of colloidal NCs is covered with the organic ligands for the passivation of dangling bonds, these organic molecules may

not be able to supply complete chemical and electronic passivation for the semiconductor NCs. For example, core-only semiconductor nanocrystals are quickly deteriorated when exposed to the atmospheric conditions due to the oxidation. Also, generated electron and hole pairs in core-only nanocrystals can be trapped by the surface atoms, resulting in the decreased PL-QY.

For the achievement of proper chemical and electronic stabilization of colloidal semiconductor NCs, heterostructured nanostructures composed of inorganic core and epitaxially grown inorganic shell have been designed and studied [48]. In addition to the effective passivation of surface atoms with the formation epitaxially grown shell, heterostructured semiconductor NCs offer great opportunities for further engineering the excitonic properties of nanocrystals by controlling the band alignment between the core and shell (Figure 2.4) [49].

For the core/shell heterostructures having Type-I like band alignment, electron and hole wavefunctions are confined in the same region of the structures, resulting in the increased wavefunction overlap and enhanced radiative recombination probability [50]. These enhanced radiative recombination rates observed in NCs with Type-I electronic structure make them highly appealing for light-emitting optoelectronic device applications. On the other hand, for the core/shell heterostructures having Type-II like band alignment, electron and hole wavefunctions are localized in the separate regions of the NCs, leading to decreased wavefunction overlap and reducing the radiative recombination probability [51]. These heterostructures are quite interesting for the light-harvesting optoelectronic applications including solar cells and photodetectors.

15

Core/Shell Heterostructures of Colloidal Semiconductor Nanocrystals

Type-I	Quasi Type-II	Type-II
Band Alignment	Band Alignment	Band Alignment
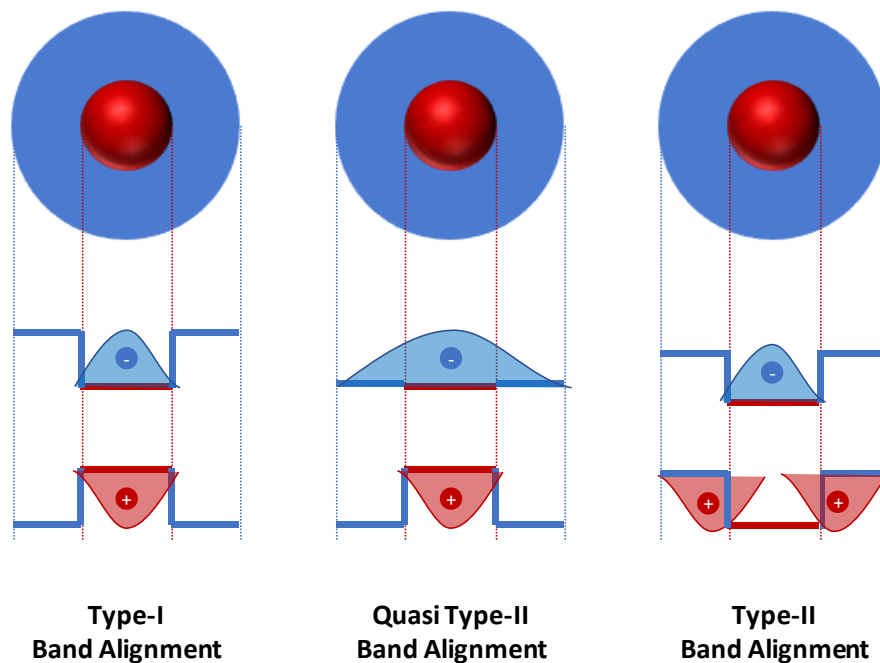
Figure 2.4. Core/shell heterostructures of colloidal semiconductor NCs having different band alignment (Type-I, quasi Type-II and Type-II) along with the localization of electron and hole wavefunctions in these architectures.

2.3.1 Nanocrystals with Type-I Heterostructures

The first successful demonstrations of core/shell heterostructured NCs having Type-I electronic structure were reported by growing CdS and/or ZnS shell layers on top of the CdSe cores [50], [52], [53]. With the formation of larger band gap CdS and ZnS shell layers around CdSe core, electron and hole wavefunctions were confined mostly to the core region. In addition, enhanced surface passivation of CdSe cores with the shell coating improved PL-QY (up to 40-50%) and enhanced stability in these heterostructured NCs. Also, these core/shell NCs exhibit continuously red-shifting

emission with increasing the thickness of shell layer, which is explained with the relaxation of the quantum confinement.

The colloidal synthesis of these core/shell heterostructured NCs was performed in two separate steps. In the first step, high-quality CdSe core NCs were synthesized and used as a seed for the subsequent shell overcoating after purification. In the second step, with the slow addition of shell precursors into the reaction mixture, the CdS and/or ZnS shell layers were epitaxially grown on CdSe core NCs. Here, the concentration of shell precursors, the injection rate of shell precursors and the shell growth temperature are highly important parameters to be optimized, avoiding the homogenous nucleation of shell precursors.

For further eliminating the risk of homogenous nucleation during the shell growth, successive ion layer adsorption and reaction (SILAR) technique was developed by the group of Peng [54]. By using this approach, they demonstrated the synthesis of large-scale and highly monodisperse CdSe/CdS core/shell colloidal NCs. With the alternating injection of certain amount of shell precursors into the reaction mixture, SILAR technique reduces the probability of homogenous nucleation of shell materials and offer highly precise shell thickness control. Therefore, with precisely adjusting the CdS shell thickness, they showed successfully tunable emission behavior from CdSe/CdS core/shell NCs. Moreover, thanks to the versatility of SILAR technique, it was further extended to the synthesis of multishell heterostructures, which is strongly required to achieve ideal semiconductor NC having highly crystalline structure and well-passivated electronic structure suppressing the tunneling of electrons and holes from core region to surface trap sites.

While CdSe/CdS core/shell material system features lower lattice mismatch enabling the formation of highly crystalline nanocrystals, they suffer from the incomplete electronic passivation owing to the lower energy barrier for the electrons [55]. On the other hand, CdSe/ZnS system exhibits improved electronic passivation with respect to CdSe/CdS core/shell NCs owing to the higher band gap of ZnS [55]. However, higher lattice mismatch observed in this material system leads to increased strain formation, creating trap sites. Therefore, carefully designed heterostructured nanocrystals are strongly required to achieve superior properties by combining the advantages of different materials.

The first demonstrations of multishell heterostructures were demonstrated with the synthesis of CdSe/CdS/ZnS core/multishell NCs [55], [56]. By growing a thin layer of CdS shell between the CdSe core and ZnS shell, formation of highly crystalline NCs was obtained with these multishell heterostructures, reducing strain formation. In addition to that, the proper electronic passivation by using both CdS and ZnS shell layers enabled the achievement of improved PL-QY (up to 70-85%) with enhanced photostability. This initial study has shown the critical importance of the multishell heterostructures and inspired the community for further investigation of various multishell architectures using simple and low-cost colloidal synthesis techniques.

To address these needs, one-pot synthesis of highly crystalline and efficient core/shell NCs was developed [57]. By using the reactivity difference between the precursors, the formation of both core and shell was achieved in a single-step synthesis. The resulting core/shell semiconductor NCs had a chemical structure with composition gradient, strongly improving their crystal quality and reducing strain formation (Figure 2.5a).

Also, the chemical composition gradient strongly modified their electronic structures, enabling the funneling of excitons into the core region and increasing the radiative recombination rates. With their promising chemical and electronic structures, these NCs possessed higher photoluminescence quantum yield (up to 85-95%) and excellent photostability. In addition, by simply adjusting the amount of the initial precursors, highly efficient blue-, green- and red-emitting semiconductor NCs can be obtained using this one-pot synthesis approach (Figure 2.5b) [58], [59].
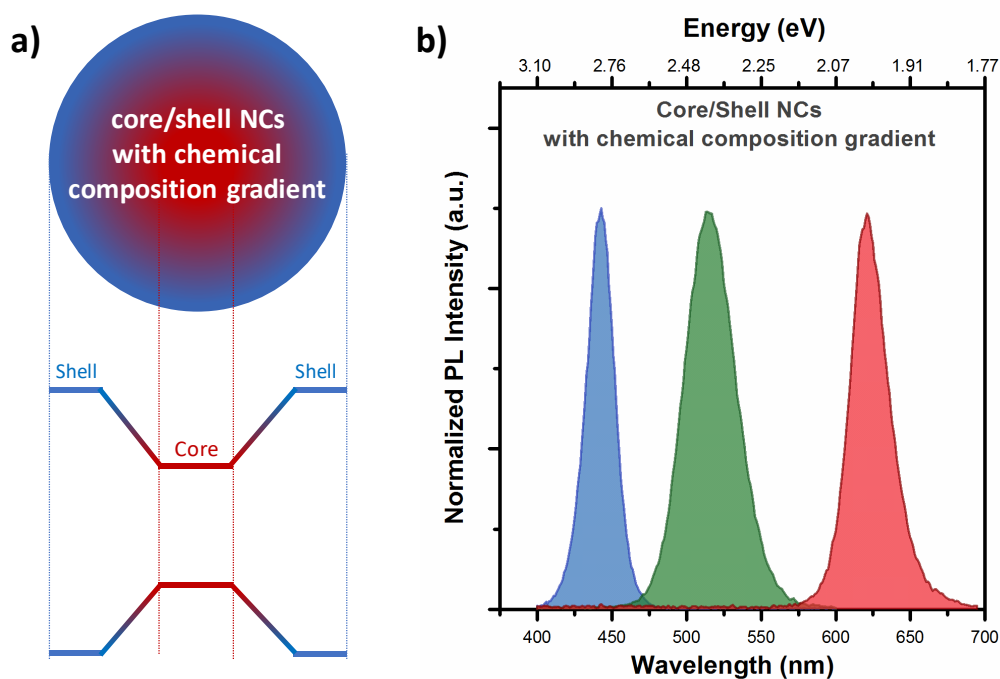
Figure 2.5. (a) Schematic drawing of the core/shell NC having chemical composition gradient structure together with their band alignment. (b) Normalized photoluminescence spectra of blue-, green- and red-emitting colloidal NCs with the chemical composition gradient structure, synthesized at our laboratories.

The strategies developed for the achievement of highly crystalline and efficient core/shell heterostructures having Type-I electronic structure was successfully extended to the colloidal synthesis of Cd- and/or heavy metal free NCs. It was shown that InP/ZnS [60], [61] and CuInS$_2$/ZnS [62], [63] core/shell NCs with higher photoluminescence quantum yield (reaching ~80%) can be also synthesized by using colloidal routes. With the higher PL-QY and enhanced photostability, core/shell heterostructures of Type-I nanocrystals have been widely used for the development of novel light-emitting optoelectronic device applications including LEDs and lasers.

2.3.2 Nanocrystals with Type-II Heterostructures

In addition to the colloidal nanocrystals having Type-I electronic structure, semiconductor NCs with Type-II electronic structure have offered unique and exciting excitonic properties [64]. With the localization of electron and hole wavefunctions in the separate regions of NCs, spatially indirect excitons are formed at the core/shell interface. With the radiative recombination of these spatially indirect excitons, they exhibit strongly red-shifted emission, which would not be accessible from a single core and/or shell material. Also, owing to the reduced overlap of the electron and hole wavefunctions in these heterostructures, they feature decreased PL-QY with elongated radiative lifetime. In addition, the reduced electron and hole wavefunction overlap enables the suppression of nonradiative Auger recombination. These appealing properties of core/shell heterostructures having Type-II band alignment make them highly promising for the light-harvesting optoelectronic applications, including solar cells and photodetectors.

20

The first demonstrations of colloidal NCs having Type-II electronic structure was shown with the synthesis of CdTe/CdSe and CdSe/ZnTe core/shell heterostructures by the group of Bawendi [51]. For both samples, strongly red-shifted emissions were observed with elongated radiative lifetimes, suggesting the formation of Type-II electronic structures. Additionally, the order of core and shell materials strongly affect excitonic properties of the resulting core/shell nanocrystal having Type-II electronic structures. For example, although both CdSe/CdTe and CdTe/CdSe core/shell heterostructures exhibit Type-II like band alignment, their emission and absorption behaviors were rather different, showing the importance of the starting core material. Furthermore, different kinds of semiconductor NCs with Type-II electronic structures including CdS/ZnSe [65] and ZnSe/ZnTe [66] were synthesized to further tune their absorption and emission behaviors.

2.3.3 Nanocrystals with Quasi Type-II Heterostructures

Colloidal semiconductor NCs with quasi Type-II electronic structure lying within the Type-I and Type-II heterostructures have also shown interesting optical properties. Owing to the similar energy levels observed in the conduction and/or valence bands between the core and shell materials, the partial separation of electron and hole pairs are obtained in these heterostructures. Among the limited numbers of material pairs having quasi Type-II band alignment, CdSe/CdS core/shell heterostructures have been the most widely studied material system [67]. With the lower energy barrier for electrons in this material system, electrons are localized through the whole structure (both the core and shell regions), while holes are confined to the CdSe core. Therefore, with the partial separation of electron and hole wavefunctions, suppression of nonradiative Auger

recombination was observed in these heterostructures. Also, the lower lattice mismatch between the CdSe and CdS materials enables the uniform growth of thick CdS shell with a reduced number of defect sites, boosting their photostability. Furthermore, the relatively lower band of CdS with respect to ZnS make a great contribution to the enhancement of the absorption cross-section in these NCs. With these appealing features, CdSe/CdS core/shell heterostructures have been investigated extensively for the development of highly stable nanocrystal LEDs and low-threshold lasers.

The initial studies on the synthesis of CdSe/CdS core/shell heterostructures with thick CdS shell (up to 20 monolayers of shell) were performed by using SILAR technique offering highly precise shell thickness control [67], [68]. Owing to the formation of thick CdS shell, these heterostructures are also known as "giant" nanocrystals. With the formation of CdS shell, these giant nanocrystals exhibit improved absorption cross-section and strongly red-shifted emission with suppressed blinking behavior [69]. Also, thanks to the reduced rate of Auger recombination in these giant core/shell nanocrystals, high-performance LEDs [70] and low-threshold gain [71] were achieved. However, the formation of thick CdS shell over a long time period and the abrupt interface at the core/shell boundary have hampered the achievement of superior performance with these heterostructures.

To further push their performance and improve the PL-QY, the synthesis of CdSe/CdS core/shell NCs having alloyed and/or gradient shell structures has been targeted. Recently, colloidal synthesis of high-quality CdSe/CdS core/shell NCs has been demonstrated with narrow emission linewidth and suppressed blinking [72]. With the slow growth rate of CdS shell at higher temperature, highly uniform and crystalline

core/shell NCs were achieved resulting in the near-unity PL-QY (Figure 2.6). Also, the higher shell growth temperature led to the formation of smooth $CdSe_xS_{1-x}$ interface owing to the enhanced interdiffusion between the core and shell regions, reducing Auger recombination rates. These CdSe/CdS core/shell heterostructures with relatively thin CdS shell (6-7 monolayers) and smooth interface had superior excitonic properties when compared to colloidal nanocrystals having similar size and enabled the achievement of low-threshold gain and lasing under two-photon optical pumping [73].
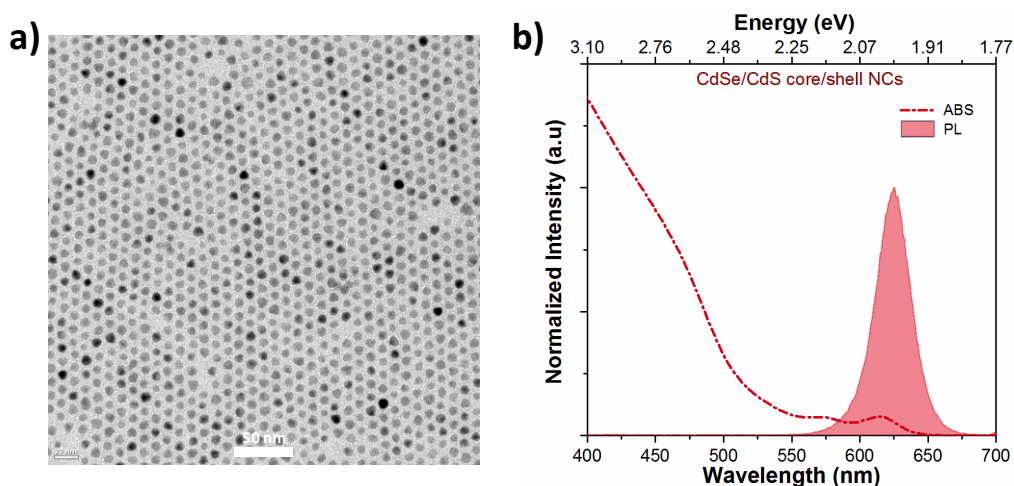
Figure 2.6. (a) High-resolution transmission electron microscopy (TEM) image of our CdSe/CdS core/shell NCs showing highly monodisperse size distribution. (b) Normalized absorption and photoluminescence spectra of our CdSe/CdS core/shell NCs with narrow emission linewidths (~28 nm).

2.4. Colloidal Quantum Wells

Thanks to the advancements in the field of the colloidal chemistry, the synthesis of semiconductor nanocrystals starting with the spherical shaped nanocrystals has been

extended to the more anisotropic and complex structures including nanorods and tetrapods [45]–[47]. Recently, synthesis of atomically-flat colloidal nanoplatelets NPLs have been also demonstrated by using colloidal approaches [15]. These colloidal NPLs feature lateral dimensions on the order of tens of nanometers with the atomic-scale vertical thickness, which can be controlled precisely with the synthesis (Figure 2.7). Also, owing to their similarity with the epitaxially grown quantum wells, these colloidal NPLs are called as colloidal quantum wells.
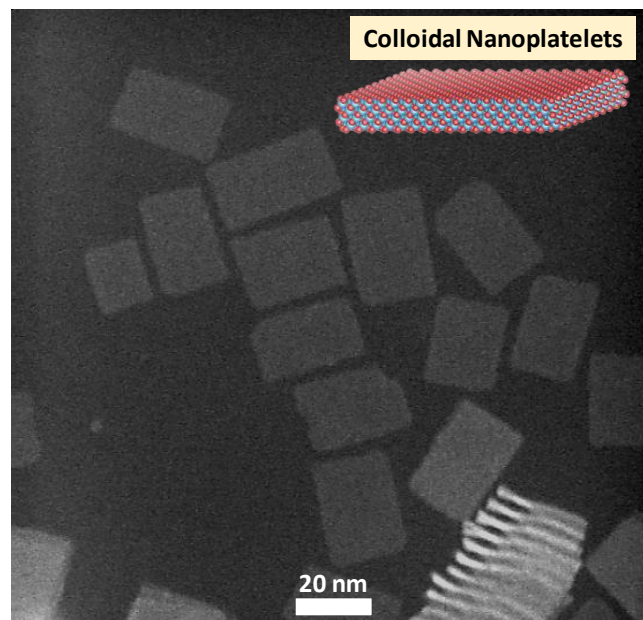
Figure 2.7. High-angle annular dark-field scanning transmission electron microscopy (HAADF-STEM) image of our colloidal NPLs with the inset showing the schematic drawing of atomically-flat colloidal NPLs.

The first synthesis of these atomically-flat NPLs were demonstrated by the group of Dubertret [15]. These colloidal CdSe NPLs having zinc blende crystal structure were synthesized with precisely controlled vertical thicknesses by slightly changing the recipe

of spherical shaped CdSe nanocrystals. It was observed that the addition of a short-chain Cd(carboxylate)$_2$ into the reaction mixture containing a long-chain Cd(carboxylate)$_2$ and Se powder within the temperature range of 180 and 240˚C promotes the lateral extension of the well-defined seeds and leads to the formation of nanoplatelets. This anisotropic growth of seeds having highly isotropic crystal structure was attributed to the lower activation energy barrier of thinner facets when compared to larger planar facets [74]. Therefore, the seeds were grown at a faster rate on thinner facets, resulting in the anisotropic-shaped nanoplatelets. It was also shown that by changing the injected amount of the short-chain Cd(carboxylate)$_2$, injection temperature and growth time, the lateral dimensions and vertical thicknesses of colloidal NPLs can be precisely tuned.

Owing to the extended lateral dimensions of colloidal NPLs larger than the exciton Bohr radius, these NPLs exhibit pure quantum confinement along their vertical thicknesses. Therefore, with their quasi 2D structure, colloidal NPLs has shown unique electronic structure and optical properties significantly different from the spherical shaped colloidal NCs [16], [17]. With the formation of quantum-well like electronic structure, sharp excitonic transitions are observed from the absorption spectra corresponding to the heavy-hole and light-hole transitions.

For the case of 4 monolayer (ML) thick CdSe NPLs, the heavy-hole and light-hole transitions are observed at ~512 and ~480 nm, respectively (Figure 2.8). In addition, these CdSe NPLs exhibit almost zero Stokes shifted emission behavior with the narrowest full-width-at-half-maximum (FWHM) value of ~8 nm when compared to other classes of semiconductor NCs [17]. This narrower emission linewidths observed in these colloidal NPL is attributed to the synthesis of atomically-flat NPLs suppressing

the inhomogeneous broadening [75]. In addition, with the strong quantum and dielectric confinement effects, these colloidal NPLs have the giant oscillator strength, leading to observation of the ultrafast radiative lifetimes [17]. Moreover, it was shown that these atomically-flat nanocrystals have extremely large linear and nonlinear absorption cross-sections [76], [77]. With these astonishing excitonic properties, these colloidal quantum wells hold great promise for the achievement of superior device performances, which may possibly challenge their epitaxial counterparts.
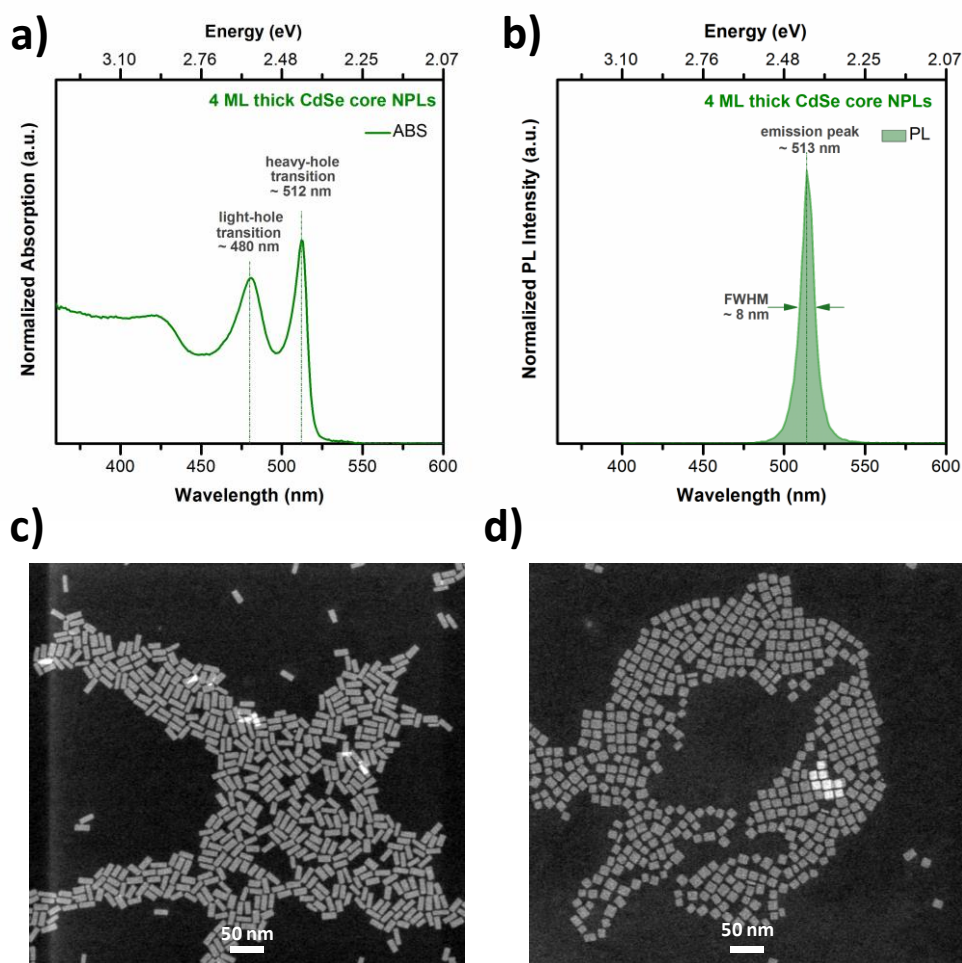
Figure 2.8. Normalized (a) absorption and (b) photoluminescence spectra of our 4 ML thick CdSe core NPLs. HAADF-STEM images of our 4 ML thick CdSe core NPLs with varying lateral dimensions from (c) rectangular-shaped to (d) almost square-shaped.

Because of their pure vertical quantum confinement, these colloidal quantum wells possess discrete absorption and emission features regardless of their lateral dimensions [78]. Although rectangular-shaped and/or square-shaped 4 ML thick CdSe NPLs can be synthesized with the same colloidal approach (Figure 2.8b), their excitonic features remain almost in the same spectral position. For the achievement of the tunable

27

absorption and emission behavior at different wavelengths, CdSe core NPLs with varying vertical thicknesses were synthesized. With the relaxation of the quantum confinement by increasing the vertical thicknesses, their excitonic features were continuously shifted to the lower energies (Figure 2.9). In addition to the CdSe core NPLs with different vertical thicknesses, colloidal synthesis of CdS [79] and CdTe [80] NPLs has been also studied to obtain further tunable excitonic properties.
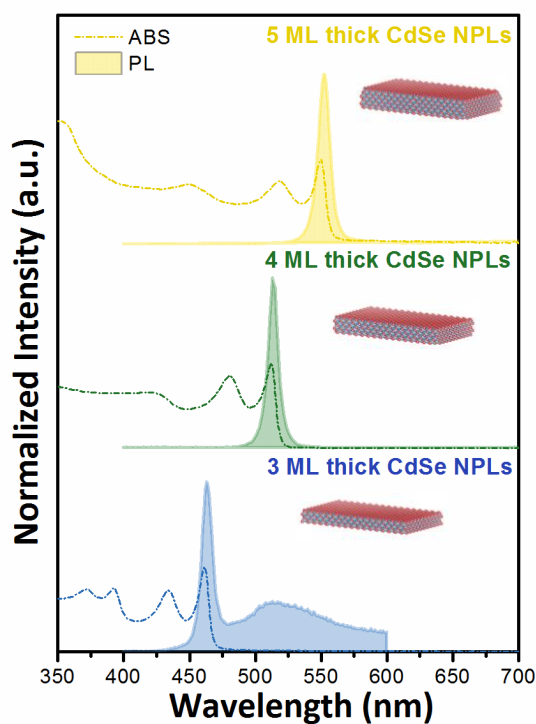
Figure 2.9. Normalized absorption and photoluminescence spectra of our CdSe colloidal NPLs having different vertical thicknesses, synthesized at our laboratories.

Similar to other classes of semiconductor nanocrystals, core-only NPLs have suffered from their lower PL-QY and decreased stability. Therefore, to achieve enhanced excitonic properties with improved stability, different heterostructures of colloidal NPLs

including core/crown (laterally grown extension) [18], [81] and core/shell (vertically grown coating) [19] structures have been designed and synthesized (Figure 2.10a). Among different kind of material combinations, CdSe and CdS have been the most widely studied materials in these heterostructures owing to the great synthesis experience developed with these material systems.
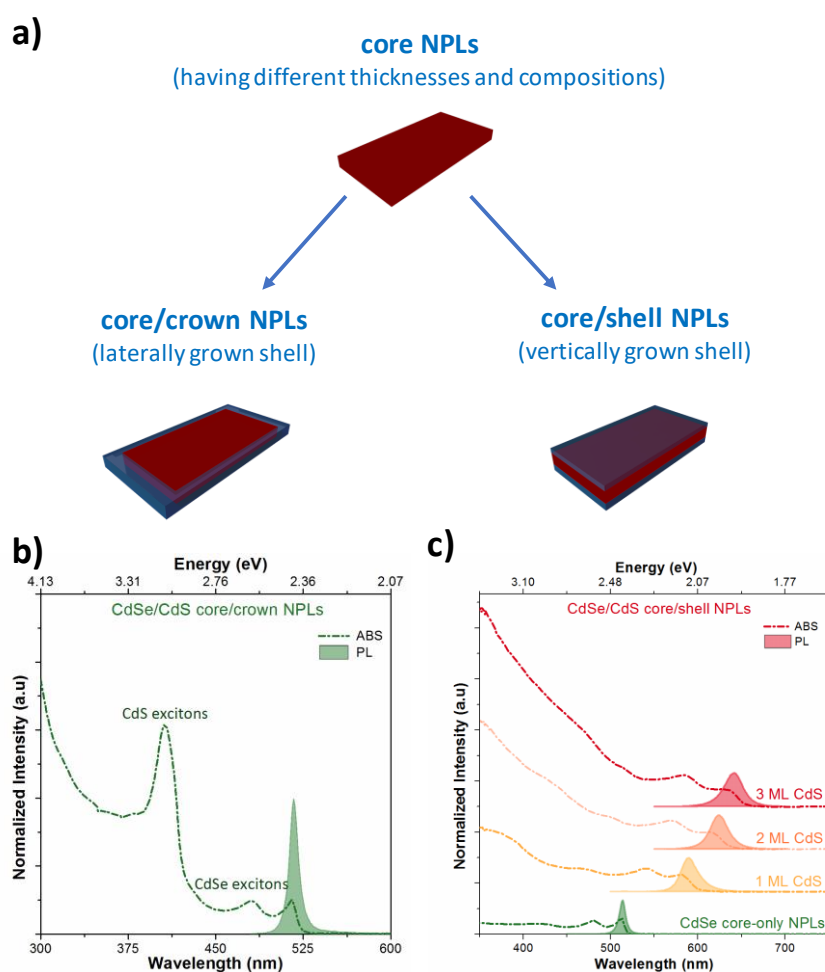
Figure 2.10. (a) Schematic drawings of core-only colloidal NPLs together with their core/crown (laterally grown shell) and core/shell (vertically grown shell) heterostructures. Normalized absorption and photoluminescence spectra of (b) our

CdSe/CdS core/crown and (c) core/shell NPLs, all of which are synthesized at our laboratories.

The first demonstration of heterostructures has been reported with the synthesis of CdSe/CdS core/crown NPLs [18], [81]. By using the freshly synthesized CdSe core NPLs as a seed, CdS crown region was grown only in the lateral direction without changing the vertical thicknesses of the starting CdSe core NPLs. Owing to the laterally extended CdS crown region, these core/crown heterostructures exhibit almost similar excitonic features with CdSe core NPLs (Figure 2.10b). However, with the sidewall passivation of inner CdSe core, they featured significantly enhanced PL-QY and stability. Also, the laterally extended CdS crown region having a higher band gap leads to increase in the absorption cross-section within the near-UV regions of the spectrum. Moreover, with the ultrafast exciton transfer from crown region to core, CdS crown region makes a great contribution to the emission of core/crown NPLs.

In addition to the core/crown heterostructures, synthesis of CdSe/CdS core/shell NPLs has been also demonstrated by using two different approaches. By using the single-step synthesis, continuous growth of CdS shell layers in the vertical direction was achieved with the co-injection of cadmium and sulfur precursors into the reaction solution [19]. On the other hand, with the alternating injection of the precursors, colloidal atomic layer deposition (c-ALD) techniques offer highly uniform growth of CdS shell with atomically precise thickness control [82]. Thus, core/shell NPLs with desired shell thicknesses can be synthesized using c-ALD technique to tune their excitonic features in a controlled way.

With the growth of CdS shell in the vertical thicknesses, CdSe/CdS core/shell NPLs exhibit red-shifted excitonic features (Figure 2.10c), which can be explained with the decreased quantum confinement effect. In addition, owing to the enhanced exciton-phonon coupling with these material combinations, the excitonic features were slightly broadened with respect to CdSe core-only NPLs. Also, thanks to the partial separation of electron and hole wavefunctions, suppression of Auger recombination was observed with reduced blinking behavior in these systems [83].

With these fascinating excitonic properties, colloidal NPLs together with their different heterostructures have been shown to be highly promising for next-generation optoelectronics, especially for low-threshold lasing and high-performance LEDs when compared to other classes of semiconductor nanocrystals. For example, under similar gain conditions, even simple CdSe-based core-only NPLs having emission in the blue spectral region with a low photoluminescence quantum yield (~10%) [84] surpassed the optical gain performance of carefully engineered and highly advanced $Cd_xZn_{1-x}S/ZnS$ core/shell nanocrystals having soft interface with almost near-unity photoluminescence quantum yield [85] in the same spectral region. In addition, by using the primitive CdSe/CdS core/crown and core/shell heterostructured NPLs, the lowest optical gain thresholds were achieved for the green- and red-emitting spectral regions [20], [86]. Furthermore, with the solution-processed LEDs by using these colloidal NPLs, spectrally narrower electroluminescence was demonstrated, showing the importance of the colloidal NPLs for the development of LEDs with high color purity. These initial findings by using simple heterostructures of NPLs have provided great motivation for us to focus on the synthesis, characterization and applications of the novel heterostructured NPLs in this thesis.

31

Chapter 3

Characterization of Colloidal Quantum Wells

In this chapter, we describe the characterization techniques used for investigating the optical and structural properties of the synthesized colloidal quantum wells. This chapter is composed of two main parts: optical characterization techniques and structural characterization techniques.

3.1 Optical Characterization Techniques

For the complete understanding of the unique excitonic properties of colloidal quantum wells having different heterostructures, we used the optical spectroscopy techniques including steady-state absorption spectroscopy, steady-state photoluminescence spectroscopy, photoluminescence excitation spectroscopy, the photoluminescence quantum yield measurements, and time-resolved fluorescence spectroscopy.

3.1.1 Steady-State Absorption Spectroscopy

The steady-state absorption spectroscopy is the most commonly used technique to determine the absorption behavior of colloidal NPLs, strongly depending on their vertical thicknesses and composition. For the steady-state absorption measurements, we have used the dispersion and/or solid samples of colloidal quantum wells, which were cleaned after the colloidal synthesis. These samples are excited with photons by varying their energies and their absorption spectra are recorded by measuring the transmission of photons through the sample. While the photons having higher energies than their band gap are absorbed by creating electron and hole pairs, the photons having lower energies are transmitted through the sample without absorption.

In addition to investigating the absorption spectra of colloidal NPLs, we have used steady-state absorption spectroscopy to determine the vertical thicknesses of the synthesized core NPLs. As an exemplary case, the absorption spectra of our CdSe core NPLs with different vertical thicknesses are presented in Figure 3.1. With the pure quantum confinement along their vertical thickness, these colloidal NPLs feature discrete excitonic absorption peaks regardless of their lateral dimensions [17]. For example, CdSe NPLs with 3, 4 and 5 ML vertical thicknesses have the first excitonic transition peak at ~460, 513 and 550 nm, respectively. Therefore, the vertical thicknesses of the synthesized NPLs can be determined simply by using steady-state absorption spectroscopy.
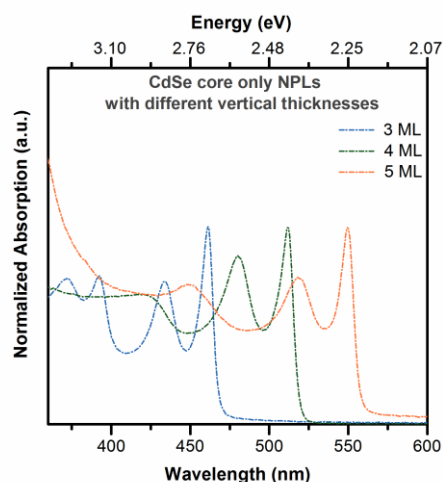
Figure 3.1. Normalized absorption spectra of our CdSe core-only NPLs having different vertical thicknesses, synthesized at our laboratories.

We have also used the steady-state absorption spectroscopy to verify the formation of core/crown and core/shell heterostructures. Since the resulting absorption behavior of core/crown and core/shell NPLs is strongly related with the thickness of the starting core NPLs, these heterostructured NPLs also exhibit discrete excitonic transitions [18], [19]. For example, in the CdSe/CdS core/crown heterostructures, while the excitonic features belonging to the CdSe core NPLs remain in the same spectral positions, a new excitonic peak appears due to the absorption within the CdS crown region (Figure 3.2a), suggesting the formation of CdSe/CdS core/crown NPLs. Similarly, CdSe/CdS core/shell NPLs exhibit discrete excitonic absorption peaks depending on the thicknesses of CdSe core and CdS shell. Thus, the number of CdS shell can be also easily estimated from the absorption spectra of CdSe/CdS core/shell NPLs (Figure 3.2b).
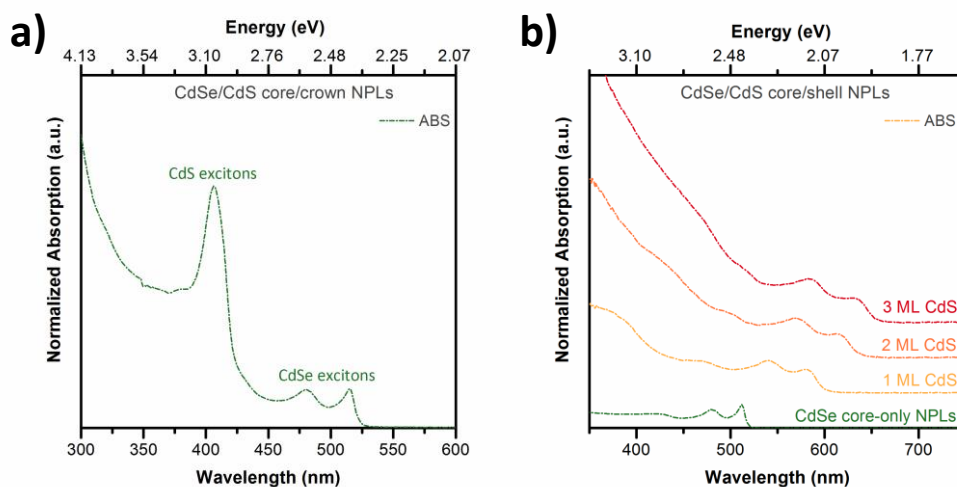
Figure 3.2. Normalized absorption spectra of (a) CdSe/CdS core/crown NPLs and (b) CdSe/CdS core/shell NPLs with different vertical thicknesses synthesized at our laboratories.

3.1.2 Steady-State Photoluminescence Spectroscopy

Steady-state photoluminescence spectroscopy is highly important for investigating the emission behavior of colloidal semiconductor NPLs. For the photoluminescence measurements, both dispersion and/or solid samples of colloidal NPLs can be used. These samples are excited with photons having higher energies than their band gap to create electron and hole pairs. These created electron and hole pairs are quickly localized to their ground state and radiatively recombined, resulting in the photoluminescence. The resulting intensity of the photoluminescence is recorded as a function of the detection wavelength and emission spectra of the samples are obtained.

As it can be seen from the normalized photoluminescence spectra of our CdSe core NPLs with varying vertical thicknesses (Figure 3.3), these core-only NPLs possess the

narrowest emission linewidths (~35 meV). This narrow emission behavior of NPLs can be explained with the synthesis of atomically-flat nanocrystals, enabling the suppression of inhomogeneous broadening [75]. Also, these core NPLs have shown discrete emission lines, enabling the estimation of their vertical thicknesses from the emission spectra [78].
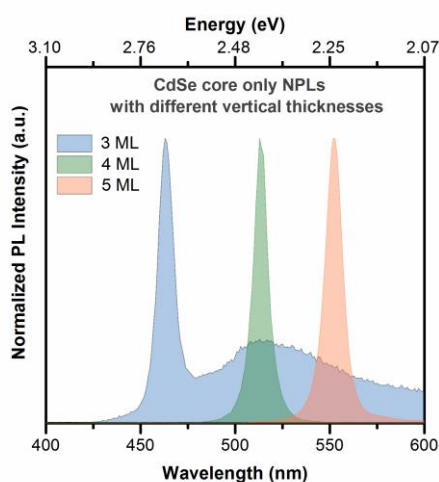
Figure 3.3. Normalized photoluminescence spectra of CdSe core-only NPLs with varying vertical thicknesses synthesized at our laboratories.

3.1.3 Photoluminescence Excitation Spectroscopy

In addition to steady-state absorption and photoluminescence measurements, the photoluminescence excitation (PLE) spectroscopy should be performed to completely understand the origin of the photoluminescence from the solution-processed NPLs. The PLE measurements was performed by using the both solution and film samples. In the PLE measurements, the change in the intensity of photoluminescence at a fixed detection wavelength is measured by varying the excitation wavelength. Therefore, it is expected

that PLE spectra of the colloidal NPLs having well-defined size, shape and composition should be similar to their absorption spectra.

In this thesis, we used the PLE spectroscopy as a relatively simple technique to analyze the structural quality of the synthesized NPLs. For example, the PLE spectrum of 4 ML thick CdSe core NPLs is given in Figure 3.4a. The observation of similar excitonic transitions between the PLE and absorption spectra clearly shows the colloidal synthesis of highly monodisperse and uniform nanoplatelets. In addition, the PLE measurements taken at different emission wavelengths of the synthesized NPLs provides valuable information about the emission broadening. For instance, the PLE measurements of 4 ML thick CdSe core NPLs taken at the lower energy emission side, the higher energy emission side and the peak of the emission have shown exactly similar excitonic transitions (Figure 3.4b), suggesting the suppressing of inhomogeneous broadening in these atomically-flat nanocrystals [75].
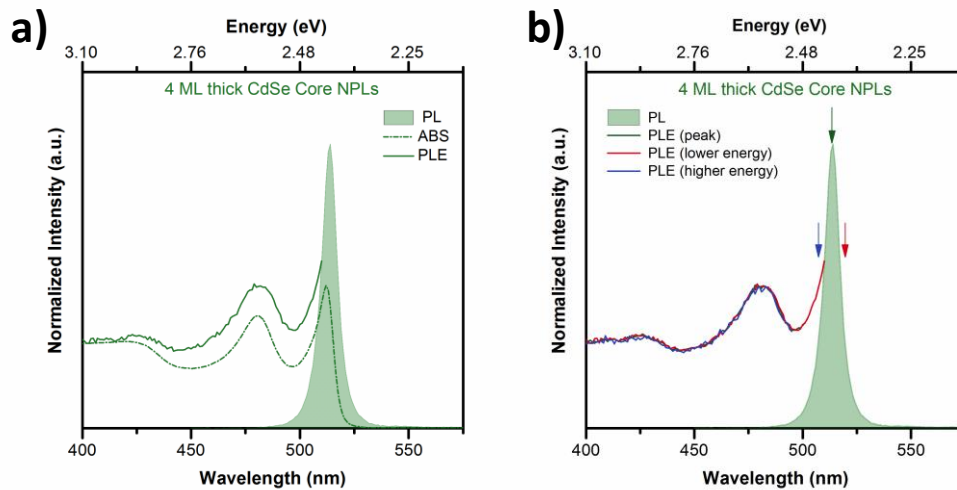
Figure 3.4. (a) Normalized photoluminescence and photoluminescence excitation spectra of our 4 ML thick CdSe core NPLs together with their absorption spectra. (b)

The photoluminescence excitation spectra of our 4 ML thick CdSe core NPLs taken at different emission wavelengths.

We have also used the PLE measurements to explain the emission broadening in the core/shell and core/crown heterostructures of NPLs. For example, with the formation of CdS shell in the vertical direction, CdSe/CdS core/shell NPLs exhibit red-shifted and broadened emission with respect to the CdSe core-only NPLs. This emission broadening observed in the core/shell NPLs can be attributed to the variation in the CdS shell thicknesses within the ensemble solution of NPLs. However, the observation of similar excitonic features from the PLE measurements of the core/shell NPLs taken at different emission wavelengths rules out this possibility and suggests that this broadening originates from the enhanced exciton-phonon coupling, commonly observed in CdSe and CdS material system (Figure 3.5a) [87]. Similarly, we have also observed significantly broadened emission in CdSe/CdTe core/crown NPLs, which can be due to the nonuniform growth of CdTe crown region and/or the composition variation in the crown region. However, by using the PLE measurements taken at different emission wavelengths of CdSe/CdTe core/crown NPLs, these probabilities have been eliminated (Figure 3.5b). This significantly broadened emission is explained with the radiative recombination of spatially indirect excitons in the NCs having Type-II electronic structure [51].
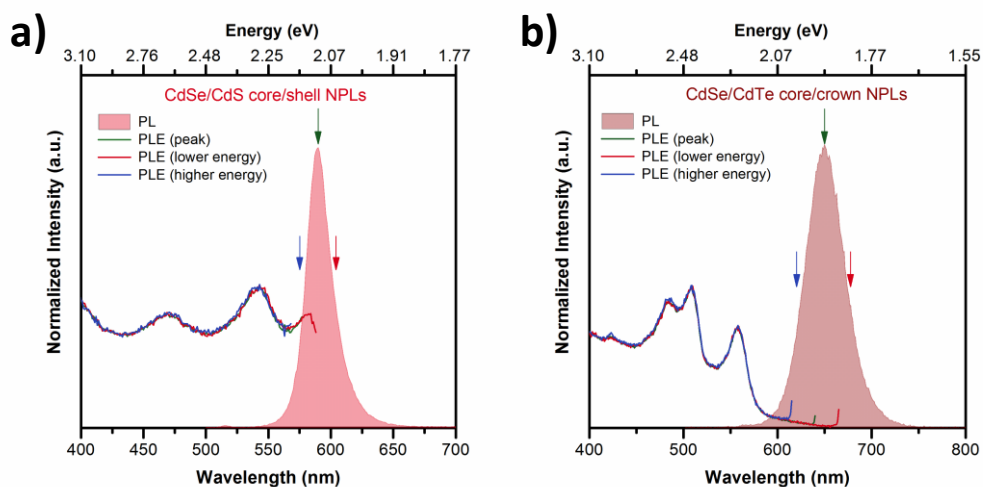
Figure 3.5. Photoluminescence excitation spectra of (a) CdSe/CdS core/shell and (b) CdSe/CdTe core/crown NPLs taken at different emission wavelengths synthesized at our laboratories.

3.1.4 Photoluminescence Quantum Yield Measurements

One of the most important design parameters of the colloidal semiconductor NCs is their photoluminescence quantum yield, which can be defined as the ratio of the number of emitted photons to the number of absorbed photons. The PL-QY measurements also give valuable information about the quality of the synthesized NCs in terms of their passivation, crystalline structure and uniformity. While well-passivated colloidal NCs with highly crystalline structure and uniform size distribution exhibit improved PL-QY, incomplete passivation of colloidal NCs together with lower crystal quality and nonuniform size distribution leads to the decreased PL-QY [88], [89].

For the determination of the PL-QY of colloidal semiconductor NCs, there are two different methods commonly used in the literature: the relative PL-QY measurements

[90] and the absolute PL-QY measurements [91]. In the relative PL-QY measurements, the PL-QY of an unknown sample is determined by comparison with a reference material having a well-known PL-QY. The measurements are performed by using the solution samples of the unknown sample and the reference material having the same absorption value at the excitation wavelength. After matching their absorption levels, their emission spectra are measured under identical conditions, including the same excitation wavelength and the same slit size. Then, the PL-QY of the samples are calculated by using the given Equation (1),

$$PL\text{-}QY_x = PL\text{-}QY_{st} \times \left(\frac{E_x}{E_{st}}\right) \times \left(\frac{A_{st}}{A_x}\right) \times \left(\frac{n_x}{n_{st}}\right)^2 \qquad (1)$$

where subscripts x and st denote the sample under test and the standard reference material, respectively. In the equation, E refers to the integrated area under the emission spectrum, A refers to fraction of the excitation wavelength absorbed and n is the refractive index of the solutions. Although the relative PL-QY measurement method is a simple approach to determine the PL-QY of the samples, it suffers from several drawbacks including the limited number of suitable reference materials and their applicability only to the solution samples. Therefore, the absolute PL-QY measurements method has become widely used technique to measure the PL-QY of the both solution and film samples.

In the absolute PL-QY measurements method, the PL-QY of a sample is determined by directly calculating the number of absorbed versus emitted photons. The measurements are performed by using an integrating sphere having fully reflecting surface. To determine the PL-QY, the measurements are taken in three different

configurations, which are shown schematically in Figure 3.6a: (i) the measurement of the spectrum without any sample inside the integrating sphere, (ii) the measurement of the spectrum when the sample is excited directly, and (iii) the measurement of the spectrum when the sample is excited in-directly with the scattered light from the surface of integrating sphere. After the measurements, the PL-QY of the sample is calculated by using the Equation (2) and (3),

$$Abs = 1 - \frac{E_{ii}}{E_{iii}} \qquad (2)$$

$$PL\text{-}QY_x = \frac{L_{ii} - (1 - Abs) \times L_{iii}}{Abs \times E_i} \qquad (3)$$

where the subscript x refers to the sample and subscripts i, ii and iii refer to the configuration of the measurements. In the equations, E refers to the excitation part of the measured spectrum and L is the emission part of the measured spectrum.
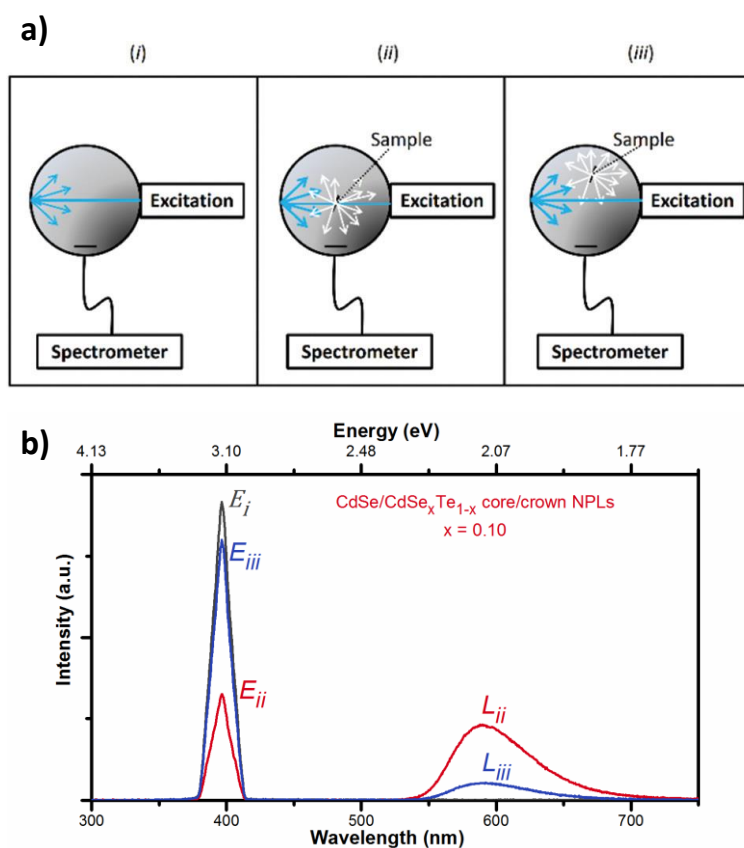
Figure 3.6. (a) Schematic demonstration of different measurement configurations used in the absolute PL-QY measurement method. Reproduced with permission from [92]. Copyright Royal Society of Chemistry 2015. (b) PL-QY measurements of CdSe/CdSe$_{1-x}$Te$_{1-x}$ core/crown NPLs (x = 0.10) performed by following the absolute PL-QY measurements method at our laboratories. While the higher energy sides of the emission spectra show the excitation spectra obtained in different measurement configurations, the lower energy sides of the spectra belong to the emission spectra of the sample obtained in different measurement configurations.

In our thesis studies, we have commonly used the absolute PL-QY measurement method offering great advantages. With this approach, the PL-QY of the both solution and film samples can be conveniently measured. Also, by changing the excitation

42

wavelength, the excitation wavelength dependent PL-QY can be measured. As an exemplary case, the measured photoluminescence spectrum of CdSe/CdSe$_{1-x}$Te$_x$ core/crown NPLs is presented in Figure 3.6b. By integrating the area under the excitation and emission spectra, we calculated their PL-QY using the given equations. With the novel heterostructured NPLs demonstrated in the thesis, we have achieved almost near-unity PL-QY (~95 %) [93].

3.1.5 Time-Resolved Fluorescence Spectroscopy

Time-resolved fluorescence (TRF) spectroscopy is a commonly used method to explore and understand the emission kinetics in these atomically-flat NPLs. For the TRF measurements, we have used both solution and film samples of colloidal quantum wells. These samples are excited by using a pulsed laser source. After the excitation, the photogenerated electron and hole pair is quickly thermalized to their lowest energy states and emits a photon through radiative recombination. By using time-correlated single photon counting unit, the time duration between the laser pulse generation and photon collection is recorded and fluorescence decay curves of the samples are obtained. The resulting fluorescence decay curves of the samples are analyzed by least chi-square fittings based on a multi-exponential fitting.

The analyses of fluorescence decay curves are quite important for the understanding of the radiative and nonradiative recombination rates in the colloidal NPLs. For example, the fluorescence decay curves of our 4 ML thick CdSe core and CdSe/CdS core/crown NPLs are presented in Figure 3.7a. The CdSe core-only NPLs exhibit a multi-exponential decay with an amplitude-averaged lifetime of ~1.9 ns. Although it is hard to

explain each lifetime components separately, the fastest lifetime component (~0.15 ns) originates from the nonradiative hole trapping, which is commonly observed in core NPLs. With the passivation of inner CdSe core with laterally extended CdS crown extension, the fastest lifetime component is eliminated and CdSe/CdSe core/crown NPLs exhibit slightly elongated an amplitude-averaged lifetime of ~3.2 ns, supporting the enhanced PL-QY of CdSe/CdS core/crown NPLs with respect to core-only NPLs [94].
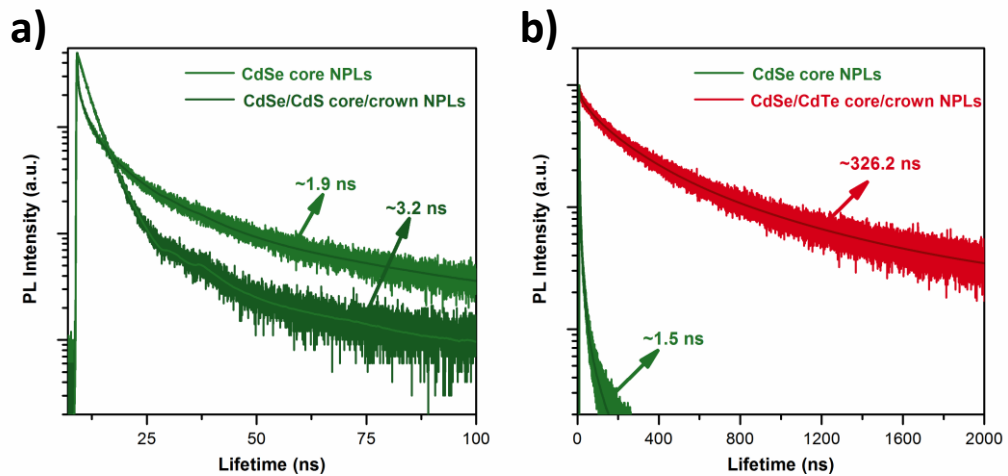
Figure 3.7. Time-resolved fluorescence decays curves of (a) CdSe core and CdSe/CdS core/crown NPLs having Type-I electronic structure and (b) CdSe core and CdSe/CdTe core/crown NPLs having Type-II electronic structure. These core and core/crown heterostructured NPLs were synthesized at our laboratories.

Also, we used TRF spectroscopy to study and figure out the excitonic behavior of colloidal heterostructured NPLs having different electronic structures. As an exemplary case, the fluorescence decay curves of 4 ML thick CdSe/CdTe core/crown NPLs are shown in Figure 3.7b. While CdSe/CdS core/crown NPLs having Type-I electronic structure feature an amplitude-averaged lifetime of ~3.2 ns, CdSe/CdTe core/crown

NPLs with Type-II electronic structure exhibit a significantly elongated amplitude-averaged radiative lifetime of ~326.2 ns, which can be explained with the separation of electron and hole wavefunctions in the heterostructures having Type-II like band alignment [95].

3.2 Structural Characterization Techniques

The resulting optical properties of the synthesized colloidal quantum wells are strongly related to their structural properties. Therefore, the complete understanding of the structural properties of the synthesized colloidal NPLs is key to designing and developing novel heterostructures of NPLs with the well-defined size, shape and composition, enabling the achievement of superior excitonic properties. Here, we present the structural characterization techniques employing transmission electron microscopy, X-Ray photoelectron spectroscopy and X-Ray diffraction to investigate the size distribution, chemical composition and crystalline structure of the synthesized colloidal NPLs having different heterostructures.

3.2.1 Transmission Electron Microscopy

Transmission electron microscopy (TEM) is a powerful structural characterization tool to study the morphology of the colloidal semiconductor NPLs including their size, shape and assembly. In addition to the morphology, TEM provides detailed information about the chemical composition and crystalline structure of the synthesized NPLs. Thus, in our thesis, we have effectively used TEM to investigate the structural properties of the core-only NPLs together with their novel heterostructures. For the sample preparation, we

have used the diluted solutions of colloidal NPLs, which are cleaned several times to remove the excess amounts of organic ligands, causing the charging issue. Then, by dropping 5 µL of the diluted solution on the copper mesh grids, the samples are kept under vacuum for the complete drying before the measurements.

The imaging of solution-processed colloidal quantum wells with TEM is also highly challenging. Due to their atomic-scale vertical thicknesses consisting of several layers of atoms, they exhibit low contrast in TEM imaging. Therefore, we have commonly used the high-angle annular dark-field scanning transmission electron microscopy (HAADF-STEM) configuration for the imaging of colloidal NPLs, enabling the enhanced contrast. As an exemplary case, HAADF-STEM images of our 4 ML thick CdSe core NPLs having different lateral dimensions are presented in Figure 3.8. From the HAADF-STEM images, the formation of highly uniform CdSe NPLs with well-defined shapes is clearly seen. With the optimized synthesis conditions, the lateral dimensions of CdSe NPLs can be tuned from rectangular shape to almost square shape without changing their vertical thicknesses.
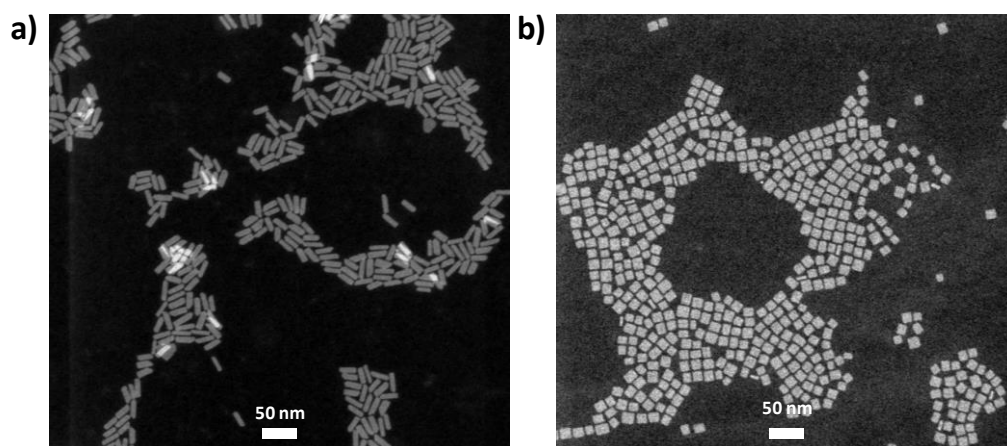
Figure 3.8. HAADF-STEM images of 4 ML thick CdSe core NPLs having (a) rectangular shape and (b) square shape, which were synthesized at our laboratories.

We have also used TEM to verify the formation of core/crown and core/shell heterostructures. HAAF-STEM images of CdSe core and CdSe/CdTe core/crown NPLs are shown in Figure 3.9. As it can be seen from the images, with the formation of CdTe crown layer in the lateral direction, CdSe/CdTe core/crown NPLs exhibit increased lateral dimensions with respect to the core-only NPLs. Also, the vertical thicknesses of core/crown NPLs are found to be the same with the starting CdSe core NPLs, indicating the growth of the crown layer in the lateral direction. In addition, the formation of core/crown heterostructure is further verified by using energy dispersive X-ray (EDX) spectroscopy from a single CdSe/CdTe core/crown NPL (Figure 3.9c). As it can be seen from Figures 3.9d and 3.9e, while the higher amount of selenium is observed in the inner region of the NPL, the higher amount of tellurium is found in the outer region of the NPL, suggesting the uniform formation of core/crown heterostructures. These imaging and spectroscopy capabilities offered by TEM have made great contributions to the understating of the structural properties of the synthesized NPLs in this thesis.

47
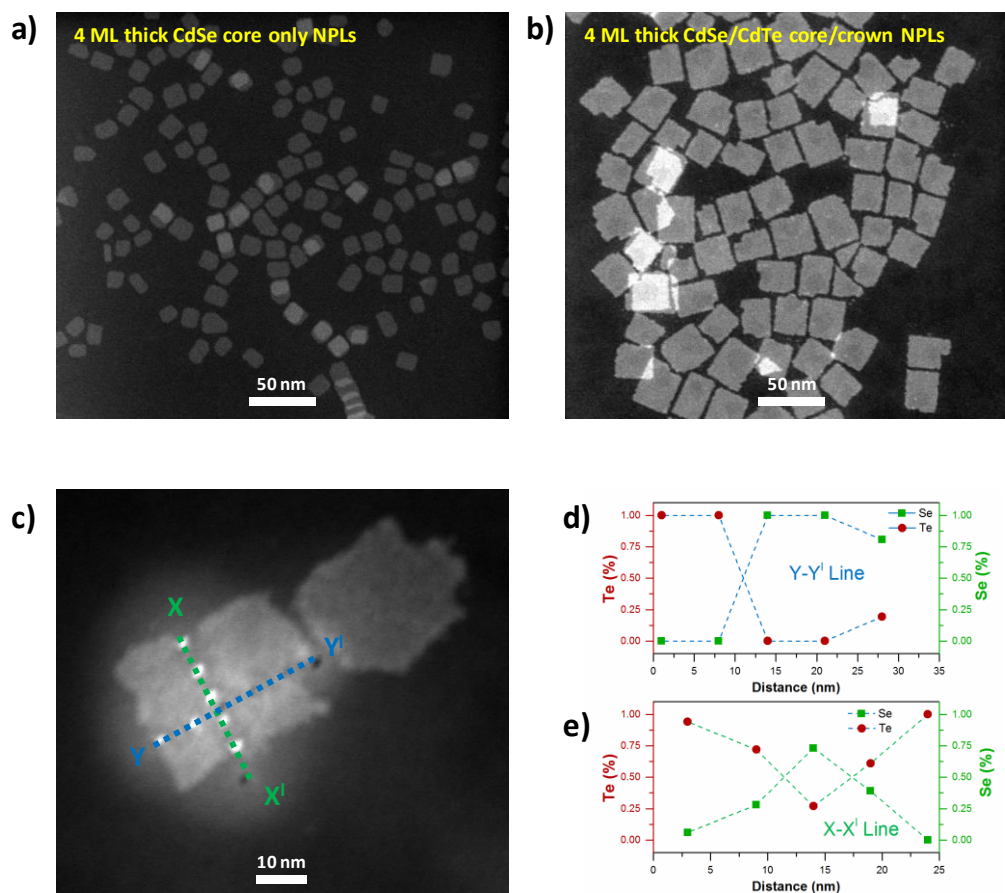
Figure 3.9. HAADF-STEM images of (a) 4 ML thick CdSe core-only NPLs and (b) 4 ML thick CdSe/CdTe core/crown NPLs. (c) HAADF-STEM image of a single CdSe/CdTe core/crown NPL together with with blue (Y−Y^l) and green lines (X−X^l) showing the EDX probe position. The line EDX analysis reporting the compositions of selenium and tellurium in the core/crown NPLs within (e) blue (Y−Y^l) and (f) green lines (X−X^l). All of these NPLs presented here were synthesized at our laboratories. Reprinted with permission from [93]. Copyright 2017 American Chemical Society.

3.2.2 X-Ray Photoelectron Spectroscopy

X-ray photoelectron (XPS) spectroscopy is a commonly used technique to analyze the surface properties of the colloidal semiconductor NPLs together with their chemical properties [96]. For the XPS measurements, the solid films are prepared by spin-coating of NPL solutions on silicon substrates. These samples are excited with the monochromatic X-rays, leading to the emission of photoelectrons from the sample. The intensity of the emitted photoelectrons from the sample is recorded as a function of their energies by the electron energy analyzer. With the analyses of the binding energy and the intensity of the emitted photoelectrons, the chemical composition of the sample is determined quantitatively using the information about the oxidation states of the elements.

In our studies, we have performed XPS to determine the elemental compositions of the synthesized NPLs. For example, the high-resolution XPS spectra of $CdSe/CdSe_{1-x}Te_x$ core/crown NPLs with different crown compositions are shown in Figure 3.10. With increasing the concentration of tellurium in the $CdSe_{1-x}Te_x$ crown region, we observed increasing contribution from the tellurium in the XPS spectra. With the fitting of the acquired high-resolution XPS spectra, we have calculated the elemental compositions of $CdSe/CdSe_{1-x}Te_x$ core/crown NPLs having different crown compositions. Also, by using the lateral sizes of the CdSe core and the $CdSe_{1-x}Te_{1-x}$ crown regions measured from the HAADF-TEM images, we have extracted the crown compositions from the calculated elemental compositions, showing the versatility of XPS.
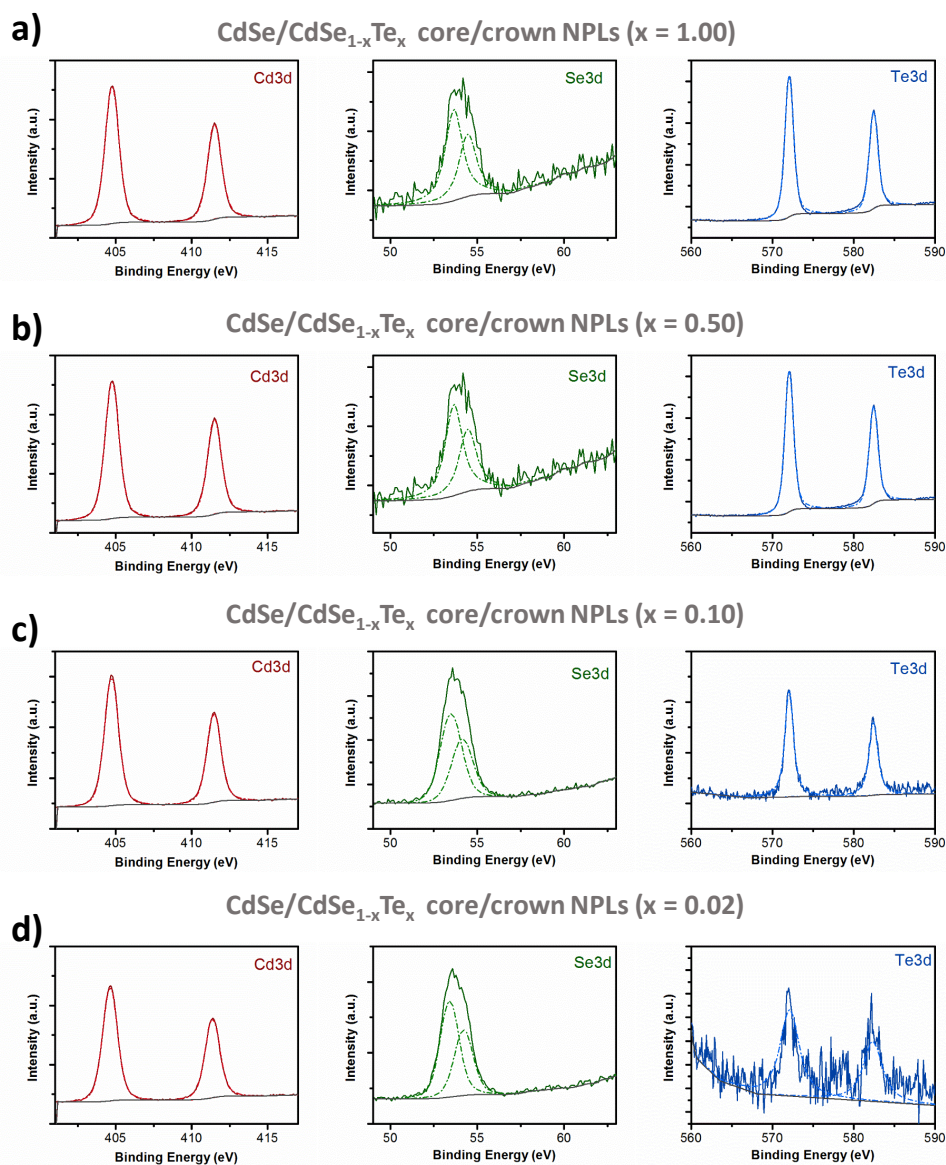
Figure 3.10. The acquired high-resolution XPS spectra of the CdSe/CdSe$_{1-x}$Te$_x$ core/crown NPLs with varying crown compositions; (a) x = 1.00, (b) x = 0.50, (c) x = 0.10 and (d) x = 0.02, synthesized at our laboratories. Reprinted with permission from [93]. Copyright 2017 American Chemical Society.

3.2.3 X-Ray Diffraction

X-ray diffraction is a unique technique for the detailed investigation of the crystal structure of the colloidal semiconductor NCs, which strongly affects their optical properties. Additionally, the crystal structure of colloidal NCs has strong influence on the final shape of the synthesized colloidal NCs. While CdSe NCs having wurtzite crystal structures promote the growth of rod-like NCs, CdSe NCs having zinc blende crystal structures trigger the formation of tetrapod-like NCs [97], showing the importance of controlling the crystal structure. For the XRD measurements, thick and uniform solid films are prepared by drop-casting highly concentrated NPL solution on the miscut silicon substrate. The samples are illuminated with the collimated beam of the monochromatic X-rays and their interaction of the samples with the incident beam is analyzed. When the interaction between the sample and the incident beam satisfies the conditions imposed by the Bragg`s Law, characteristic diffraction patterns are achieved with the formation of constructive interference. From these characteristic diffraction patterns, the crystalline structure of a sample is identified with the detailed information about its crystalline quality and chemical composition.

In our thesis, we have performed XRD measurements to determine the crystal structure of core and core/crown NPLs. The XRD patterns of 4 ML thick CdSe core NPLs are presented in Figure 3.11. These atomically-flat CdSe NPLs exhibit zinc blende crystal structure, which is supported with the characteristic diffractions observed from the (022) and (113) planes. Also, colloidal CdSe NPLs feature broader diffraction peaks, which is explained with the finite crystalline size of these NPLs. Moreover, the relative intensities of the diffraction peaks are observed to be slightly different than their bulk

counterparts, suggesting the formation of anisotropic shapes of nanoplatelets with the preferred growth direction.
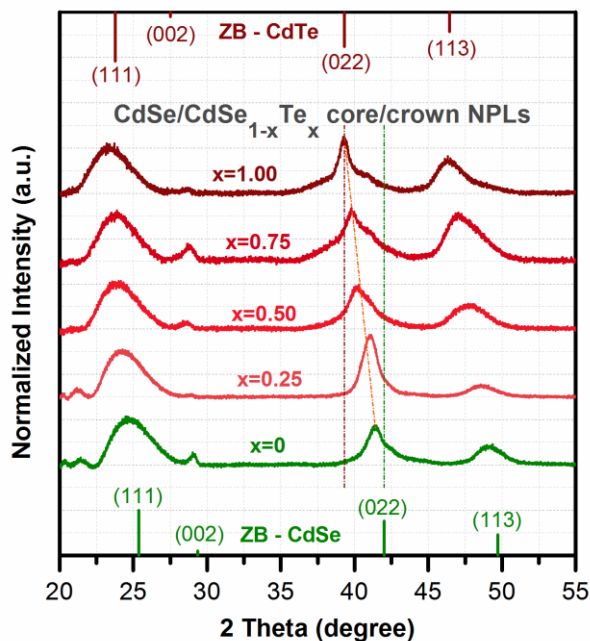
Figure 3.11. Powder XRD patterns of 4 ML thick CdSe core NPLs and CdSe/CdSe$_{1-x}$Te$_x$ core/crown NPLs having different crown compositions synthesized at our laboratories. Reprinted with permission from [93]. Copyright 2017 American Chemical Society.

We have also used XRD to investigate the crystal structures of CdSe/CdSe$_{1-x}$Te$_x$ core/crown NPLs having different crown compositions. From the XRD patterns of CdSe/CdSe$_{1-x}$Te$_x$ core/crown NPLs, it is clearly seen that, with the epitaxially-grown crown layer, these heterostructured NPLs preserve their initial zinc blende crystal structure. Also, with increasing the tellurium composition in the CdSe$_{1-x}$Te$_x$ crown region, the diffraction peaks are shifted to the lower angles suggesting the formation alloyed crown region. Furthermore, by using the Vegard`s law for the (022) plane, we

52

have estimated the composition of the $CdSe_{1-x}Te_x$ crown, which strongly agrees with the results obtained from the XPS and TEM. These findings have shown the importance of the XRD methods to determine not only the crystal structure of colloidal NPLs but also their chemical compositions.

Chapter 4

CdSe/CdS/CdS Core/Crown/Shell Heteronanoplatelets

This chapter of the thesis is based on the publication "Platelet-in-Box Colloidal Quantum Wells: CdSe/CdS@CdS Core/Crown@Shell Heteronanoplatelets," **Y. Kelestemur**, B. Guzelturk, O. Erdem, M. Olutas, K. Gungor, and H. V. Demir, Advanced Functional Materials 26 (21), 3570-3579 (2016). Reprinted with permission from [94]. Copyright 2016 WILEY-VCH Verlag GmbH & Co. KGaA, Weinheim.

4.1 Motivation

With their appealing properties, colloidal nanoplatelets have become highly promising for next-generation solution-processed optoelectronic device applications. However, similar to other classes of colloidal semiconductor nanocrystals [56], [97], core-only NPLs have suffered from the poor stability owing to their large surface area that result in lower photoluminescence quantum yield [98]. The stability issues and low PL-QY

become more dramatic especially for the solid films of these NPLs since they have tendency to form needle-like stacks due to strong van der Walls forces [99]. For these stacked NPLs, strongly quenched photoluminescence has been reported arising from ultra-efficient exciton transport assisted hole trapping [100].

Up to now, to enhance stability and PL-QY of NPLs, core/crown [18], [81], [95], [101], [102] and core@shell [19], [82] architectures have been synthesized and studied intensively. Among different varieties of core/crown (C/C) NPLs, CdSe/CdS C/C NPLs have been one of the most widely studied material systems. Since CdS crown layer is grown only in the lateral direction, the confinement in the vertical thickness is not changed and thus there is no noticeable change observed in the emission spectrum of CdSe/CdS C/C NPLs as compared to the CdSe core-only NPLs. However, with the passivation of trap sites originating from the sidewall of core-only NPLs, PL-QY can be greatly increased in the C/C NPLs. Also, with the formation of CdS crown layer, absorption cross-section in the near-UV and blue spectral ranges is substantially enhanced due to excitonic absorption in the larger band gap CdS. Furthermore, the CdS crown layer acts as a light-harvesting antenna, where the excitons photogenerated in the CdS crown layer are rapidly transferred to the CdSe core region, and makes contribution to the core emission. Therefore, with their enhanced optical properties, CdSe/CdS C/C NPLs have been shown to boost the optical gain performance in the NPLs [20]. However, due to lack of proper passivation on their larger lateral surfaces, they still suffer from serious stability issues.

Also, recently with the synthesis of core@shell (C@S) architectures, the optical properties of NPLs have been shown to be enhanced with respect to the core-only NPLs

since exciton is further confined within the core of the heterostructure and away from the lateral surface traps and possible dangling bonds [19]. Generally, shell growth in NPLs has been carried out using two different approaches: one-pot synthesis [19] and colloidal atomic-layer-deposition (c-ALD) technique [82]. In both cases, with the formation of shell layers, a significant amount of spectral redshift is observed in the absorption and emission spectra depending on the thickness and composition of the shell layers. This arises due to the relaxing vertical confinement of the electron and holes (thus, excitons) and changing the dielectric medium in the C@S NPLs. Although a significant amount of broadening of the emission is also observed in the C@S NPLs with respect to the core-only NPLs, the C@S architecture still features narrower emission bandwidths when compared to other classes of colloidal semiconductor nanocrystals including quantum dots and nanorods [87]. Also, a higher level of photoluminescence quantum yield (up to 80%) is achieved for CdSe@CdS C@S NPLs synthesized with one-pot synthesis. In addition, CdSe@CdS C@S NPLs, due to the separation of electron and hole wave functions, exhibit suppressed Auger recombination (AR) with reduced blinking behavior. With their promising properties, light-emitting diodes having narrower emission bandwidths [21] and optically pumped lasers with very low threshold [86] have been demonstrated by using NPLs in the C@S architecture. However, due to the formation of trap sites during the shell growth, the performance of C@S NPLs has been shown to be limited [87]. Therefore, to achieve further enhancement in the excitonic properties of NPLs, newly designed architectures are highly welcomed.

Here, we have developed and demonstrated the synthesis of CdSe/CdS@CdS core/crown@shell (C/C@S) NPLs resembling a platelet-in-box structure and report their systematic characterization. Starting with the CdSe core NPLs, a crown layer of CdS is

grown only in the lateral directions. In these CdSe/CdS C/C NPLs, with the passivation of periphery of the starting CdSe core NPLs, a faster nonradiative decay component (~0.15 ns) originating from the fast hole trapping is eliminated, which results in enhanced PL-QY (up to 90%). Then, by using colloidal atomic-layer-deposition technique, smooth CdS shell layers are deposited on both the core-only and C/C NPLs with atomically precise shell thickness control. With the formation of CdS shells, in both cases, a large redshift is observed in the absorption and emission spectra along with the spectral broadening of the excitonic features. When compared to C@S NPLs, C/C@S NPLs exhibit significantly enhanced absorption cross-section in the blue spectral region owing to CdS crown layer and improved PL-QY due to better passivation of the sidewalls of the inner CdSe core. In addition, amplitude-averaged fluorescence lifetimes of the C/C@S NPLs are found to be increased as a function of the increasing CdS shell thickness, which can be well explained by the delocalization of electron wavefunctions into the CdS shell layer leading to a quasi Type-II electronic structure. On the other hand, in the C@S NPLs, amplitude-averaged lifetimes are observed to remain almost constant as a function of the CdS shell thickness, which is attributed to the competition between the elongated radiative decay due to quasi Type-II character and increased nonradiative decay due to the created traps during shell growth. Suppression of trap sites in the C/C@S NPLs has been further evidenced by temperature-dependent photoluminescence study and time-resolved fluorescence spectroscopy (TRF). Lifetime broadening effect (observed for different lifetimes in the low energy side and in the high energy side of the emission peak) is considerably suppressed in the C/C@S NPLs as compared to that in the C@S NPLs. Finally, with their enhanced optical properties, the C/C@S NPLs achieve higher optical gain performance as compared to the C@S and C/C NPLs. Optical

gain threshold as low as ~20 $\mu J/cm^2$ is shown thanks to the increased PL-QY, enhanced absorption cross-section and eliminated trap sites in the C/C@S NPLs.

4.2 Colloidal Synthesis and Experiments

Chemicals. Cadmium nitrate tetrahydrate ($Cd(NO_3)_2 \cdot 4H_2O$) (99.999% trace metals basis), sodium myristate (>99%), technical-grade 1-octadecene (ODE), selenium (Se) (99.999% trace metals basis), sulfur (S) (99.998% trace metals basis), cadmium acetate dihydrate ($Cd(OAc)_2 \cdot 2H_2O$) (>98%), technical-grade oleic acid (OA) (90%), technical-grade oleylamine (OAm) (70%), N-methylformamide (NMF) (99%), and ammonium sulfide solution (40–48 wt% in H_2O) were purchased from Sigma-Aldrich. Hexane, ethanol, methanol, toluene, and acetonitrile were purchased from Merck Millipore and used without any further purification.

Preparation of Cadmium Myristate. Cadmium myristate was prepared according to the recipe given in the literature [18]. For a typical synthesis, 1.23 g of cadmium nitrate tetrahydrate was dissolved in 40 mL of methanol and 3.13 g of sodium myristate was dissolved in 250 mL of methanol. After complete dissolution of cadmium nitrate tetrahydrate and sodium myristate powders, solutions were mixed and stirred vigorously around 1 h. Then, the cadmium myristate powders were precipitated by using centrifuge and dissolved in methanol. The washing step with methanol was followed at least three times to remove any unreacted and/or excess precursors. After successive washing steps, the precipitated part was completely dried under vacuum overnight.

Synthesis of the CdSe Core NPLs. CdSe nanoplatelets having four complete monolayers of CdSe with an additional layer of Cd atoms were synthesized with a

slightly modified recipe from the literature [18]. For a typical synthesis, 340 mg of cadmium myristate, 24 mg of Se and 30 mL of ODE were loaded into a 100 mL three-neck flask. The solution was degassed at 100 °C for an hour. After degassing step, the solution was heated to 240 °C under argon atmosphere. When the solution color becomes bright yellowish (generally around 180–200 °C), 110–120 mg of cadmium acetate dihydrate was swiftly added to the reaction solution. After 10 min growth at 240 °C, 1 mL of OA was injected and the temperature of the solution was decreased to room temperature. The cadmium precursor injection temperature and the growth time were found to be important for the resulting shape and size of CdSe core NPLs. After the purification step with ethanol, CdSe core NPLs are dissolved in hexane and stored for the subsequent CdS crown and CdS shell growth.

Preparation of Anisotropic Growth Solution for CdS Crown Region. Anisotropic growth solution was prepared following the previously published procedure with slight modifications [18]. For the preparation of cadmium precursor, 480 mg of cadmium acetate dihydrate, 340 µL of OA, and 2 mL of ODE were loaded in a three-neck flask. The solution was heated to 100 °C under ambient atmosphere with rigorous stirring and it was also regularly sonicated. Until the formation of whitish color homogeneous gel, heating and sonication steps were followed alternatingly. When the cadmium precursor was prepared, it was mixed with 3 mL of sulfur precursor (0.1 M S-ODE stock solution) and used for the CdS crown coating.

Synthesis of CdSe/CdS Core/Crown NPLs. For typical CdS crown coating, 1 mL of CdSe core NPLs dissolved in hexane (having an optical density of ~1 at 350 nm), 5 mL of ODE and 100 µL of OA were loaded into a 50 mL three-neck flask. The solution was

degassed at 100 °C for the complete removal of hexane, water, and any other organic solvents. After that, the solution was heated to 240 °C under argon flow for the coating of CdS crown region. When the temperature reaches 240 °C, certain amount of anisotropic growth mixture was injected at the rate of 8 mL/h. After the injection of anisotropic growth mixture was finished, the resulting mixture was further annealed for 5 min at 240 °C. Finally, the solution was cooled down to room temperature for the purification step. The as-synthesized CdSe/CdS core/crown NPLs were precipitated by using ethanol. Finally, the precipitated NPLs were dissolved in hexane and stored for the following CdS shell coating steps. According to the desired CdS crown size, the injection amount of anisotropic growth mixture was tuned. Also, with the addition of OA to the reaction mixture, more uniform CdS crown growth with enhanced colloidal stability was achieved.

Synthesis of CdSe@CdS Core@Shell and CdSe/CdS@CdS Core/Crown@Shell NPLs. Both CdSe@CdS C@S and CdSe/CdS@CdS C/C@S NPLs were synthesized by using the colloidal atomic-layer-deposition technique [82]. We use CdSe core-only and CdSe/CdS core/crown NPLs as seeds for the subsequent CdS shell coating. For a typical CdS shell deposition, 3 mL of N-methylformamide (NMF) and 3 mL of seed NPLs dissolved in hexane were mixed. With the addition of 50 µL of sulfur precursor (Ammonium sulfide solution), NPLs are transferred from hexane to NMF. After 5 min shaking and stirring for complete reaction, the NPLs were precipitated with the addition of acetonitrile and toluene. For complete removal of excess sulfur precursor, the washing step was repeated at least two times. Then, precipitated NPLs were dissolved in 3 mL of fresh NMF for the next cadmium deposition step. After complete dissolution of NPLs, 2 mL of cadmium precursor (0.2 M cadmium acetate-NMF) was added and waited for 5

min to complete reaction. The NPLs were then precipitated with the addition of acetonitrile and toluene. Resultantly, 1 ML CdS shell was formed on the CdSe core or CdSe/CdS core/crown NPLs. For further increasing the CdS shell thickness, this process was followed in the same way. Finally, the core@shell and/or core/crown@shell NPLs with surfaces terminated with cadmium were precipitated and dispersed in hexane with the addition of excess amount of OAm.

For the TRF measurements, core-only, core/crown, core@shell, and core/crown@shell NPLs were precipitated with the addition of ethanol. Then, they were dissolved in hexane and the TRF measurements were conducted with the samples cleaned only one times to prevent removal of surface ligands and stacking issues, which significantly change the decay kinetics of NPLs. On the other hand, for the optical gain study, we performed the same washing procedure with ethanol at least two times for the achievement of highly close packed and uniform films form NPLs.

4.3 Results and Discussion

In this study, CdSe/CdS@CdS core/crown@shell (C/C@S) NPLs having a novel 3D architecture have been synthesized in three separate steps. First, we started with the synthesis of CdSe core NPLs having 4 ML of CdSe with an additional layer of Cd atoms by using a slightly modified recipe from the literature (see the Experimental Section for details) [18]. When compared to CdSe NPLs having different vertical thicknesses, these CdSe core NPLs have been preferred in this study because of their optimized synthesis condition and higher stability. Absorption and PL emission spectra of these CdSe core NPLs are given in Figure 4.1a. With their quantum well-like electronic structure, the

sharp excitonic features around 480 and 511 nm corresponding to electron/light-hole and electron/heavy-hole transitions, respectively, are clearly observed from the absorption spectrum. Also, they feature narrower emission linewidth (~8 nm) with a PL-QY of ~30%. From HAADF-STEM image (Figure 4.1b), formation of almost square-shaped CdSe core-only NPLs (with lateral dimensions of 11.1 ± 1.4 nm and 14.4 ± 1.7 nm) can be clearly seen. These core NPLs have been used as a seed for the subsequent synthesis of core/crown (C/C), core@shell (C@S) and core/crown@shell (C/C@S) architectures.
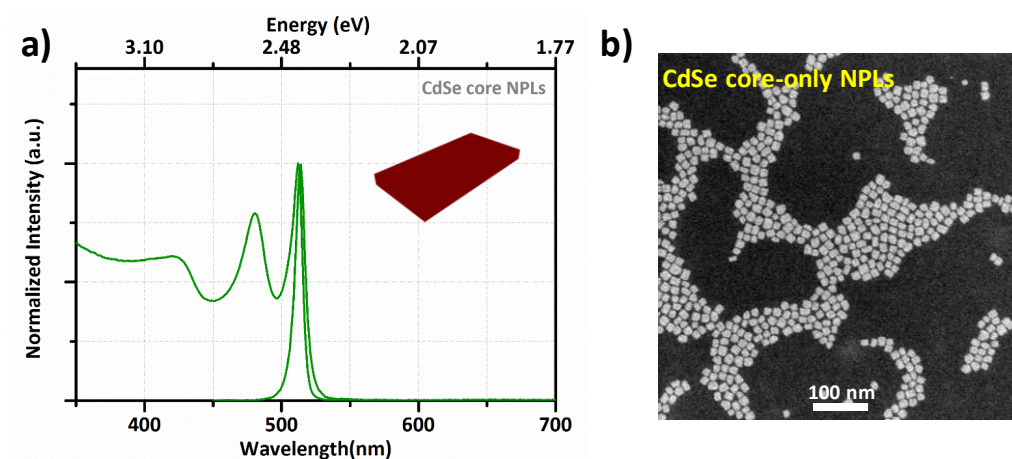
Figure 4.1. (a) Normalized absorption and photoluminescence spectra of CdSe core-only NPLs and (b) HAADF-STEM image of CdSe core-only NPLs. Reprinted with permission from [94]. Copyright 2016 WILEY-VCH Verlag GmbH & Co. KGaA, Weinheim.

In the second step, CdSe/CdS C/C NPLs have been synthesized using core-seeded approach following a previously published procedure with slight modifications (see the Experimental Section) [18]. By using cadmium acetate as a cadmium precursor, anisotropic growth of CdS layer is achieved and CdS crown layer is grown only in the lateral direction. Also, varying the amount of injected solution, CdSe/CdS C/C NPLs

with different crown sizes have been prepared. As it can be seen from Figure 4.2a, with the formation of small CdS crown layer, a new absorption peak around ~406 nm becomes apparent corresponding to the band gap of CdS NPLs having the same thickness with CdSe core NPLs. With the increased size of the CdS crown layer, this absorption peak becomes more pronounced and significantly enhances the absorption cross-section of the resulting NPLs in the blue spectral region. Also, by using photoluminescence excitation spectroscopy (Figures 4.2b, 4.2c, and 4.2d), it is shown that this CdS crown layer acts as an antenna, where excitons formed in the CdS crown region are transferred to the CdSe core region, and makes a major contribution to the emission. On the other hand, owing to the only lateral growth of CdS crown layer, no significant change is observed in the excitonic features of the CdSe core NPLs. The slight redshift (~3-4 nm) in the absorption and emission peaks is attributed to the change of dielectric constants due to the formation of the CdS crown layer. In addition, with the passivation of the periphery of the CdSe core NPLs, a substantially higher PL-QY (up to 90%) is obtained depending on the size of the CdS crown layer.
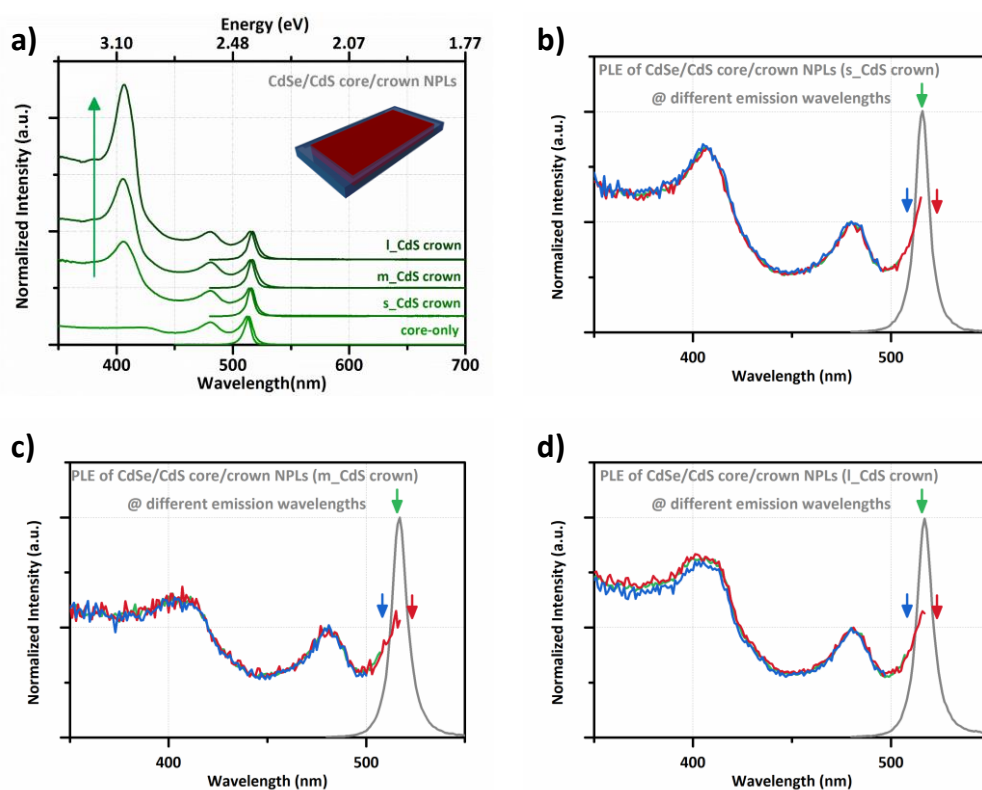
Figure 4.2. (a) Normalized absorption and photoluminescence spectra of CdSe core and CdSe/CdS core/crown NPLs having different crown sizes. Normalized photoluminescence excitation spectra of (b), (c) and (d) CdSe/CdS core/crown NPLs having different crown sizes taken at different emission wavelengths. Reprinted with permission from [94]. Copyright 2016 WILEY-VCH Verlag GmbH & Co. KGaA, Weinheim.

While the CdSe/CdS C/C NPLs having a narrower CdS crown width suffer from the incomplete and/or uneven growth of the CdS crown layer, the CdSe/CdS C/C NPLs having a wide enough layer suffer from the formation of cracks, which may act as a trap site. With the addition of a small amount of oleic acid, the stability and quality of the CdS crown layer can be greatly improved when compared to our previous synthesis.

Nevertheless, it is not easy to achieve sharp boundaries in CdSe/CdS C/C NPLs similar to CdSe/CdTe C/C NPLs (Figure 4.3) [95], [102]. Therefore, optimized CdS crown layer coating is essential to achieve high optical performance from CdSe/CdS C/C NPLs.
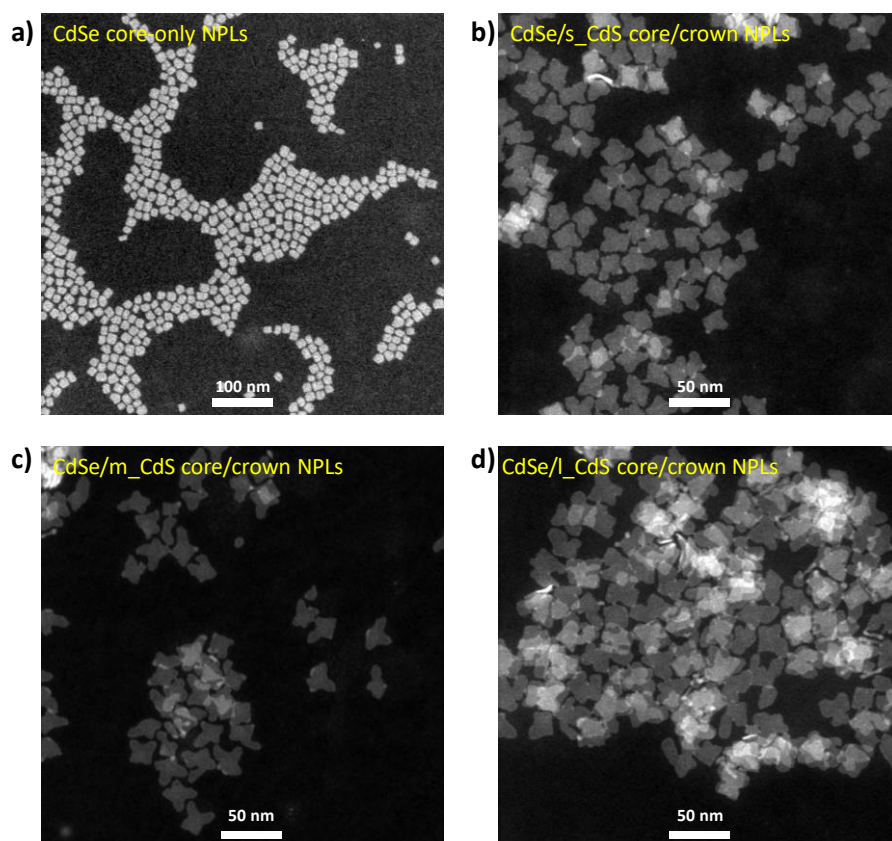
Figure 4.3. HAADF-STEM images of (a) CdSe core-only and CdSe/CdS core/crown NPLs with (b) small, (c) medium, and (d) large CdS crown size. Reprinted with permission from [94]. Copyright 2016 WILEY-VCH Verlag GmbH & Co. KGaA, Weinheim.

In the last step, CdS shell coating has been performed for both the CdSe core-only and the CdSe/CdS C/C NPLs having different crown sizes by using c-ALD technique [82]. As compared to the CdS shell growth with one-pot synthesis, c-ALD offers great

65

advantages including the formation of smooth CdS shell layer with atomically precise shell thickness control. As it can be seen from Figures 4.4a and 4.4b, with the formation of CdS shell, a significant amount of red-shifting in the absorption and emission spectra has been observed for both the core@shell and the core/crown@shell NPLs. This strongly red-shifting behavior can be explained with the growth of CdS shell in the vertical direction, making the initially very tight quantum confinement relatively relaxed. Owing to quasi Type-II like band alignment between CdSe and CdS material systems, electrons can spread across the whole structure (throughout both the CdSe core and CdS shell regions), while holes are mostly confined to the CdSe core region. Therefore, with the separation of electron and hole wavefunctions, strongly red-shifted emission can be obtained. Also, when compared to the C@S NPLs having the same CdS shell thickness, the C/C@S NPLs exhibit an additional red-shifting in their absorption and emission spectra. For example, while the C@S NPLs with 1 ML CdS shell thickness dissolved in hexane have an emission peak around ~589 nm, the C/C@S NPLs with the same CdS shell thickness possess its emission peak around ~610 nm.
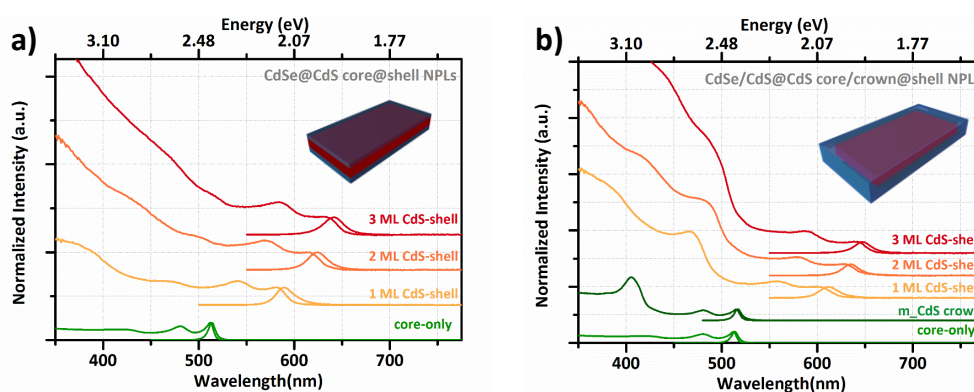
Figure 4.4. Normalized absorption and photoluminescence spectra of (a) CdSe@CdS core@shell, and (b) CdSe/CdS@CdS core/crown@shell NPLs with varying CdS shell

thicknesses. Reprinted with permission from [94]. Copyright 2016 WILEY-VCH Verlag GmbH & Co. KGaA, Weinheim.

This additional red-shifting in the C/C@S NPLs could possibly be originated from two potential sources: a nonuniform CdS shell coating and/or change in dielectric constant, which is known to be effective. Therefore, to check out the first hypothesis, transmission electron microscopy TEM and photoluminescence excitation spectroscopy have been performed. From the HAADF-STEM images (Figure 4.5), the thickness of the CdSe/CdS@CdS core/crown@shell NPLs having 2 ML CdS shell is determined as ~2.7 nm, which matches with the estimated thickness of ~2.5 nm.
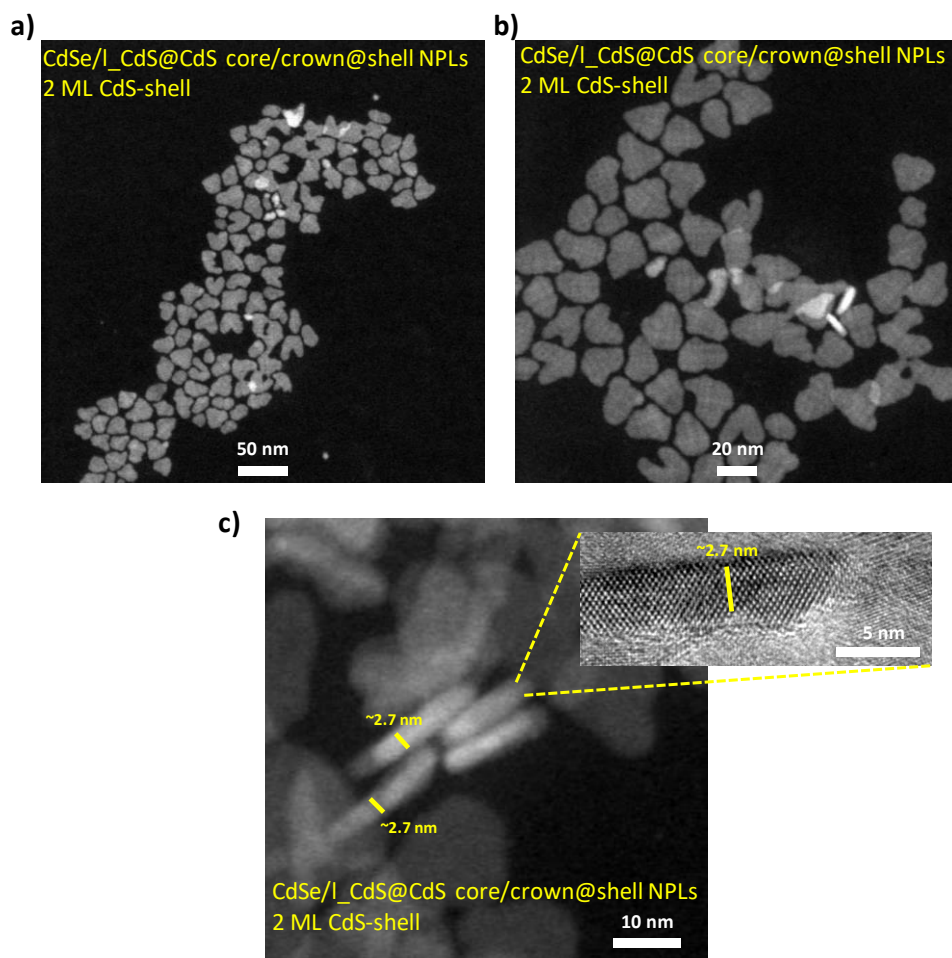
Figure 4.5. HAADF-STEM images of (a), (b) and (c) the CdSe/l_CdS@CdS core/crown@shell NPLs having 2 ML CdS shell thickness at different magnifications. High-resolution TEM image of the CdSe/l_CdS@CdS core/crown@shell NPLs having 2 ML CdS shell is given in the inset. Reprinted with permission from [94]. Copyright 2016 WILEY-VCH Verlag GmbH & Co. KGaA, Weinheim.

Also, the PLE spectra taken at the lower energy side, the higher energy side and the peak of the emission exhibit the same excitonic transitions, which suggest that there is no considerable inhomogeneous broadening (Figure 4.6). This rules out the possibility of CdS shell thickness variations and thus the nonuniform CdS shell coating of the

C/C@S NPLs is not possible because variation in shell-thickness would cause NPL sub-populations with varying excitonic transitions, which would result in an inhomogeneous broadening in the emission and absorbance spectra. Therefore, this additional red-shifting in the C/C@S NPLs is explained with the difference in the effective dielectric constant. With the encapsulation of the CdSe core region by the CdS crown and CdS shell regions leading to a platelet-in-box structure, the dielectric constant of the C/C@S NPLs has indeed been significantly increased when compared to the C@S NPLs, resulting in additional red-shifting in absorption and emission spectra. Also, similar trends observed between the CdSe core-only NPLs and the CdSe/CdS core/crown NPLs further suggest that the additional shifting from C@S to the C/C@S NPLs originate from the difference in the dielectric constant.
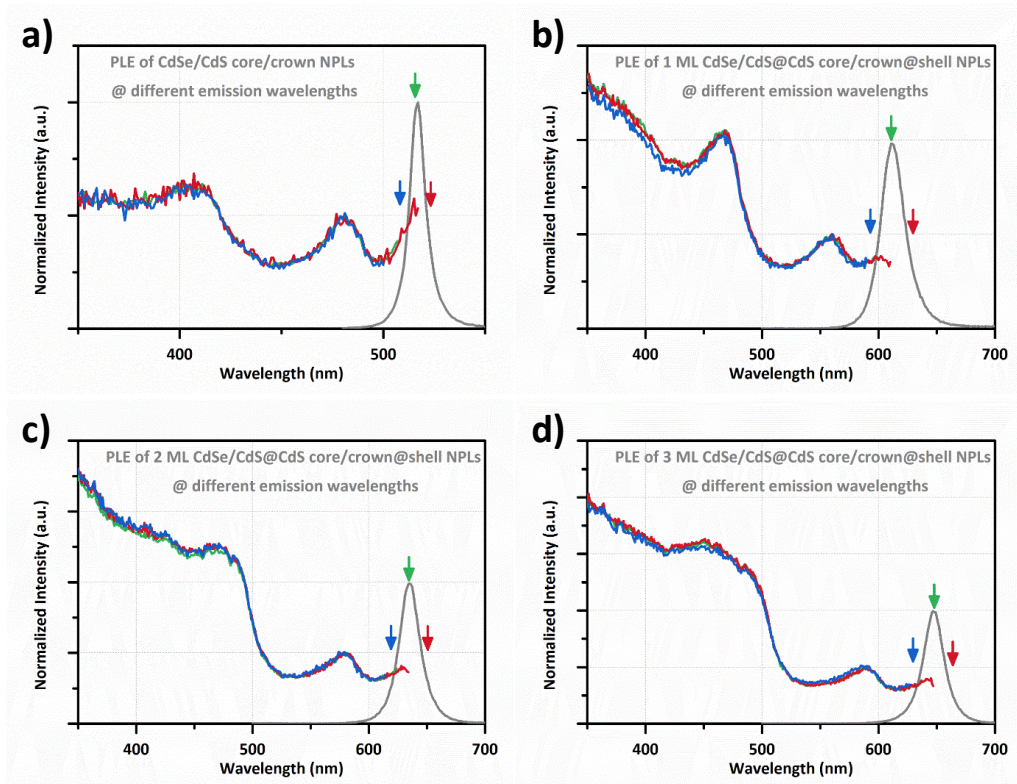
Figure 4.6. Photoluminescence excitation spectra of (a) CdSe/CdS core/crown NPLs having medium crown size and CdSe/CdS@CdS core/crown@shell NPLs having (b) 1 ML CdS shell, (c) 2 ML CdS shell and (d) 3 ML CdS shell taken at different emission wavelengths. Reprinted with permission from [94]. Copyright 2016 WILEY-VCH Verlag GmbH & Co. KGaA, Weinheim.

In addition to strongly red-shifted light-hole and heavy-hole transitions with the emission peak, broadening of the emission bandwidths in the C@S and C/C@S NPLs has been observed when compared to the CdSe core-only NPLs. While the CdSe core-only NPLs exhibit FWHM of ~35-40 meV, the C@S and C/C@S NPLs have FWHM of ~62–90 meV. This broadening was previously reported in the C@S NPLs regardless of the shell deposition method and attributed to the enhanced exciton–phonon coupling

upon the deposition of CdS shell [87]. Also, we have observed that structural quality of the seed NPLs (either the CdSe core or the CdSe/CdS C/C NPLs) is responsible for the broadening of emission bandwidth. Depending on the quality of seed NPLs, the FWHM of the C@S, and C/C@S NPLs ranges from ~62 to 90 meV. For example, while the CdSe/CdS@CdS C/C@S NPLs having medium CdS crown size exhibit FWHM of ~62 meV, the CdSe@CdS C@S NPLs exhibit FWHM of ~76 meV. The decreased broadening in the PL emission of the C/C@S NPLs having medium crown size can be explained with the passivation of trap sites in the CdSe core-only NPLs. On the other hand, the C/C@S NPLs having smaller and larger crown sizes exhibit broader PL emission bandwidths (~90 meV) when compared to the C@S NPLs due to incomplete and/or uneven growth of CdS crown layer (for the smaller crown) and formation of cracks in the CdS crown layer (for the larger crown).

We have also measured the PL-QY of both the C@S and C/C@S NPLs by using relative PL-OY measurement technique with Rhodamine 6G. Up to now, we have synthesized different C@S and C/C@S NPLs by using various CdSe core and CdS crown sizes. Regardless of the CdSe core size, CdS crown size and CdS shell thickness, the C/C@S NPLs are found to be consistently exhibiting higher PL-QY (up to ~40%) than that of the C@S NPLs. Also, with increasing the CdS shell thickness, decreasing of the PL-QY is observed for both the C@S and the C/C@S NPLs. This decreasing trend of PL-QY with increasing the shell thickness can possibly be attributed to our shell deposition method, which was performed at room temperature under ambient atmosphere, resulting in the formation of defect sites. For example, the PL-QY of CdSe/CdS@CdS C/C@S NPLs (with medium crown size) having 1 and 3 ML CdS shell thickness are ~36% and ~18%, respectively. Similarly, for the CdSe@CdS C@S NPLs

having 1 and 3 ML CdS shell thickness are ~20% and ~8%, respectively. The increased PL-QY of the C/C@S NPLs with respect to the C@S NPLs has shown the importance of sidewall passivation of the CdSe core NPLs.

To develop a better understanding of the excitonic properties of the CdSe core based hetero-NPLs in different architectures including CdSe/CdS C/C, CdSe@CdS C@S, and CdSe/CdS@CdS C/C@S NPLs, we performed time-resolved fluorescence spectroscopy. In-solution samples of NPLs (dissolved in hexane), which were gently cleaned, are used for TRF measurements to avoid stacking issue. Previously, it has been shown that NPLs have tendency to form column-like stacks depending on concentration of NPL solution, ligand concentration, and cleaning procedures [98]–[100]. In the stacked NPL assemblies, ultrafast energy transfer among the NPLs [20] assists hole-trapping, which alters excitonic properties including significantly accelerated overall fluorescence decay rates with almost completely quenched photoluminescence [100]. Therefore, sample quality is highly crucial to correctly analyze resulting excitonic properties of different architectures of hetero-NPLs.

Fluorescence decay curves of our CdSe core-only NPLs, CdSe/CdS C/C NPLs having different crown sizes, CdSe@CdS C@S and CdSe/CdS@CdS C/C@S NPLs with different shell thicknesses are presented in Figure 4.7. These decay curves are analyzed by decay functions, which are sum of exponential decays, resulting in reduced χ^2 about 1 with uniform residuals. For the CdSe core-only NPLs, a multi-exponential decay is observed with an amplitude-averaged fluorescence lifetime (τ_{av}) of ~1.86 ns. This multi-exponential decay kinetics of the CdSe core-only NPLs has been previously observed from both single and ensemble measurements and attributed to the presence of several

radiative decay channels in NPLs [75], [76]. Although it is hard to interpret these distinct lifetime components one by one, the fastest lifetime component (~0.15 ns) is attributed to the nonradiative decay pathway originating from the fast hole-trapping due to incomplete passivation of Cd atoms on the surface [103], [104]. Also, with increasing the lateral size of CdSe core-only NPLs, the contribution of the fastest lifetime component has been shown to become more pronounced accompanied with decreased PL-QY [76]. This finding strongly supports the discussions above and shows the importance of peripheral passivation of sidewalls of the core-only NPLs.
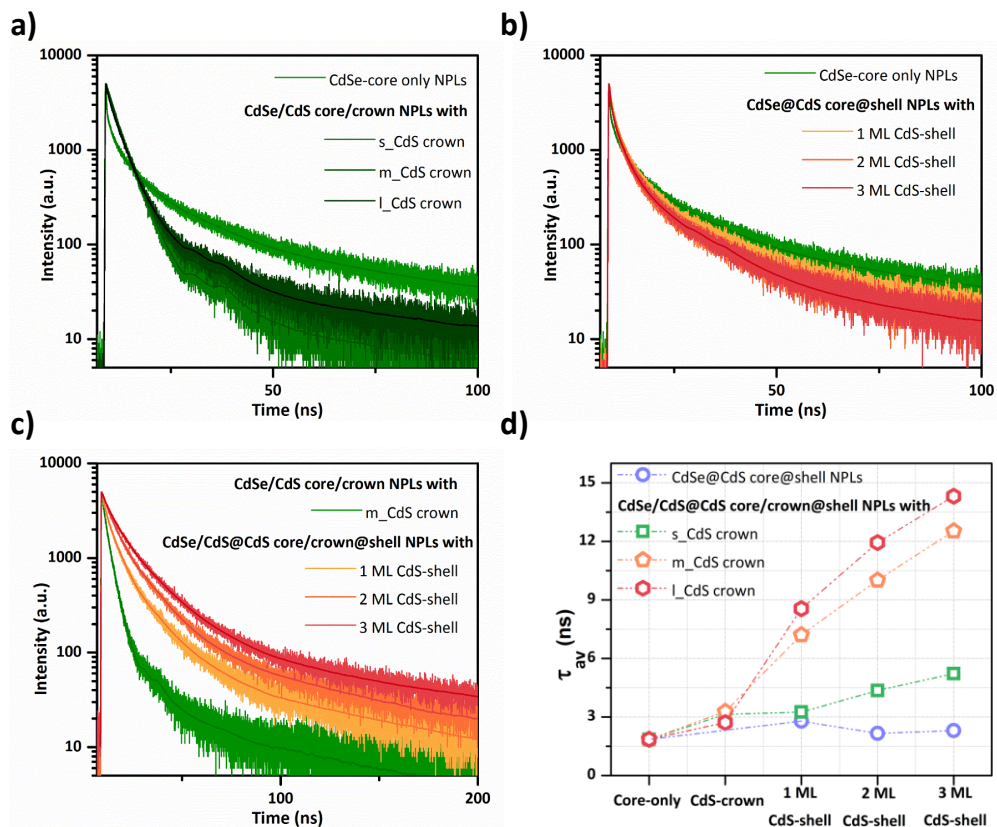
Figure 4.7. Time-resolved fluorescence spectroscopy measurements of (a) CdSe core-only NPLs and CdSe/CdS core/crown NPLs with varying CdS crown size, (b) CdSe@CdS core@shell NPLs, and (c) CdSe/CdS@CdS core/crown@shell NPLs with

different CdS shell thicknesses. (d) Amplitude-averaged fluorescence lifetime of the core, core/crown, core@shell, and core/crown@shell NPLs having different CdS crown sizes as a function of the shell thickness. Reprinted with permission from [94]. Copyright 2016 WILEY-VCH Verlag GmbH & Co. KGaA, Weinheim.

With the formation of the CdS crown layer (only in the lateral direction), amplitude-averaged fluorescence lifetimes are slightly increased to 3.13 and 3.28 ns for having smaller and medium crown sizes, respectively. As it can be seen from Figure 4.7a, with the sidewall passivation of CdSe core-only NPLs, the fastest decay component completely disappears. This also explains the much higher PL-QY (up to 90%) of the CdSe/CdS C/C NPLs with respect to the CdSe core-only NPLs. On the other hand, with the formation of larger CdS crown size, we start to observe the fastest lifetime component (~0.36 ns) again due to the formation of cracks with continuing crown growth. Therefore, there is an optimum crown size in the NPLs, as discussed previously [20]. However, the CdSe/CdS C/C NPLs having larger crown size still exhibit longer τ_{av} of ~2.72 ns with respect to the CdSe core-only NPLs (~1.86 ns). This slightly elongation in τ_{av} of the CdSe/CdS C/C NPLs can again be attributed to the change in the effective dielectric constant with the formation of CdS crown layer. Since the CdS crown layer is grown only in the lateral direction, this does not cause any change in the tight vertical confinement.

With the growth of CdS shell (in the vertical direction), increased τ_{av}'s are observed for the CdSe/CdS@CdS C/C@S NPLs. This increasing trend of τ_{av} is explained with the delocalization of electrons into the CdS shell region owing to the lower energy barrier for electrons between CdSe and CdS material systems. Also, with increasing thickness

74

of the CdS shell layer, the separation of electron and hole wavefunctions is further increased, resulting in an elongated amplitude-averaged fluorescence lifetime. In addition, the increased CdS crown size in the CdSe/CdS@CdS C/C@S NPLs results in further elongated τ_{av}. For example, while τ_{av} of the C/C@S NPLs with small lateral size increases from 3.13 (for the CdSe/CdS C/C NPLs) to 5.23 ns (for the 3 ML CdSe/CdS@CdS C/C@S NPLs), those of the C/C@S NPLs with medium crown size increase from 3.28 (for the CdSe/CdS C/C NPLs) to 12.54 ns (for the CdSe/CdS@CdS C/C@S NPLs with 3ML CdS shell) owing to the uniform coating of CdS crown layer and complete passivation of CdSe core sidewalls. On the other hand, τ_{av} of the CdSe@CdS C@S NPLs remains almost constant upon the growth of CdS shell. This can possibly be explained with the competition between the elongated radiative decay components owing to the formation of CdS shell and the fast nonradiative decay components due to the trap formation because of the shell growth. The decreasing PL-QY also strongly supports the increased nonradiative decay in the CdSe@CdS C@S NPLs with increasing CdS shell thickness.

To provide further insight into the emission kinetics of the CdSe@CdS C@S and the CdSe/CdS@CdS C/C@S NPLs, we performed temperature-dependent PL spectroscopy. Temperature-dependent PL spectra of these CdSe@CdS C@S and CdSe/CdS@CdS C/C@S NPLs (having 2 ML CdS shell thicknesses) are given in Figures 4.8a and 4.8b, respectively. For both samples, we observe decreased intensity of the photoluminescence with increasing temperature. Such quenching in the emission has also previously been observed in different classes of semiconductor nanocrystals and attributed to the surface/interface defects, which act as carrier trapping centers at higher temperatures, resulting in nonradiative recombination and decreasing the photoluminescence [105].

Therefore, strongly quenched emission with increasing temperature can be explained with the existence of a large number of trap sites. In our study, we observed that, at 297 K the CdSe@CdS C@S NPLs maintain ~11.5% of their initial photoluminescence intensity measured at 50 K, while the CdSe/CdS@CdS C/C@S NPLs sustain ~32.2% for the same temperature range. This indicates that in the core/crown@shell NPLs, the PL-QY is better preserved at high temperatures as compared to the core@shell NPLs, as another advantages of the C/C@S heterostructure. Thus, the better preservation of photoluminescence with increasing temperature in the CdSe/CdS@CdS C/C@S NPLs may suggest reduced surface/interface defects with respect to those of the CdSe@CdS C@S NPLs owing to the additional passivation of CdSe core periphery with CdS crown layer.
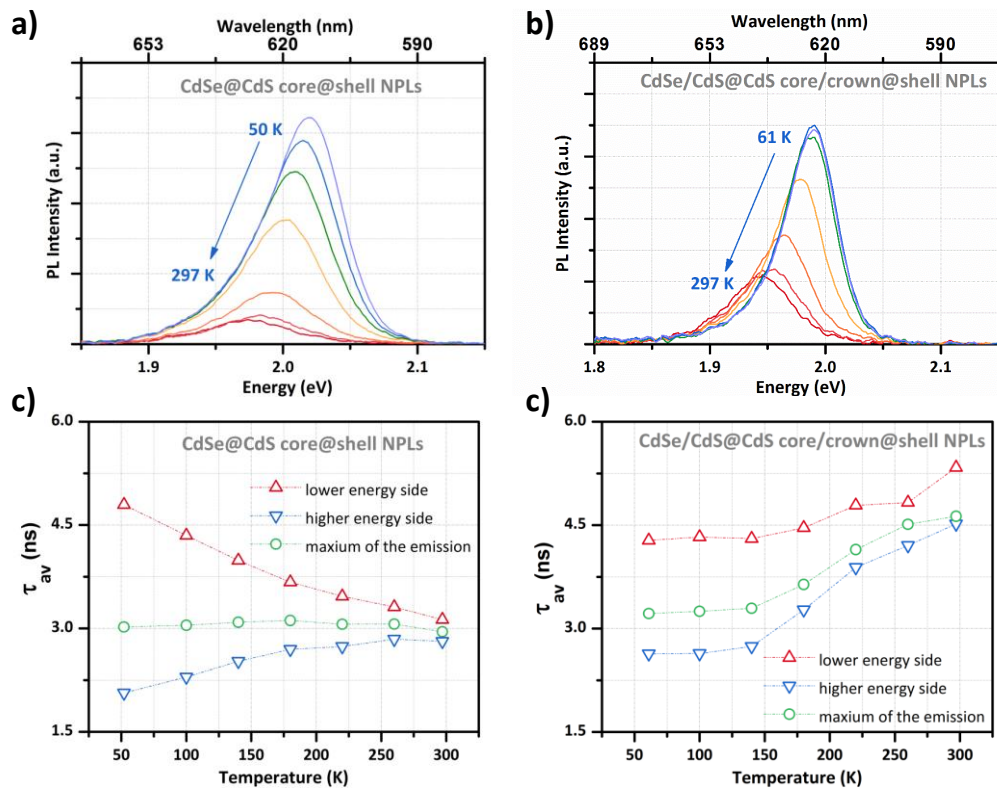
Figure 4.8. Temperature dependent PL spectra of (a) CdSe@CdS core@shell NPLs and (b) CdSe/CdS@CdS core/crown@shell NPLs having 2 ML CdS shell thicknesses. Amplitude-averaged fluorescence lifetimes (τ_{av}) of these (c) core@shell and (d) core/crown@shell NPLs at the lower energy side, at the higher energy side and at the maximum of emission. Reprinted with permission from [94]. Copyright 2016 WILEY-VCH Verlag GmbH & Co. KGaA, Weinheim.

Also, another significant point observed in the temperature-dependent steady-state PL spectra of the CdSe@CdS C@S and the CdSe/CdS@CdS C/C@S NPLs is their asymmetric emission profile, which can be observed even at room temperature. With decreasing temperature, their asymmetric behavior becomes more pronounced with a long tail on the lower energy side of the emission (Figure 4.8a). To unravel this

asymmetric emission behavior, we performed temperature-dependent TRF spectroscopy at the lower energy side, at the higher energy side and at the emission peak. τ_{av}'s of the C@S and C/C@S NPLs at different temperatures are shown in Figures 4.8c and 4.8d, respectively. Unlike the CdSe core-only NPLs exhibiting accelerated decay rate with decreasing temperature, τ_{av} of the CdSe@CdS C@S NPLs remains almost the same with decreasing temperature. On the other hand, when we analyze τ_{av} in the lower and higher energy sides of the emission peak, different trends are observed with decreasing temperature. While τ_{av} is continuously increasing from 3.13 to 4.80 ns at the lower energy side as a function of the decreasing temperature, the opposite behavior is obtained for the lifetime measured for the higher energy side (τ_{av} decreasing from 2.81 to 2.06 ns).

This kind of asymmetric emission along with significant lifetime broadening has also been observed in epitaxially grown thin-film quantum wells and explained with the charge carrier localization in the active traps sites, which can be steam from to the surface/interface defects and strain formation [106]–[108]. Owing to charge carrier localization in the trap sites, emission from these trap sites originate at a lower energy than the bandgap energy accompanied with longer radiative lifetimes. Recently, similar behavior has been also observed by Dubertret group in the CdSe@CdS C@S NPLs and attributed to the formation of defects upon the shell deposition and surface defects [87]. Here, we demonstrate that in contrast to the CdSe@CdS C@S NPLs, the CdSe/CdS@CdS C/C@S NPLs exhibit less asymmetric emission with suppressed lifetime broadening, which we attribute to the enhanced passivation of the CdSe core-only NPLs and the reduced number of traps sites with the formation of CdS crown layer. As it can be seen from Figure 4.8d, by decreasing the temperature, accelerated decay

rates are achieved from both the lower and higher energy sides of the emission. With these important findings, it can be concluded that, with the formation of the CdS crown layer, the interface/surface defects are suppressed and favorable optical properties can be achieved by the proposed core/crown@shell architecture.

Recently, colloidal NPLs have been shown to be highly promising for low threshold lasing owing to their suppressed Auger recombination, giant oscillator strength and increased absorption cross-section, enabling high performance all-colloidal nanocrystal lasers [20], [73], [76], [84], [86], [109]. Also, when compared to other classes of colloidal semiconductor nanocrystals, their higher gain coefficients, broader gain bandwidth, and longer gain lifetime make them highly favorable for practical lasing applications [84]. It has been demonstrated that even simple CdSe core-only NPLs having different thicknesses surpass the optical gain performance levels of custom designed colloidal nanocrystals emitting in the same spectral range. For example, 3 ML CdSe core-only NPLs having emission in the blue spectral region with a lower PL-QY (~10%) [84] exhibit desirably lower gain thresholds than carefully engineered $Cd_xZn_{1-x}S/ZnS$ core/shell quantum dots having smooth interface with almost near-unity PL-QY [85]. This is mainly facilitated by the large absorption cross-section of the NPLs. Furthermore, the absence of inhomogeneous broadening also allows for enhanced optical gain performance with reduced losses due to the intrinsic absorption over a wider spectral range. In addition, it has been demonstrated that by using the CdSe/CdS core/crown [20] and CdSe@CdS core@shell [86] architectures, further better optical gain performance can be achieved thanks to their increased absorption cross-section and suppressed AR with respect to the CdSe core-only NPLs. In this study, to achieve even further enhanced properties, we studied systematically optical gain performances of

CdSe/CdS@CdS core/crown@shell NPLs along with the CdSe core-only, CdSe/CdS core/crown and CdSe@CdS core@shell NPLs.

For the optical gain measurements, highly close-packed and uniform films were prepared on bare quartz substrates with spin-coating of the concentrated solutions of NPLs. The samples were excited with a femtosecond laser beam having a wavelength of 400 nm (providing 120 fs laser pulses at a 1 kHz repetition rate) by using stripe-excitation geometry. The laser beam was focused (over an excitation area of ~200 µm by 5 mm as measured by an optical profilometer, Newport) on the samples by using a cylindrical lens. The collected PL spectra for the samples are presented in Figure 4.9. For the CdSe core-only NPLs, when the excitation intensity exceeds ~76 µJ/cm^2, a red-shifted amplified spontaneous emission (ASE) spectrum is obtained. This red-shifted ASE peak is previously observed in the CdSe core-only NPLs and attributed to the biexcitonic gain [110], [111]. Also, when compared to the previous reports on NPLs, our CdSe core-only NPLs exhibit slightly high gain thresholds. This is possibly due to the different NPL lateral sizes and qualities leading to different optical gain performances [76]. Next, we studied optical gain performance of CdSe/CdS C/C NPLs, which were synthesized by using the same CdSe core-only NPLs. With the formation of CdS crown layer, we observed significantly decreased gain threshold (down to ~32 µJ/cm^2) with a red-shifted ASE peak, which remains almost in the same spectral position compared to the core-only NPLs. The enhancement of the absorption cross-section in the C/C NPLs makes great contribution to help to decrease the gain threshold, which has been already demonstrated [20]. Besides the increased absorption cross-section, the passivation of trap sites in the C/C NPLs results in higher optical quality and helps to enhance optical gain performance.
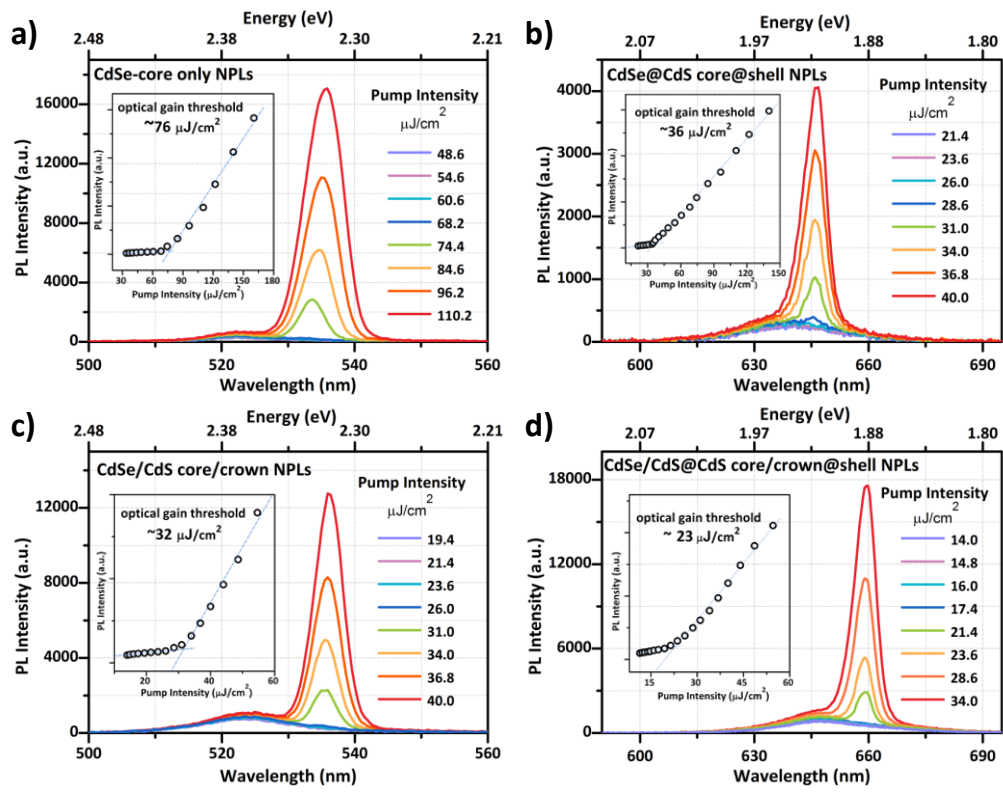
Figure 4.9. Optical gain performances of CdSe-based NPLs having different architectures. Amplified spontaneous emission spectra of (a) CdSe core-only NPLs, (b) CdSe@CdS core@shell NPLs having 2 ML CdS shell thickness, (c) CdSe/CdS core/crown NPLs, and (d) CdSe/CdS@CdS core/crown@shell NPLs having 2 ML CdS shell thickness. The insets show the integrated PL intensity as a function of the excitation intensity. Reprinted with permission from [94]. Copyright 2016 WILEY-VCH Verlag GmbH & Co. KGaA, Weinheim.

To achieve further improved gain threshold, we studied the optical gain performance in the core@shell and core/crown@shell NPLs having 2 ML CdS shell thicknesses. With the formation of 2 ML CdS shell layer, the CdSe@CdS core@shell NPLs exhibit lower gain threshold (~36 $\mu J/cm^2$) with respect to the CdSe core-only NPLs. In this case, the lower gain threshold of the core@shell NPLs can be attributed to suppressed AR rates

owing to quasi Type-II electronic structure, where the electron and hole wavefunctions overlap is reduced. Also, the staircase-type relation between AR and NPL volume observed in the colloidal quantum wells, further helps with the suppression of AR in the C@S NPLs [84]. Finally, with the combination of the enhanced absorption cross-section and the suppressed AR, we achieved the lowest gain threshold (~23 $\mu J/cm^2$) from the CdSe/CdS@CdS core/crown@shell NPLs having 2 ML CdS shell. Here, the better peripheral passivation of the CdSe core-only NPLs in the C/C@S architecture also contributes to the decreased gain threshold, which results in high optical quality films and suppressed nonradiative energy transfer rates between the NPLs.

Figure 4.10 shows the intensity of the amplified spontaneous emission in the core/crown@shell sample for pump laser shots up to 2.5×10^7 that correspond to overall 6 h of continuous excitation (pump laser is at 1 kHz repetition rate). The excitation intensity was chosen to be 35 $\mu J/cm^2$, which is above the ASE threshold of the sample (~20 $\mu J/cm^2$). ASE intensity shows a slight increase in the first 2 h of excitation, which we attribute to the annealing of the sample under the excitation condition due to slight heating up the sample. Almost after 6 h of continuous pumping, the ASE intensity drops just slightly. As compared to the CdSe core-only and CdSe/CdS core/crown NPLs, which have shown stable ASE only for several minutes of excitation (~1×10^6 pump shots) [20] the core/crown@shell NPLs depict much greater stability. Thus, the core/crown@ shell architecture will be very promising to overcome the stability problems of the existing NPL architectures. Also, as compared to tailor-made core/shell quantum dots and nanorods with low gain [73], the stability of the ASE in the core/crown@shell NPLs is better. Thanks to the complete passivation of the structure

with the crown and shell layers, excitons in the core/crown@shell NPLs stay away from the potentially reactive surface traps or defects.
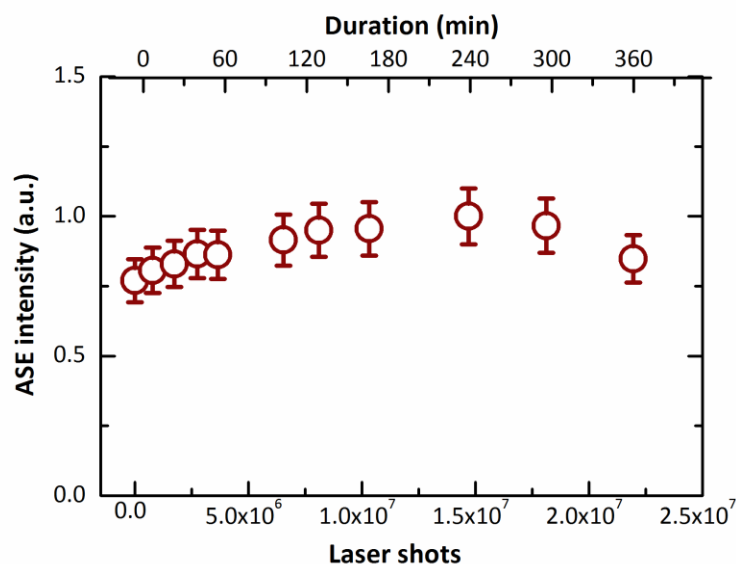
Figure 4.10. Intensity of the amplified spontaneous emission in the core/crown@shell NPLs as a function of pump laser shots (per pulse energy density of 35 μJ/cm^2). The optical gain in the core/crown@shell NPLs is highly stable even for 6 h of continuous excitation. Reprinted with permission from [94]. Copyright 2016 WILEY-VCH Verlag GmbH & Co. KGaA, Weinheim.

4.4 Summary

In summary, we have reported the first account of CdSe/CdS@CdS core/crown@shell NPLs having a novel 3D architecture resembling platelet-in-box heterostructure and studied their excitonic kinetics. Here, we have shown the critical importance of peripheral growth with laterally extending crown layer before the vertical shell growth to push the gain performance from NPLs. With the formation of CdS crown layer

covering around the periphery of the CdSe core-only NPLs, trap sites are strongly passivated in the CdSe/CdS@CdS C/C@S NPLs. Thus, these C/C@S NPLs exhibit systematically higher PL-QY when compared to the CdSe@CdS C@S NPLs regardless of the CdSe core size, CdS crown size, and CdS shell thickness. In addition to the enhanced PL-QY, more symmetric emission behavior, along with suppressed lifetime broadening, observed in the CdSe/CdS@CdS C/C@S NPLs by decreasing temperature also confirms the effective passivation of these trap sites. In addition, when compared to the C@S NPLs, the C/C@S NPLs exhibit significantly enhanced absorption cross-section with reduced re-absorption effect. Enabled by these major advancements in the excitonic behavior, the proposed C/C@S NPLs exhibit the lowest gain threshold among different architectures of NPLs. These findings can provide an important guideline for the colloidal synthesis of highly efficient and stable NPLs, which can enable high-performance optoelectronic devices possibly challenging epitaxially-grown thin-film quantum well devices.

Chapter 5

CdSe$_x$S$_{1-x}$ Alloyed Heteronanoplatelets

This chapter of the thesis is based on the publication "Alloyed Heterostructures of CdSe$_x$S$_{1-x}$ Nanoplatelets with Highly Tunable Optical Gain Performance," **Y. Kelestemur**, D. Dede, K. Gungor, C. F. Usanmaz, O. Erdem, and H. V. Demir, Chemistry of Materials 29 (11), 4857–4865 (2017). Reprinted with permission from [112]. Copyright 2017 American Chemical Society.

5.1 Motivation

In addition to the fascinating excitonic properties of colloidal nanoplatelets, their higher gain coefficient, broader gain bandwidth and longer gain lifetime make them highly desirable for practical lasing applications [84]. In this respect, optical gain and lasing performances of core-only [20], [84], [86], [94], [109], [113], core/crown [20], core/shell [84], [86], [94], [114] and core/crown/shell [94] NPLs have been studied extensively. Although core-only NPLs generally exhibit relatively higher gain threshold with low photostability, the synthesis of different heterostructures further reduces their gain thresholds to record low levels with enhanced photostability. However, due to the pure

vertical quantum confinement observed in NPLs, their optical gain and lasing performance are limited in terms of spectral tunability compared to colloidal quantum dots (CQDs). For example, 4 ML thick CdS and CdSe core NPLs exhibit discrete amplified spontaneous emission peaks at ~432 [86] and ~534 [113] nm, respectively.

To obtain tunable excitonic properties in a wide spectral range, colloidal synthesis of NPLs with different vertical thicknesses, heterostructures and compositions have been studied. By optimizing the synthesis conditions, core-only NPLs having different thicknesses can be synthesized to tune their optical properties [78]. However, owing to pure vertical confinement observed in NPLs, they exhibit discrete emission and absorption behavior regardless of their lateral size. For example, CdSe NPLs having 3, 4 and 5 ML of vertical thicknesses terminated by Cd atoms on both sides always exhibit emission peak at ~460, 513 and 550 nm, respectively [78]. In addition, core/crown [18], [81], [95], [101], [102] and core/shell [19], [82] heterostructures of NPLs have been synthesized to further extend their spectral tunability. Nonetheless, the resulting excitonic properties of core/crown and core/shell NPLs have been shown to be strongly depend on the vertical thickness of the starting core NPLs. For instance, 4 ML thick CdSe/CdS and CdSe/CdTe core/crown NPLs always exhibit similar emission behavior independent of their crown size. In addition to the colloidal synthesis of NPLs with different heterostructures, CdTe [80] and CdS [79] based NPLs have been synthesized to obtain tunable excitonic properties. Even though pure population of CdS and CdTe NPLs having different vertical thicknesses has been synthesized successfully, they suffer from the lower PL-QY and stability issues.

To achieve further tunable excitonic properties in colloidal NPLs, homogeneous alloying can be used as a highly effective approach which has not been studied extensively. Previously, several studies have been reported the synthesis of homogeneously alloyed $CdSe_xS_{1-x}$ core-only NPLs, showing tunable absorption spectra by adjusting the sulfur compositions [115], [116]. However, the synthesized $CdSe_xS_{1-x}$ core-only NPLs exhibit low PL-QY (~10-20%) with the limited emission tunability in the spectral range of ~490-510 nm [117]. Therefore, engineered heterostructures of alloyed NPLs have been greatly required to obtain enhanced excitonic properties, enabling the achievement of highly tunable and low-threshold gain performance.

To overcome these limitations, we synthesized core/crown and core/shell heterostructures of $CdSe_xS_{1-x}$ alloyed core NPLs and systematically studied their resulting excitonic properties including spontaneous emission and stimulated emission performance. By synthesizing $CdSe_xS_{1-x}$/CdS core/crown NPLs, we achieved enhanced PL-QY (up to 60%), without changing the emission spectrum of $CdSe_xS_{1-x}$ alloyed core NPLs. Furthermore, with the synthesis of $CdSe_xS_{1-x}$/CdS core/shell NPLs, we further extended the tunable emission behavior of $CdSe_xS_{1-x}$ NPLs. These effective excitonic properties of alloyed core/crown and alloyed core/shell heterostructures with the reduced re-absorption enabled us to achieve highly tunable optical gain performance from $CdSe_xS_{1-x}$ based NPLs. Compared to CdSe core based NPLs, these $CdSe_xS_{1-x}$ based NPLs with relatively low gain thresholds are highly promising candidates for future lasing applications.

5.2 Colloidal Synthesis and Experiments

Chemicals. Cadmium nitrate tetrahydrate ($Cd(NO_3)_2 \cdot 4H_2O$) (99.999% trace metals basis), cadmium acetate dihydrate ($Cd(OAc)_2 \cdot 2H_2O$) (>98%), sodium myristate (>99%), technical-grade 1-octadecene (ODE), selenium (Se) (99.999% trace metals basis), sulfur (S) (99.998% trace metals basis), technical-grade oleic acid (OA) (90%), technical-grade oleylamine (OAm) (70%), N-methylformamide (NMF) (99%), and ammonium sulfide solution (40-48 wt. % in H_2O) were purchased from Sigma-Aldrich. Hexane, ethanol, methanol, toluene, and acetonitrile were purchased from Merck Millipore and used without any further purification.

Preparation of cadmium myristate. For the preparation of cadmium myristate, we followed previously published recipe in the literature [18]. In a typical synthesis, 1.23 g of cadmium nitrate tetrahydrate was dissolved in 40 mL of methanol and 3.13 g of sodium myristate was dissolved in 250 mL of methanol by continuous stirring. When the complete dissolution was achieved, both solutions were mixed and stirred around 1 h. Then, bulky solutions of cadmium myristate were centrifuged and precipitates dissolved in methanol for further cleaning. For the complete removal of excess precursors and better purification, this procedure was repeated at least three times. At the end, the precipitated part was dried under vacuum overnight.

Synthesis of the 4 ML thick CdSe$_x$S$_{1-x}$ alloyed core NPLs. For the synthesis of 4 ML thick CdSe$_x$S$_{1-x}$ alloyed core NPLs, we modified the commonly used recipe of 4 ML thick CdSe core NPLs [18]. 340 mg of cadmium myristate, 20 mg Se and 30 mL of ODE were added in a 100 mL three-neck flask. The solution was degassed under vacuum at 95 °C around 1 h. Then, the temperature of the solution was set to 240 °C under argon

flow. At 100 °C, the desired amount of sulfur precursor (S/ODE, 0.2 M) was injected rapidly to tune the composition of $CdSe_xS_{1-x}$ alloyed core NPLs. For example, for the synthesis of $CdSe_xS_{1-x}$ NPLs having sulfur composition (1-x) of 0.15, 0.25 and 0.30, we injected 0.25, 0.50 and 1.00 mL of sulfur precursors, respectively. When the temperature was reached to ~195 °C, 70 mg of cadmium acetate dihydrate was added. After 10 min growth at 240 °C, 1 mL of OA was injected and the solution was moderately cooled to room temperature. Below 120 °C, 5 mL of hexane was injected for better dissolution of NPLs. In the purification state, NPLs were precipitated by addition of ethanol and then kept in hexane solution.

Thanks to the formation of alloyed $CdSe_xS_{1-x}$ NPLs, the resulting optical properties can be determined with the injected amount of S precursor. Moreover, the temperature at which cadmium acetate dihydrate is added is important to eliminate the formation of other species having different emission properties.

Preparation of anisotropic growth solution for CdS crown region. For the lateral growth of CdS crown region, Cd and S precursors were prepared according to the well-known procedure with slight modifications [18]. 480 mg of cadmium acetate dihydrate, 340 μL of OA, and 2 mL of ODE were loaded in a 50 mL three-neck flask. The solution was heated to 120 °C under ambient atmosphere with rigorous stirring and it was also regularly sonicated. Alternating steps of heating and sonication followed until whitish homogeneous gel formed. When the cadmium precursor was ready, it was mixed with 3 mL of S/ODE (0.1 M) precursor and then used for the coating of CdS crown for the alloyed NPLs.

Synthesis of 4 ML-thick CdSe$_x$S$_{1-x}$/CdS core/crown NPLs. For the lateral growth of alloyed CdSe$_x$S$_{1-x}$ cores with CdS crown region, 5 mL of ODE, 100 μL of OA and 1 mL of 4 ML thick CdSe$_x$S$_{1-x}$ dissolved in hexane (100 μL CdSe$_x$S$_{1-x}$ NPLs dissolved in 3 mL of hexane having an optical density of ~1 at 350 nm) were loaded into a 50 mL three-neck flask and degassed at 80°C for the removal of excess solvents. Under argon flow, solution was heated up to 240 °C. Around 190-195 °C, the injection of CdS anisotropic growth mixture was started and 0.70 mL of this mixture was injected at a rate of 8 mL/h. The amount of injected precursor determines the crown size with the desired optical properties. After the injection of anisotropic growth mixture, CdSe$_x$S$_{1-x}$/CdS core/crown NPLs were further annealed for 5 min at 240 °C and cooled down to room temperature. For the cleaning of the resulting core/crown NPLs, ethanol was used for precipitation and then the precipitated NPLs dissolved in hexane.

Synthesis of CdSe$_x$S$_{1-x}$/CdS core/shell NPLs. By using the colloidal atomic-layer-deposition technique, CdSe$_x$S$_{1-x}$/CdS core/shell NPLs were synthesized [82]. According to this well-known procedure, 3 mL of N-methylformamide (NMF) and 3 mL of core NPLs dissolved in hexane were mixed. With the addition of 50 μL of sulfur precursor (ammonium sulfide solution (40-48 wt. % in H$_2$O)), NPLs were transferred from non-polar hexane to highly polar NMF. For a complete sulfur coating, the solution was stirred around 5 min and excess sulfur was removed in the following washing steps. In this step, acetonitrile and toluene were added to precipitate NPLs and then 3 mL of fresh NMF was added for complete dissolution. For the next cadmium deposition step, 2 mL of cadmium precursor (0.2 M cadmium acetate dihydrate in NMF) was added and waited for 5 min for the reaction. The NPLs were then precipitated with the addition of acetonitrile and toluene. As a result of these processes, 1 ML CdS shell was formed on

the $CdSe_xS_{1-x}$ alloyed core NPLs. To increase the shell thickness, this process was repeated in a similar way. Finally, with the addition of OAm to the solution of NPLs terminated by Cd atoms, the core/shell NPLs dissolved in NMF can be transferred to hexane.

Absorption and Steady-State Photoluminescence. UV-Vis absorption and photoluminescence spectra of NPLs together with their photoluminescence excitation spectra were taken by using Cary 100 UV−vis and Cary Eclipse fluorescence spectrophotometer, respectively.

Photoluminescence Quantum Yield Measurements. The PL-QY measurements of NPLs were performed according to the methodology described by de Mello et al [91]. Our PL-QY measurement setup was equipped with an Ocean Optics Maya 2000 spectrometer, an integrating sphere, a xenon lamp and a monochromator. For the PL-QY measurements, freshly prepared dispersion samples of core-only, core/crown and core/shell NPLs were used and excited at a wavelength of 400 nm.

Time-Resolved Photoluminescence Spectroscopy. The time-resolved photoluminescence measurements were taken by using Pico Quant FluoTime 200 spectrometer. Dispersion samples of NPLs were excited with a picosecond pulsed laser having a wavelength of 375 nm and the fluorescence decay curves were recorded with TimeHarp time-correlated single-photon counting (TCSPC) unit. The FluoFit software was used for the reconvolution mode fitting of the decay curves to account for the instrument response function (IRF).

Transmission Electron Microscopy. TEM images of NPLs were acquired with FEI Tecnai G2 F30 operated at 300 kV in the high-angle annular dark-field scanning transmission electron microscopy configuration. For the sample preparation, NPLs were cleaned with ethanol at least two times to remove excess ligands. Then, 5 µL of diluted NPL solution was dropped on a 200 mesh copper grid and kept under vacuum for the complete drying before the imaging.

X-Ray Photoelectron Spectroscopy. To determine the elemental composition of alloyed $CdSe_xS_{1-x}$ core NPLs, we performed XPS measurements by using the Thermo Scientific K-Alpha X-ray photoelectron spectrometer. The samples for XPS were prepared by spin-coating of NPL solutions on silicon substrates ($\sim 1 \times 1$ cm^2). The acquired high-resolution spectra of $CdSe_xS_{1-x}$ core NPLs with varying sulfur compositions were analyzed by using the Avantage software.

5.3 Results and Discussion

In this study, we prepared $CdSe_xS_{1-x}$ alloyed NPLs together with their core/crown and core/shell heterostructures to obtain highly tunable excitonic properties. First, we started with the synthesis of 4 ML thick $CdSe_xS_{1-x}$ core NPLs having an additional layer of Cd atoms and used them as a seed for the further synthesis of core/crown and core/shell NPLs. For the synthesis of $CdSe_xS_{1-x}$ core NPLs, we modified the recipe of 4 ML thick CdSe core NPLs (see the experimental section for details) [18]. By the addition of a certain amount of sulfur precursor after the degassing, we succeeded in the formation of highly uniform $CdSe_xS_{1-x}$ alloy and depending on the amount of injected sulfur precursor, the composition of $CdSe_xS_{1-x}$ was tuned in a precisely controlled way. The HAADF-STEM images of $CdSe_xS_{1-x}$ alloyed core NPLs with various compositions

feature a rectangular shape and uniform size distribution regardless of the sulfur composition (Figure 5.1a). While lateral sizes of $CdSe_xS_{1-x}$ alloyed core NPLs were observed to be generally increased with increasing the amount of sulfur, their thicknesses were found to be the same with the 4 ML thick CdSe core-only NPLs. Also, the elemental composition of $CdSe_xS_{1-x}$ alloyed core NPLs is determined by using X-ray photoelectron spectroscopy (Figure 5.1b). It was measured that the elemental composition of sulfur can be increased up to $(1-x) = 0.30$ with a 1 mL of sulfur precursor injection. Further increasing the amount of sulfur resulted in the formation of mixed population of NPLs with excess amount of colloidal quantum dots so that it is not easy to achieve pure population of $CdSe_xS_{1-x}$ alloyed core NPLs with cleaning procedures.
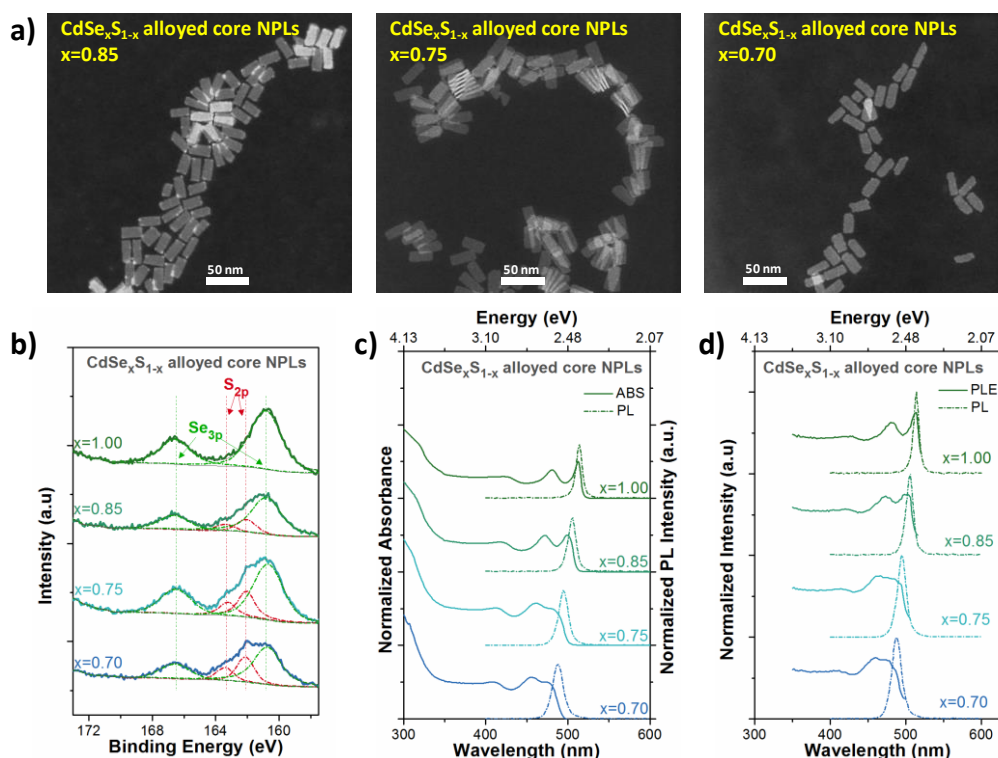
Figure 5.1. (a) HAADF-STEM images of $CdSe_xS_{1-x}$ alloyed core NPLs having different sulfur compositions, (b) high-resolution X-ray photoelectron spectra of spin-coated thin

films of CdSe$_x$S$_{1-x}$ alloyed core NPLs, (c) normalized absorbance and photoluminescence (PL) spectra of CdSe$_x$S$_{1-x}$ alloyed core NPLs, showing continuous blue-shifted excitonic features, (d) photoluminescence excitation spectra of CdSe$_x$S$_{1-x}$ alloyed core NPLs. Reprinted with permission from [112]. Copyright 2017 American Chemical Society.

After structural characterization of CdSe$_x$S$_{1-x}$ alloyed core NPLs having the same vertical thicknesses, we performed optical characterization including absorption, photoluminescence and photoluminescence excitation spectroscopy. Absorption spectra of CdSe$_x$S$_{1-x}$ alloyed core NPLs are presented in Figure 5.1c. From the absorption spectrum of CdSe core NPLs, splitting of sharp excitonic features including light-hole (~480 nm) and heavy-hole (~512 nm) transitions are clearly visible, indicating formation of the quantum well like electronic structure [17]. In CdSe$_x$S$_{1-x}$ alloyed core NPLs, these sharp excitonic features were slightly broadened and continuously shifted to the higher energies by increasing the sulfur composition. Also, the PL of CdSe$_x$S$_{1-x}$ alloyed core NPLs exhibits similar behavior with the absorption. For example, while CdSe core-only NPLs have their emission peak at ~513 nm with a FWHM of ~40 meV, CdSe$_x$S$_{1-x}$ alloyed core NPLs having the highest sulfur composition of (1-x) = 0.30 possess theirs at ~ 488 nm with a FWHM of ~80 meV. Here the blue-shifting in excitonic features can be explained with the increase of the energy band gap due to the alloying. On the other hand, slight broadening could be attributed to the variation in the composition and/or inhomogeneous alloying of NPLs. However, the similar excitonic transitions observed from the PLE spectra of CdSe$_x$S$_{1-x}$ core NPLs taken at different emission wavelengths has ruled out this possibility and strongly suggested the formation of CdSe$_x$S$_{1-x}$ core NPLs having homogenously alloyed crystal structure (Figure 5.2). Therefore, the

broadening of the excitonic features may most likely be due to the enhanced exciton-phonon coupling commonly observed in this material system [87].
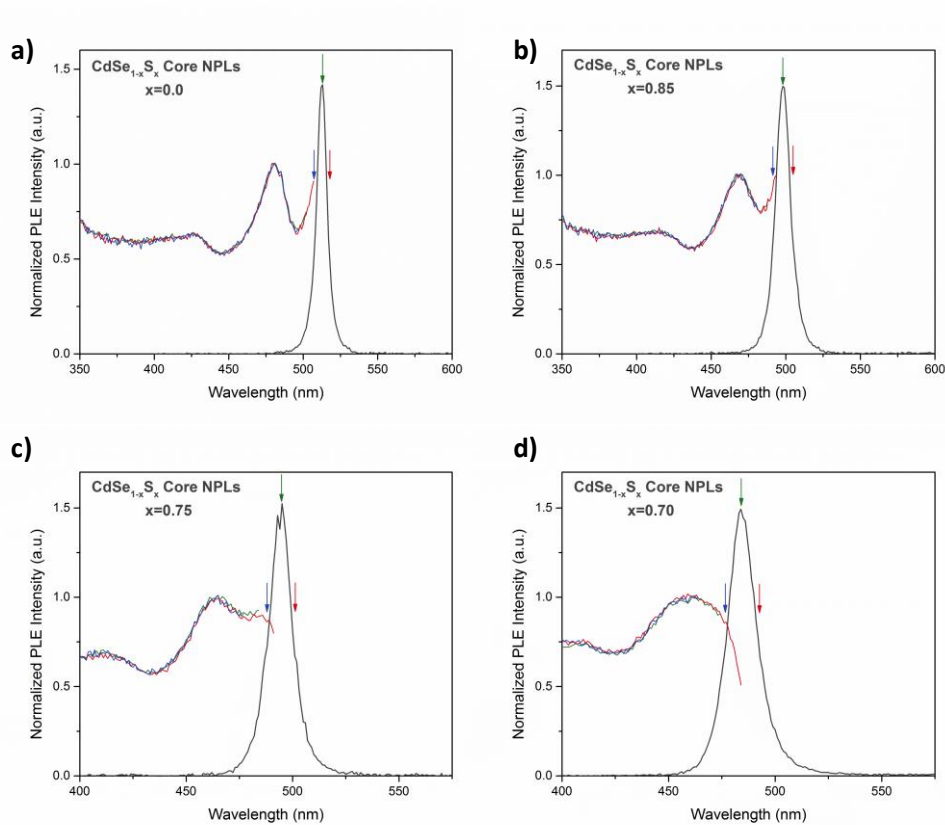
Figure 5.2. Normalized photoluminescence excitation spectra of $CdSe_xS_{1-x}$ NPLs taken at different emission wavelengths with various sulfur compositions (a) x = 0.0, (b) x = 0.85, (c) x = 0.75, and (d) x = 0.70. Reprinted with permission from [112]. Copyright 2017 American Chemical Society.

Although the emission of the $CdSe_xS_{1-x}$ alloyed core NPLs was demonstrated to be shifted to higher energies with increasing sulfur composition, they suffered from the decreased PL-QY (~10-20%) and the stability issue with respect to CdSe core-only NPLs, which can be explained with the increased surface trap sites owing to their

extended lateral size. To achieve better optical properties and enhanced stability without changing the emission behavior of CdSe$_x$S$_{1-x}$ alloyed core NPLs, we synthesized CdSe$_x$S$_{1-x}$/CdS core/crown NPLs. The formation of CdS crown extension only in the lateral direction and passivation of sidewalls can greatly enhance the PL-QY of NPLs without changing the spectral position of the emission [94]. By using the freshly synthesized CdSe$_x$S$_{1-x}$ alloyed core NPLs as seeds, we prepared core/crown NPLs using a slightly modified recipe (see the experimental section for details). HAADF-STEM images of CdSe$_x$S$_{1-x}$/CdS core/crown NPLs having different sulfur compositions are shown in Figure 5.3a. In comparison to CdSe$_x$S$_{1-x}$ core NPLs, lateral sizes of the core/crown NPLs are found to be increased, while the vertical thicknesses remained the same, suggesting the formation of core/crown heterostructures. It is also important to note that, although we used highly uniform and rectangular-shaped CdSe$_x$S$_{1-x}$ alloyed core NPLs as seeds, the formation of CdS crown region was nonuniform in the lateral direction, which is typically observed for the CdSe/CdS core/crown NPLs in the literature [18], [20], [81].
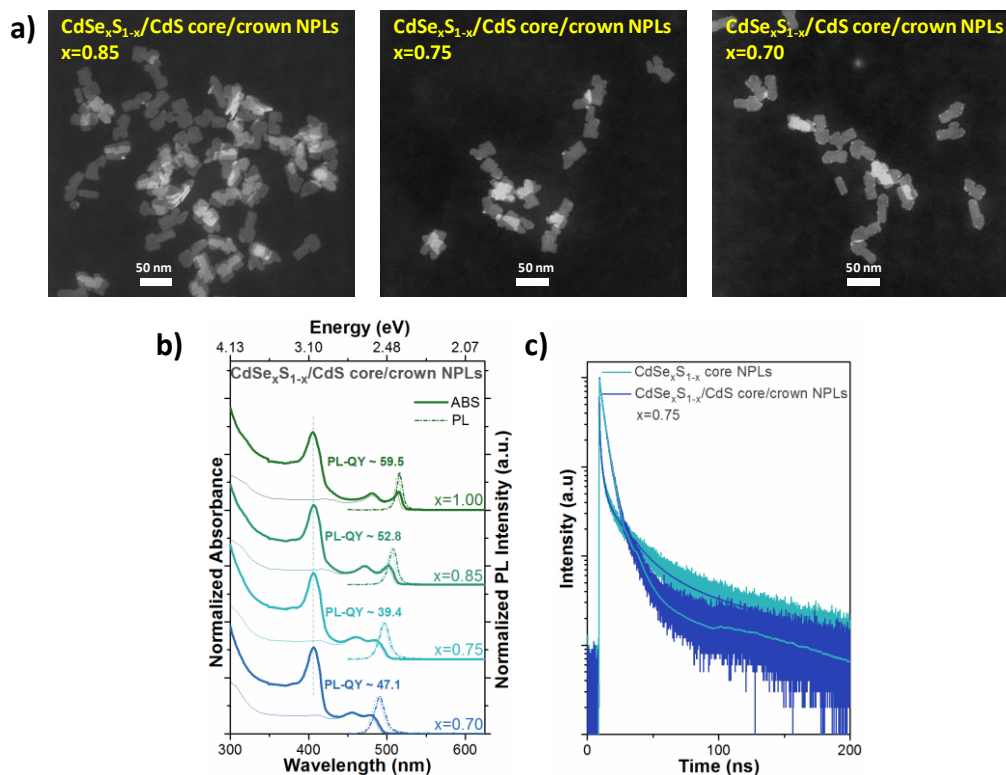
Figure 5.3. (a) HAADF-STEM images of CdSe$_x$S$_{1-x}$/CdS alloyed core/crown NPLs having different sulfur compositions, (b) normalized absorbance and photoluminescence spectra of CdSe$_x$S$_{1-x}$/CdS core/crown NPLs and (c) time-resolved fluorescence decay curves of CdSe$_x$S$_{1-x}$ alloyed core and CdSe$_x$S$_{1-x}$/CdS core/crown NPLs for the case of x = 0.75. Reprinted with permission from [112]. Copyright 2017 American Chemical Society.

Compared to the CdSe$_x$S$_{1-x}$ core NPLs, CdSe$_x$S$_{1-x}$/CdS core/crown NPLs exhibit substantially improved optical properties along with enhanced stability. The absorption spectra of CdSe$_x$S$_{1-x}$/CdS core/crown NPLs were presented in Figure 5.3b together with that of CdSe$_x$S$_{1-x}$ core NPLs for a better comparison. It is clearly seen that the excitonic features of CdSe$_x$S$_{1-x}$ core NPLs remained almost in the same spectral position with the formation of CdS crown region, which can be explained by the unchanged quantum

confinement in the core/crown heterostructures due to the growth of CdS region being only in the lateral direction. Furthermore, regardless of sulfur composition, a new absorption peak emerged at the same wavelength (~405 nm) in the absorption spectra of $CdSe_xS_{1-x}$/CdS core/crown NPLs, which corresponds to the bandgap of 4 ML thick CdS NPLs [79]. These two findings strongly support that the synthesized $CdSe_xS_{1-x}$ core NPLs have a homogenously alloyed structure with the same vertical thickness. Otherwise, we would observe a shifting in the excitonic features belonging to the both core and crown regions.

With the growth of CdS only in the lateral direction, $CdSe_xS_{1-x}$/CdS core/crown NPLs exhibit almost similar emission peaks with respect to $CdSe_xS_{1-x}$ core NPLs. The slightly red-shifted emission (~2-3 nm) can be related to the change in the dielectric constant [18]. Also, with the passivation of sidewalls of the $CdSe_xS_{1-x}$ core NPLs, $CdSe_xS_{1-x}$/CdS core/crown NPLs exhibit remarkable improvement in PL-QY (up to 60%) regardless of sulfur composition. For a better understanding of the increased PL-QY, we also performed time-resolved fluorescence spectroscopy by using in-solution samples. Fluorescence decay curves of the samples were fitted by using four-exponential functions due to the complex decay kinetics observed in the NPLs [75], [118]. The multi-exponential decays were convolved with the instrument response function of the excitation laser to account for its pulse width (~230 ps). The fluorescence decay curves and their analysis results are summarized in the supporting information (Figure 5.4 and Table 5.1, and 5.2). For example, the amplitude-averaged fluorescence lifetime of $CdSe_xS_{1-x}$ core NPLs (x=0.75) was measured to be ~0.90 ns with the fastest nonradiative decay component (0.15 ns), which is attributed to the hole trapping commonly observed in NPLs [100], [103]. Thanks to the passivation of sidewalls in the $CdSe_xS_{1-x}$/CdS

98

core/crown NPLs, the amplitude-averaged lifetime of the core/crown NPLs (x=0.75) was increased to ~3.78 ns by the suppression of the fastest nonradiative decay component. The similar behavior was also observed for the other $CdSe_xS_{1-x}/CdS$ core/crown NPLs having different sulfur compositions, suggesting the enhanced PL-QY of the core/crown NPLs.
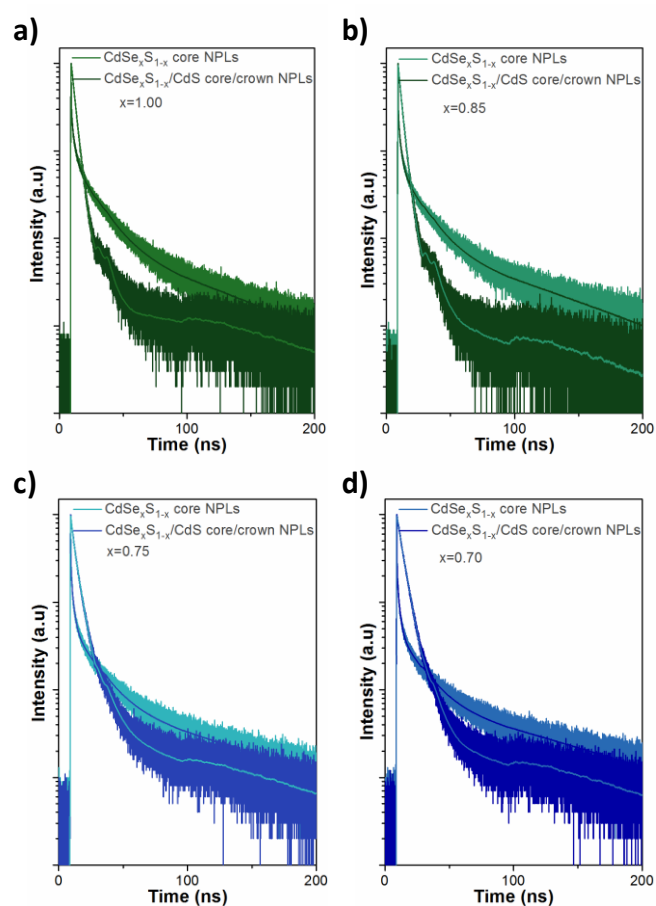
Figure 5.4. Time-resolved fluorescence decay curves of $CdSe_xS_{1-x}/CdS$ core/crown NPLs together with their core for the case of (a) x = 1.00, (b) x = 0.85, (c) x = 0.75 and (d) x = 0.70. Reprinted with permission from [112]. Copyright 2017 American Chemical Society.

Table 5.1. Analysis of time-resolved fluorescence decay curves of $CdSe_xS_{1-x}$ alloyed core NPLs with different sulfur composition. Reprinted with permission from [112]. Copyright 2017 American Chemical Society.

$CdSe_xS_{1-x}$ core-only NPLs	TRF Decay Components								Amplitude-average Lifetimes ($\frac{\sum A_i \times \tau_i}{\sum A_i}$)
	τ_1 (ns)	τ_2 (ns)	τ_3 (ns)	τ_4 (ns)	A_1	A_2	A_3	A_4	τ_{av} (ns)
x = 1.00	76.7	15.3	2.3	0.15	105	765	1953	21670	1.12
x = 0.85	83.2	14.9	2.0	0.13	96	611	1874	23780	0.91
x = 0.75	87.8	14.9	1.9	0.15	88	496	1830	21920	0.90
x = 0.70	101.0	15.1	1.8	0.14	85	423	1710	22180	0.87

Table 5.2. Analysis of time-resolved fluorescence decay curves of $CdSe_xS_{1-x}$/CdS core/crown NPLs with different sulfur composition. Reprinted with permission from [112]. Copyright 2017 American Chemical Society.

$CdSe_xS_{1-x}$/CdS core/crown NPLs	TRF Decay Components								Amplitude-average Lifetimes ($\frac{\sum A_i \times \tau_i}{\sum A_i}$)
	τ_1 (ns)	τ_2 (ns)	τ_3 (ns)	τ_4 (ns)	A_1	A_2	A_3	A_4	τ_{av} (ns)
x = 1.00	152.0	9.0	3.0	1.0	16	346	10045	1780	3.10
x = 0.85	202.0	16.9	3.4	1.2	6	92	7750	4325	2.83
x = 0.75	156.0	16.7	4.4	0.9	21	255	8006	4035	3.78
x = 0.70	200.0	19.7	5.0	1.1	15	132	9508	2147	4.70

With the synthesis of $CdSe_xS_{1-x}$/CdS core/crown NPLs, we obtained improved optical properties including the enhanced absorption cross-section and the increased PL-QY. However, due to the formation of CdS crown region only in the lateral direction, $CdSe_xS_{1-x}$/CdS core/crown NPLs exhibit emission almost in the same spectral position with $CdSe_xS_{1-x}$ core NPLs. To achieve further spectral tunability with $CdSe_xS_{1-x}$ core

NPLs, we synthesized $CdSe_xS_{1-x}/CdS$ core/shell NPLs by using the c-ALD technique [82]. With atomically precise shell thickness control offered by c-ALD technique, we achieved highly uniform growth of CdS layers. HAADF-STEM images of $CdSe_xS_{1-x}/CdS$ core/shell NPLs having 3 ML of CdS shell are presented in Figure 5.5a. As it can be seen from the HAADF-STEM images, the growth of CdS shell layer is highly uniform and $CdSe_xS_{1-x}/CdS$ core/shell NPLs preserve their initial rectangular shape during the shell growth process.
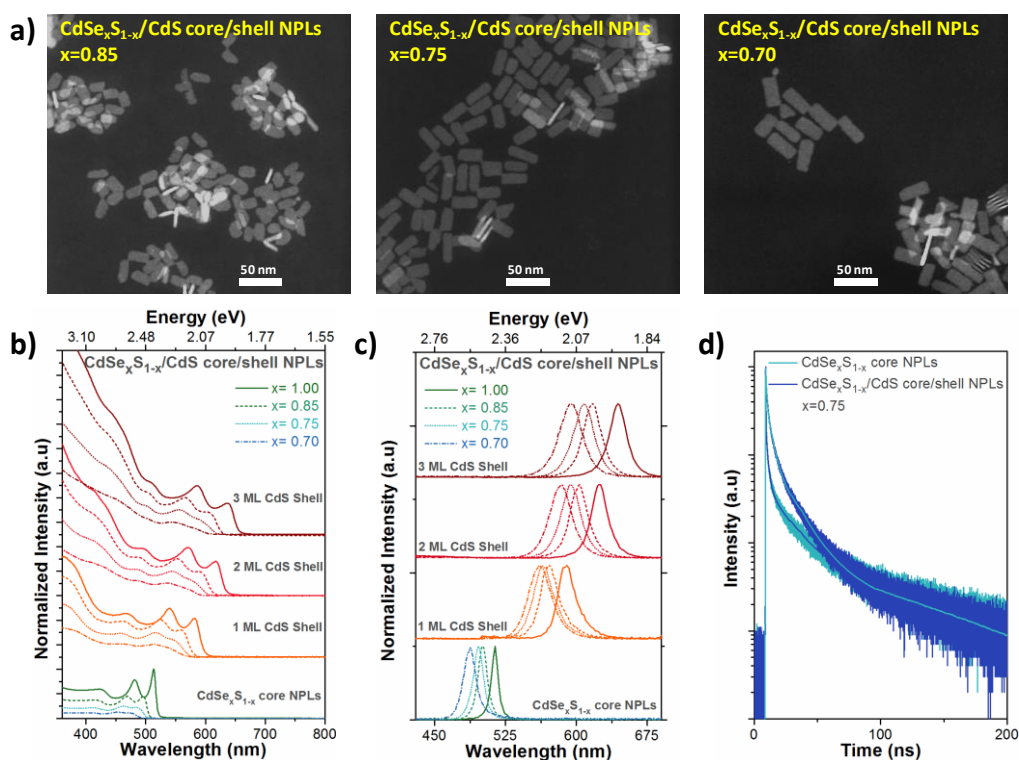
Figure 5.5. (a) HAADF-STEM images of $CdSe_xS_{1-x}/CdS$ core/shell NPLs having 3 ML CdS shell thicknesses, (b) normalized absorbance spectra of $CdSe_xS_{1-x}/CdS$ core/shell NPLs with different sulfur composition and CdS shell thicknesses, (c) PL spectra of $CdSe_xS_{1-x}/CdS$ core/shell NPLs with varying sulfur composition and CdS shell thicknesses, and (d) time-resolved fluorescence decay curves of $CdSe_xS_{1-x}$ alloyed core

and $CdSe_xS_{1-x}/CdS$ core/shell NPLs having 3 ML CdS shell for the case of x = 0.75 (d).

Reprinted with permission from [112]. Copyright 2017 American Chemical Society.

We also studied the highly tunable optical properties of $CdSe_xS_{1-x}/CdS$ core/shell NPLs. The absorption spectra of $CdSe_xS_{1-x}/CdS$ core/shell NPLs having different CdS shell thicknesses are presented in Figure 5.5b. With the formation of CdS shell layers in the vertical direction, we observed red-shifting and broadening in the excitonic features of $CdSe_xS_{1-x}/CdS$ core/shell NPLs regardless of their sulfur compositions. While the red-shifting of excitonic features can be explained with the relaxation of the quantum confinement depending on the increased vertical thickness of NPLs, the broadening of excitonic features can be attributed to the enhanced exciton-phonon coupling.

Similarly, we observed the red-shifted emission behavior for $CdSe_xS_{1-x}/CdS$ core/shell NPLs and achieved tunable emission within the spectral range of 560-650 nm depending on the shell thickness and sulfur composition of the starting $CdSe_xS_{1-x}$ core NPLs (Figure 5.5c). However, the PLs of $CdSe_xS_{1-x}/CdS$ core/shell NPLs were found to be significantly broadened with respect to that of $CdSe_xS_{1-x}$ core NPLs. For example, CdSe core NPLs exhibit the FWHM values of ~35-40 meV, whereas CdSe/CdS core/shell NPLs having 3 ML CdS shell have the FWHM values of ~65-70 meV. In addition, we observed that the broadening of the emission bandwidths is strongly related with sulfur composition. We showed that the emission bandwidth of core/shell NPLs continuously broadened with increasing sulfur composition and reached ~100 meV for the $CdSe_xS_{1-x}/CdS$ core/shell NPLs having 3 ML CdS shell and the highest amount of sulfur composition (x = 0.70). This finding also supports that the broadening comes from the increased exciton-phonon coupling. Furthermore, by using in-solution samples, the

formation core/shell structure was further verified with the TRF measurements. Owing to the partial separation of electron and hole wavefunctions in the $CdSe_xS_{1-x}/CdS$ core/shell NPLs, increased radiative fluorescence lifetimes were measured with respect to their $CdSe_xS_{1-x}$ cores (Figure 5.6, Tables 5.3 and 5.4). As it can be seen from Figure 5.5d, the amplitude-averaged fluorescence lifetime was increased from ~0.71 to ~2.75 ns for the $CdSe_xS_{1-x}/CdS$ core/shell NPLs with x=0.75 having 3 ML CdS shell. It is also important to note that when we compared the fluorescence lifetimes of $CdSe_xS_{1-x}/CdS$ core/shell NPLs with those of $CdSe_xS_{1-x}/CdS$ core/crown NPLs, core/shell NPLs exhibit faster fluorescence lifetimes despite their increased electron and hole wavefunctions delocalization. This can be attributed to the lower PL-QY of core/shell NPLs, increasing the contribution of the faster nonradiative decay components. Therefore, owing to the competition between the faster nonradiative component originating from the trap sites and the elongated radiative component with the increased electron delocalization, we observed faster fluorescence lifetimes from the core/shell NPLs with respect to core/crown NPLs.
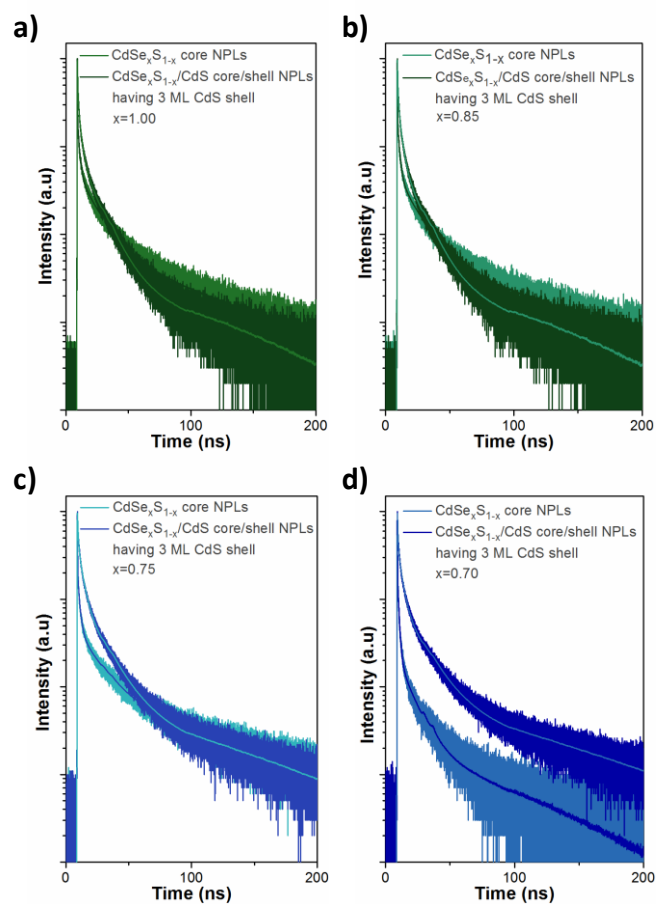
Figure 5.6. Time-resolved fluorescence decay curves of CdSe$_x$S$_{1-x}$/CdS core/shell NPLs having 3 ML CdS shell together with their core for the case of (a) x = 1.00, (b) x = 0.85, (c) x = 0.75, and (d) x = 0.70. Reprinted with permission from [112]. Copyright 2017 American Chemical Society.

Table 5.3. Analysis of time-resolved fluorescence decay curves of CdSe$_x$S$_{1-x}$ core NPLs used for the CdS shell coating. Reprinted with permission from [112]. Copyright 2017 American Chemical Society.

CdSe$_x$S$_{1-x}$ core-only NPLs	TRF Decay Components								Amplitude-average Lifetimes ($\frac{\sum A_i \times \tau_i}{\sum A_i}$)
	τ_1 (ns)	τ_2 (ns)	τ_3 (ns)	τ_4 (ns)	A_1	A_2	A_3	A_4	τ_{av} (ns)
x = 1.00	71.5	13.6	1.6	0.09	81	443	1507	33340	0.48
x = 0.85	73.1	13.4	1.6	0.10	75	426	1569	29360	0.52
x = 0.75	92.1	15.6	1.7	0.12	86	358	1501	25120	0.71
x = 0.70	60.5	10.6	1.2	0.10	26	209	1508	30860	0.26

Table 5.4. Analysis of time-resolved fluorescence decay curves of CdSe$_x$S$_{1-x}$/CdS core/shell NPLs having 3 ML CdS shell. Reprinted with permission from [112]. Copyright 2017 American Chemical Society.

CdSe$_x$S$_{1-x}$/CdS core/shell NPLs	TRF Decay Components								Amplitude-average Lifetimes ($\frac{\sum A_i \times \tau_i}{\sum A_i}$)
	τ_1 (ns)	τ_2 (ns)	τ_3 (ns)	τ_4 (ns)	A_1	A_2	A_3	A_4	τ_{av} (ns)
x = 1.00	76.1	12.6	2.3	0.30	37	816	3124	12880	1.43
x = 0.85	74.1	12.5	2.5	0.32	37	765	3372	12233	1.50
x = 0.75	96.0	15.5	3.5	0.45	61	1067	3793	9560	2.75
x = 0.70	99.5	15.6	3.1	0.36	71	927	3520	11088	2.33

After the optical and structural characterization of CdSe$_x$S$_{1-x}$ alloyed core NPLs and their different heterostructures, we have studied their optical gain performance. For the optical gain measurements, we prepared highly close-packed films by spin-coating highly concentrated NPL solutions on fused silica substrates. The samples were excited with the stripe configuration by using femtosecond laser beam (400 nm, 120 fs laser

pulses at a 1 kHz repetition rate). Pump-fluence dependent PL spectra of NPLs were collected via a fiber coupled to the spectrometer. As an exemplary case, pump-fluence dependent PL spectra of $CdSe_xS_{1-x}$ core, $CdSe_xS_{1-x}/CdS$ core/crown and core/shell NPLs ($x = 0.75$) are presented in Figures 5.7a, 7b and 7c respectively. For the $CdSe_xS_{1-x}$ core-only NPLs ($x = 0.75$), when the excitation fluence exceeded ~292 $\mu J/cm^2$, we observed slightly red-shifted (~6 nm) ASE peak at 508 nm having a narrower bandwidth (6-7 nm) with respect to spontaneous emission (Figure 5.7a). This red-shifted ASE peak can be attributed to the biexcitonic gain observed in semiconductor nanocrystals having Type-I electronic structure [110], [111]. Also, while we observed comparable gain threshold for $CdSe_xS_{1-x}$ core NLPs having different sulfur compositions, we achieved the lowest gain threshold (~146 $\mu J/cm^2$) from the $CdSe_xS_{1-x}$ core NLPs with x=0.85. Although we expected increased gain threshold from the $CdSe_xS_{1-x}$ core NLPs with increasing sulfur compositions owing to their decreased PL-QY and reduced absorption cross-section, $CdSe_xS_{1-x}$ core NLPs exhibit the relatively lower gain thresholds when compared to CdSe core NPLs. The better optical gain performance of $CdSe_xS_{1-x}$ core NLPs can be explained with the reduced amount of re-absorption, which seems to be major concern of NPLs due to their almost zero Stokes-shifted emission. In addition to that, further studies including ultrafast spectroscopy should be undertaken for a better understanding of the relation between the optical gain performance and sulfur composition.
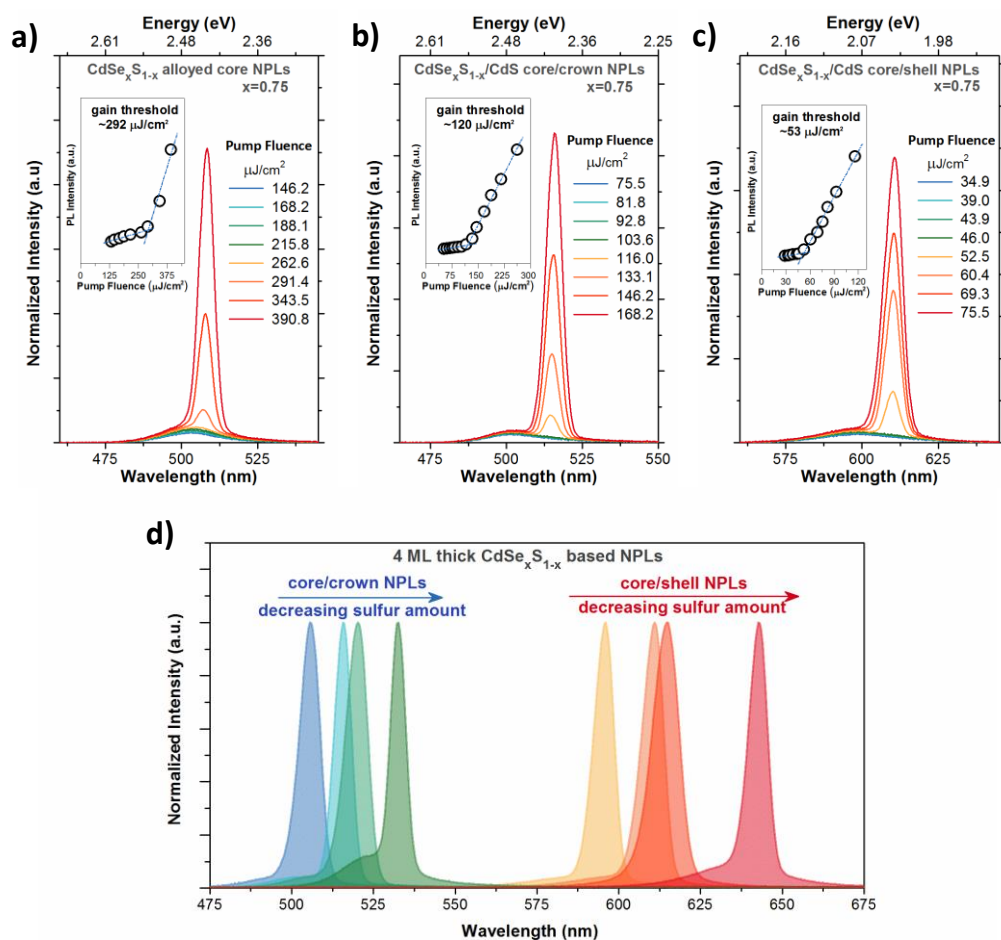
Figure 5.7. Optical gain performances of CdSe$_x$S$_{1-x}$/CdS core/crown and core/shell NPLs having different sulfur compositions. As an exemplary case for x = 0.75 amplified spontaneous emission spectra of (a) CdSe$_x$S$_{1-x}$ core-only NPLs, (b) CdSe$_x$S$_{1-x}$/CdS core/crown NPLs, (c) CdSe$_x$S$_{1-x}$/CdS core/shell NPLs having 2 ML CdS shell at different excitation fluence. In the insets, the integrated PL intensity are given as a function of the pump fluence. (d) Normalized ASE spectra of CdSe$_x$S$_{1-x}$/CdS heterostructures showing highly tunable gain performance varying with the incorporated sulfur amount. Reprinted with permission from [112]. Copyright 2017 American Chemical Society.

We have also studied the optical gain performance of different heterostructures of $CdSe_xS_{1-x}$ based NPLs. Further decreased gain thresholds are expected from $CdSe_xS_{1-x}/CdS$ core/crown NPLs thanks to their enhanced absorption cross-section and sidewall passivation of core NPLs with the CdS crown region. As it can be seen from Figure 5.7b, $CdSe_xS_{1-x}/CdS$ core/crown NPLs (x=0.75) exhibit slightly red-shifted ASE peak (515 nm) with reduced gain threshold of ~120 $\mu J/cm^2$ in comparison to $CdSe_xS_{1-x}$ core-only NPLs (x=0.75). We also observed decreased gain threshold with the $CdSe_xS_{1-x}/CdS$ core/crown NPLs comprising different sulfur compositions, indicating the importance of the crown formation. In addition, to further realize the spectral tunability of ASE with reduced gain threshold, we studied the optical gain performances of $CdSe_xS_{1-x}/CdS$ core/shell NPLs having 2 ML of CdS shell. Similarly, with the formation of CdS shell, we obtained lower gain thresholds with respect to $CdSe_xS_{1-x}$ core-only NPLs for all sulfur compositions. From the $CdSe_xS_{1-x}/CdS$ core/shell NPLs (x=0.75), we achieved a red-shifted ASE peak located at ~610 nm with the lowest gain threshold of 53 $\mu J/cm^2$ when compared to core-only, core/crown and core/shell NPLs used in this study. The improved performance of core/shell NPLs can be explained with the further suppressed Auger recombination owing to partial separation of electron and hole wavefunctions. Also, reduced amount of re-absorption enables us to achieve decreased gain thresholds with $CdSe_xS_{1-x}$ based heterostructures of NPLs despite their lower PL-QY.

Finally, as it can be seen from Figure 5.7d, with the synthesis of alloyed heterostructures of $CdSe_xS_{1-x}$ core NPLs, we have achieved extended spectral tunability of the optical gain obtained from colloidal NPLs. In previous studies, low-threshold optical gain has been demonstrated by using colloidal NPLs emitting in the blue, green,

108

yellow and red spectral regions [84]. However, thanks to pure vertical quantum confinement, they exhibit discrete ASE peaks at ~490 nm for blue-, ~534 nm for green-, 575 nm for yellow- and ~640 nm for red-emitting NPLs. Here, by using $CdSe_xS_{1-x}/CdS$ core/crown and core/shell NPLs, we have accomplished to fill the gaps and shown tunable ASE peaks within the range of 500-535 nm and 590-640 nm. Here it is also possible to further extend the spectral tunability by tailoring the sulfur composition of $CdSe_xS_{1-x}$ core-only NPLs and the adjusting the thickness of the CdS shell.

5.4 Summary

In summary, we have reported the synthesis of core/crown and core/shell heterostructures of $CdSe_xS_{1-x}$ core-only NPLs together with their resulting excitonic properties, enabling the achievement of highly tunable and low-threshold gain performance. With the synthesis of $CdSe_xS_{1-x}/CdS$ core/crown NPLs, we demonstrated improved PL-QY, enhanced absorption cross-section and increased stability without changing the emission spectra of $CdSe_xS_{1-x}$ core-only NPLs. On the other hand, with the synthesis of $CdSe_xS_{1-x}/CdS$ core/shell NPLs, we realized highly tunable emission for NPLs covering a wide range of the spectrum between 560-650 nm depending on the sulfur composition and shell thickness. Also, we studied the optical gain performances of different heterostructures of $CdSe_xS_{1-x}$ alloyed NPLs offering great advantages including reduced re-absorption and spectrally tunable optical gain range. Considering the emission of $CdSe_xS_{1-x}$ based NPLs covering a wide spectral range, we demonstrated highly tunable ASE with low gain thresholds (~53 $\mu J/cm^2$). These findings have shown the importance of the colloidal synthesis of engineered heterostructured NPLs for the achievement of superior excitonic properties and the significant potential for the

utilization of NPLs for the next-generation optoelectronic devices including lasers and

LEDs owing to their profoundly tunable excitonic properties.

Chapter 6

CdSe/CdTe Core/Crown Heteronanoplatelets

This chapter of the thesis is based on the publication "Type-II Colloidal Quantum Wells: CdSe/CdTe Core/Crown Heteronanoplatelets," **Y. Kelestemur**, M. Olutas, S. Delikanli, B. Guzelturk, M. Z. Akgul, and H. V. Demir, The Journal of Physical Chemistry C 119 (4), 2177-2185 (2015). Reprinted with permission from [95]. Copyright 2015 American Chemical Society.

6.1 Motivation

With the ease of facile colloidal synthesis of semiconductor nanocrystals, different kinds of core/shell architectures can be designed and synthesized with great control over their size distribution and shape uniformity [53], [54], [97]. Also, with the favorable selection of core and shell materials, electronic structure of semiconductor nanocrystals can be engineered to achieve either Type-I or Type-II electronic structure, which is highly critical for various applications [51], [111], [119]. For example, with the coating of higher band gap shell material, Type-I electronic structure can be achieved where both

electrons and holes are confined to the core. Because of the confinement of the electron and hole inside the core region, higher oscillator strength and higher PL-QY can be obtained [52]. Recently, semiconductor nanocrystals having Type-I electronic structure have been synthesized with almost near-unity PL-QY [120], and this makes them highly promising candidates for the next generation LEDs [121] and lasing applications [122].

In contrast to Type-I semiconductor nanocrystals, semiconductor nanocrystals having Type-II electronic structure, where there is a significantly reduced overlap between electron and hole wave functions, show different and interesting properties [51], [64]. First, they exhibit strongly red-shifted emission originating from the radiative recombination of electron and hole across the core-shell interface, which would otherwise not be possible to achieve from either only core or only shell materials. Second, as a result of the separation of electron and hole wave functions, a reduced level of oscillator strength is observed with significantly increased radiative lifetime. In addition, thanks to the reduced oscillator strength, suppression of Auger recombination is also reported in Type-II semiconductor nanocrystals [119], [123]. Therefore, with these attractive properties, Type-II nanocrystals are highly promising as light harvesting materials for photovoltaic and photoconduction applications, where efficient removal of excited charges is highly desired [124]. However, when compared to the routinely synthesized highly efficient and stable Type-I semiconductor nanocrystals, Type-II semiconductor nanocrystals have suffered from the poor stability and impeded charge extraction. To date, different core/shell heterostructures including spherical forms [51], [65], rods [125], [126], tetrapods [44], and barbells [127], [128] having Type-II band alignment have been synthesized and studied for the increased stability and enhanced charge extraction. Although higher PL-QY and stability have been reported for the

spherical core/shell heterostructures having Type-II band alignment [129], they suffer from the limited charge extraction since either electron or hole is always trapped inside the core of a spherical particle. On the other hand, while asymmetric core/shell heterostructures such as barbells and tetrapods enable more efficient charge extraction with respect to spherical ones, their inferior film formation limits the device performance [64]. Therefore, new architectures of colloidal semiconductor nanocrystals enabling efficient charge extraction and high-quality film formation are welcomed for enhanced light-harvesting purposes.

Recently, as a subclass of colloidal semiconductor nanocrystals, colloidal NPLs have been introduced, which offer exciting properties owing to their quasi-1D confinement making them colloidal counterparts of quantum wells [15], [17]. These NPLs exhibit extremely narrow emission bandwidth with tunable peak emission via changing the thickness of the NPLs. In addition, assorted structures of NPLs having vertically grown shell region [19] and/or laterally extended crown region [18], [81] can be synthesized with a precise control of the shell thickness and the crown width. With the formation of shell and crown region, core/shell and core/crown NPLs exhibit enhanced PL-QY and stability, which is indispensable for various advanced optoelectronic applications. For example, by using core/shell and core/crown NPLs having Type-I electronic structure, LEDs with a narrower emission bandwidth [21] and solution-processed laser with lower lasing threshold [20] have been demonstrated, respectively. However, NPLs having Type-II electronic structure have not previously been studied. Recently, during the review process of our work, the report by Pedetti et al. appeared to show the synthesis and characterization of CdSe/CdTe core/crown NPLs having Type-II electronic structure using a different cadmium precursor [102].

113

Here, in an independent study, we report the synthesis of CdSe/CdTe core/crown NPLs having Type-II electronic structure with varying crown width by using core-seeded lateral shell growth approach. With the laterally grown CdTe crown region, atomically-flat CdSe/CdTe core/crown NPLs are achieved, which is highly promising for efficiently removal of excited carriers. The epitaxial growth of CdTe crown layer is verified by using transmission electron microscopy with quantitative EDAX analysis and X-ray diffraction. In these Type-II nanoplatelets, we systematically study the optical properties via tailoring the size of the CdTe crown layer. Strongly red-shifted photoluminescence (up to ~150 nm) is observed, which would not be possible to achieve from only 4 ML thick CdSe NPLs or CdTe NPLs. The fluorescence lifetimes of the Type-II NPLs are measured to be 2 orders of magnitude greater than those of the core-only Type-I NPLs due to the presence of the spatially indirect excitons at the Type-II interface. Moreover, we extend the fluorescence time-resolved study and analyze temperature-dependent emission kinetics of CdSe/CdTe core/crown NPLs for a deeper understanding of their excitonic behavior. Although amplitude-averaged lifetimes of CdSe/CdTe core/crown NPLs slightly decrease with decreasing temperature, the fluorescence radiative lifetime components of CdSe/CdTe core/crown NPLs exhibit increasing behavior. Finally, we report an effective ligand exchange procedure to achieve water-soluble CdSe/CdTe core/crown NPLs, which may enable high quality film formation by using a layer-by-layer approach.

6.2 Colloidal Synthesis and Experiments

Chemicals. Cadmium nitrate tetrahydrate ($Cd(NO_3)_2 \cdot 4H_2O$) (99.999% trace metals basis), sodium myristate (>99%), technical grade 1-octadecene (ODE), selenium (Se)

(99.999% trace metals basis), cadmium acetate dihydrate (Cd(OAc)$_2$·2H$_2$O) (>98%), technical grade oleic acid (OA) (90%), technical grade trioctylphosphine (TOP) (90%), tellurium (Te) (99.997% trace metals basis), and 3-mercaptopropionic acid (>99%) were purchased from Sigma-Aldrich. Hexane, methanol, and ethanol were purchased from Merck Millipore.

Preparation of Cadmium Myristate. The preparation of cadmium myristate is followed by the recipe given in the literature [18]. Briefly, 1.23 g of cadmium nitrate tetrahydrate is dissolved in 40 mL of methanol, and 3.13 g of sodium myristate is dissolved in 250 mL of methanol. After complete dissolution, solutions are mixed and stirred strongly for around 1 h. Then, the solution is centrifuged and the precipitated part is dissolved in methanol. This washing step with methanol is performed at least three times for the removal of excess precursors. After that, the final precipitated part is kept under vacuum for about 24 h for drying.

Synthesis of 4 ML Thick CdSe Nanoplatelets. 4 ML thick CdSe NPLs are synthesized according to the recipe given in the literature [18]. For a typical synthesis, 170 mg of cadmium myristate, 12 mg of Se, and 15 mL of ODE are loaded into a three-neck flask. The solution is degassed at room temperature for half an hour to remove excess oxygen and volatile solvents. Then, the solution is heated to 240 °C under argon atmosphere. When the temperature reaches 195 °C, 80 mg of cadmium acetate dihydrate is introduced swiftly into the reaction. After the growth of CdSe NPLs at 240 °C for around 10 min, 0.5 mL of OA is injected and the temperature of the solution is decreased to room temperature. CdSe NPLs synthesized with this recipe exhibit peak emission at 513 nm, and other side products including NPLs having different thicknesses can be removed by

115

size-selective precipitation. Finally, 4 ML thick CdSe NPLs are dissolved and stored in hexane.

Preparation of Anisotropic Growth Mixture for CdTe Crown Region. Anisotropic growth mixture is prepared with a slightly modified recipe, which is used for the growth of CdS crown region [18]. First, cadmium precursor is prepared. Briefly, 480 mg of cadmium acetate dihydrate, 340 µL of OA, and 2 mL of ODE are loaded into a three-neck flask. The solution is heated to 150 °C under air with continuous stirring while also regularly sonicated. When a homogeneous gel having whitish color is formed, the solution is cooled down to room temperature. For the tellurium precursors, both Te-TOP (0.1 M) solution having an excess amount of TOP and Te-TOP-ODE (0.03 M) solution, which is achieved by the dilution of Te-TOP (1 M) solution with ODE, are prepared inside the glovebox.

Synthesis of 4 ML Thick CdSe/CdTe Core/Crown Nanoplatelets. CdSe/CdTe core/crown NPLs are synthesized using the core-seeded approach. For achieving a higher PL-QY, we have performed syntheses with slight modifications. In the first case, a certain amount of 4 ML thick CdSe NPLs dissolved in hexane and 5 mL of ODE were loaded into a three-neck flask. The solution was degassed at room temperature for 1 h for the complete removal of hexane. Then, the solution was further degassed at 100 °C for the removal of water and any other organic residuals. After that, the temperature was set to 240 °C under an argon atmosphere for the growth of the CdTe crown region. When the temperature reached 240 °C, anisotropic growth mixture including 2 mL of cadmium precursor and 3 mL of tellurium precursor having an excess amount of TOP was injected at the rate of 2.0 mL/h. Finally, with the addition of 0.5 mL of OA, the reaction was

cooled down to room temperature. However, due to an excess amount of TOP, the resulting CdSe/CdTe core/crown NPLs exhibit lower PL-QY (<5%) with partial and/or nonuniform coating of CdTe crown region. Recently, it has been demonstrated that while the presence of TOP in the reaction solution decreases the stability of CdSe core NPLs, the presence of carboxylates in the reaction solution preserves the stability of CdSe core NPLs [102]. Therefore, the amount of TOP in the Te precursor is critical in obtaining high quality CdSe/CdTe core/crown NPLs.

In the case of modified synthesis to achieve a higher PL-QY and uniform coating of CdTe crown region, Te-TOP-ODE (0.03 M) solution is used as a tellurium precursor and a calculated amount of cadmium precursor is added at the beginning of the reaction. For the synthesis, 2 mL of 4 ML thick CdSe NPLs dissolved in hexane (having optical density of 0.5 at 350 nm), 5 mL of ODE, 40 µL of OA, and 0.39 mL of cadmium precursors were loaded into a three-neck flask. The solution was degassed at room temperature for 1 h for the complete removal of hexane. Then, the solution was further degassed at 100 °C for the removal of water and any other organic residuals. Subsequently, the temperature of the solution was set to 240 °C under argon atmosphere for the growth of CdTe crown region. When the temperature reached 240 °C, 1 mL of tellurium precursor (Te-TOP-ODE (0.03 M)) was injected at the rate of 8 mL/h and the synthesis was allowed to react at 240 °C for 15 min (including injection) before cooling to room temperature. Finally, with the addition of 0.5 mL of OA, the reaction was cooled down to room temperature. By doing so, we achieved the highest PL-QY up to 40−50% with highly uniform coated CdTe crown region. In addition, depending on the desired size of CdTe crown region, the amount of cadmium and tellurium precursors could be

changed. For the further characterization of CdSe/CdTe core/crown NPLs, they were cleaned with successive precipitation and dispersed in hexane.

Ligand Exchange with 3-Mercaptopropionic Acid (MPA). After the synthesis of CdSe/CdTe core/crown NPLs, ligand exchange is performed to achieve water-soluble colloidal NPLs. For a typical ligand exchange procedure, 250 μL of MPA is mixed with 15 mL of methanol and the mixture is shaken vigorously to homogeneously distribute MPA. Then, 30 mL of hexane is slowly added into the mixture. Afterward, NPLs dissolved in 2 mL of hexane are added dropwise while sonicating the mixture. After 30 min of sonication, the mixture is centrifuged at 4500 rpm until all of NPLs precipitate. The supernatant is discarded, and the precipitate is dissolved in deionized water. Then, the NPL solution is centrifuged at 2000 rpm for 5 min for the removal of the aggregated NPLs. The precipitate is discarded, and the resulting clear aqueous solution of NPLs is used for further studies.

6.3 Results and Discussion

In this study, 4 ML thick CdSe/CdTe core/crown NPLs having Type-II electronic structure are synthesized using the core-seeded approach. First, CdSe NPLs having 4 ML thickness are synthesized with a slightly modified recipe from the literature [18]. The absorption and photoluminescence spectra of 4 ML CdSe NPLs are given in Figure 6.1a. They have very sharp excitonic absorption peak at 513 nm corresponding to the electron/heavy-hole transition with a FWHM of ~8 nm. They exhibit a moderately high PL-QY (30−50%) when compared to bare CdSe core colloidal quantum dots. In addition, owing to the quantum well like structure of the NPLs, separation of heavy- and light-hole transitions is clearly observed in their absorption spectra. Moreover, depending on

the synthesis parameters including the reaction temperature and time, the lateral dimensions of the NPLs can be tuned and either rectangular- or square-shaped NPLs can be achieved. As it can be seen from the HAADF-STEM images in Figures 6.1b, 4 ML CdSe NPLs, which are synthesized with the recipe given above, result in almost square shape with lateral dimensions of 17.33 ± 1.51 nm and 13.31 ± 1.98 nm.
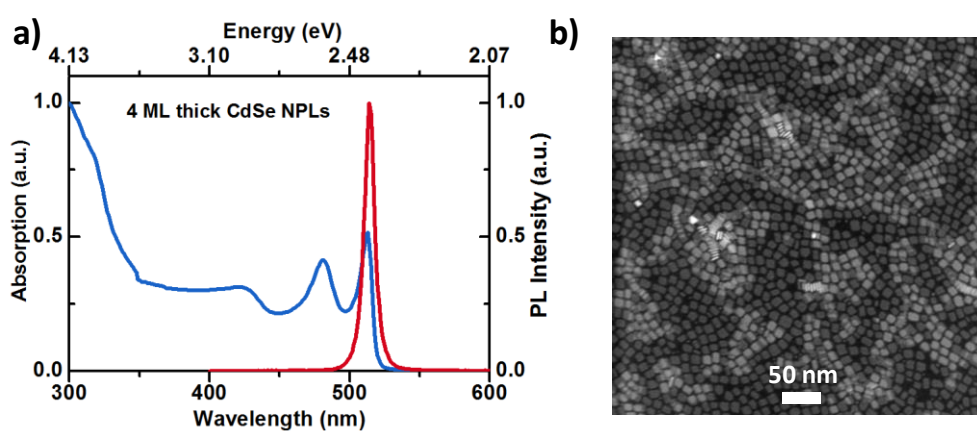
Figure 6.1. (a) Normalized absorption and photoluminescence spectra of 4 ML thick CdSe NPLs dissolved in hexane. (b) HAADF-STEM images of the 4 ML thick CdSe NPLs with a scale bar of 50 nm. Reprinted with permission from [95]. Copyright 2015 American Chemical Society.

By using the freshly synthesized CdSe NPLs as the seeds, CdSe/CdTe core/crown NPLs are synthesized with a continuous injection of crown precursors at higher temperatures. Thanks to the anisotropic growth of cadmium acetate precursor, only lateral growth of CdTe is achieved. In addition, by simply changing the amount of injection, CdSe/CdTe core/crown NPLs with varied crown sizes are synthesized. Absorption spectra of CdSe/CdTe core/crown NPLs having a higher PL-QY are shown in Figure 6.2b. As it can be seen from the absorption spectra, the sharp excitonic

transitions, which correspond to the electron/light-hole and electron/heavy-hole of CdSe, remain almost in the same spectral position during the growth of CdTe crown. These non-shifting excitonic features have also been observed for Type-I core/crown CdSe/CdS NPLs [18], [81] and confirmed the growth of CdTe region only in the lateral direction. Otherwise, with the coating of CdTe region in the vertical direction, spectral shifting of the absorption peaks would be observed as a result of the delocalization of electron and hole wave functions across the whole structure. In addition, an absorption feature appearing within the spectral region of 550−560 nm emerges and becomes comparable to the electron/light-hole and electron/heavy-hole transitions of CdSe NPLs as the CdTe crown is grown larger. This red-shifted sharp absorption peak (∼556 nm) thus corresponds to the formation of excitons in the 4 ML thick CdTe crown layer [80], and the intensity of this peak can be tuned by changing the size of the CdTe crown layer. Also, it was shown that higher concentration of OA results in formation of extended CdTe crown region and enhances the absorption of crown region [102]. However, for the CdSe/CdTe core/crown NPLs synthesized by using an excess amount of TOP, the excitonic peak corresponding to 4 ML thick CdTe crown layer could not observed clearly, which can be attributed to the nonuniform and/or partial coating of CdTe crown region. Moreover, an absorption tail extending into the lower energy side of the absorption spectra is observed, and this can be attributed to the intermediate transitions at the core/crown interface owing to the Type-II band alignment [126], [128]. Therefore, the growth of CdTe crown region occurs only in the lateral direction and both CdSe core and CdTe crown regions make contributions to the absorption. These features observed from the absorption spectra clearly indicate the formation of CdSe/CdTe core/crown NPLs having Type-II band alignment.
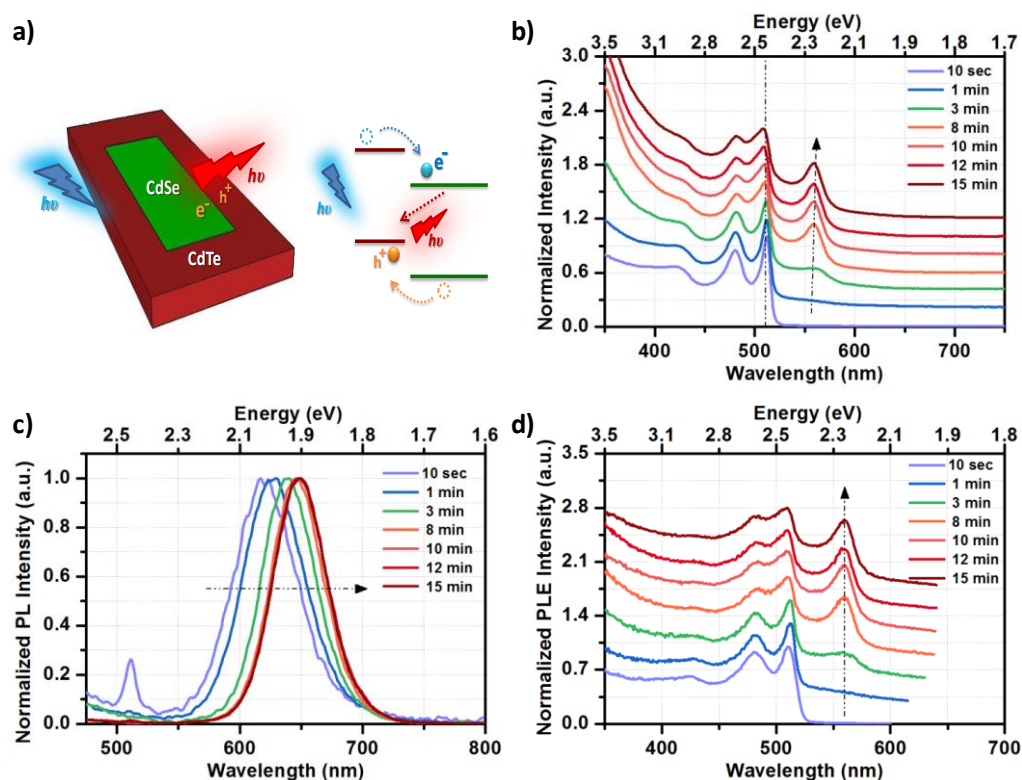
Figure 6.2. Optical characterization of 4 ML thick CdSe/CdTe core/crown NPLs having a higher PL-QY. (a) Schematic representation of carrier photogeneration in both CdSe core and the CdTe crown regions, transfer to core/crown interface, and subsequent radiative recombination resulting in Type-II emission. (b) Normalized absorption, (c) normalized photoluminescence, and (d) normalized photoluminescence excitation spectra of the CdSe/CdTe core/crown NPLs dissolved in hexane with varied crown size. Reprinted with permission from [95]. Copyright 2015 American Chemical Society.

In addition to the absorption spectra of CdSe/CdTe core/crown NPLs having a higher PL-QY, the photoluminescence spectra are presented in Figure 6.2c. As it can be seen from the PL spectra, with a small amount of anisotropic growth mixture injection, the narrower emission of 4 ML thick CdSe NPLs is completely quenched and a broader emission that is strongly red-shifted as compared to the core-only NPLs is observed from

the resulting CdSe/CdTe core/crown NPLs. Owing to the smaller Bohr radius of hole for CdTe (∼1.12 nm) [102], a very small layer coating of CdTe crown results in strongly red-shifted emission, which can be explained with the intermediate transition across the Type-II core/crown interface. Moreover, as the crown size is grown larger, the emission is continuously shifted from ∼620 to ∼660 nm, which can be attributed to the lateral confinement of CdTe crown region in addition to the vertical confinement. However, with the further injection of crown precursor, the emission peak remains almost in the same spectral position. Contrary to narrower emission line width of CdSe NPLs around 35 meV, the CdSe/CdTe core/crown NPLs exhibit broad emission line width, which is changing between 150 and 180 meV depending on the reaction time. While the CdSe/CdTe core/crown NPLs exhibit emission line width of ∼180 meV at the early stage of crown growth, the line width decreases down to ∼150 meV with the continuous injection of crown precursors. This behavior of CdSe/CdTe core/crown NPLs can be explained with the nonuniform coating of the CdTe crown region in the early stages of the crown growth. With the conformal coating of CdTe crown region at later stages, the line width starts to decrease during the reaction. Yet, the PL-QY and emission line width of CdSe/CdTe core/crown NPLs are strongly dependent on the reaction kinetics. For example, the excess amount of TOP used in the tellurium precursor promotes partial and/or nonuniform coating of CdTe crown region and results in lower PL-QY (<5%) with broader emission line width of ∼200 meV. On the other hand, Te-TOP-ODE precursors having a lesser amount of TOP result in conformal coating of CdTe crown region with higher PL-QY (up to 40-50%) and narrower emission line width (∼150 meV).

For a better understanding of the origin of strongly red-shifted emission, we also performed photoluminescence excitation spectroscopy as shown in Figure 6.2d. As it can be seen from the PLE spectra of the CdSe/CdTe NPLs in the early stages of the crown growth, which are measured at the peak emission wavelength, the electron/light-hole and electron/heavy-hole transitions of CdSe NPLs are clearly observed. This indicates that this red-shifted emission originates from the excitons in the CdSe core. Moreover, the contribution from the CdTe crown layer starts to appear at the lower energy side with increasing size of the CdTe crown region. Then, by further increasing the size of CdTe crown region, it evolves into a sharp peak around 556 nm, which corresponds to the 4 ML thick CdTe crown region [80]. Finally, it can be concluded that the red-shifted emission originates from excitons formed in both the CdSe core region and the CdTe crown region, which is expected for Type-II materials [64], [125].

Moreover, by using transmission electron microscopy, quantitative EDX analysis, and X-ray diffraction, structural characterization of CdSe/CdTe core/crown NPLs was performed. HAADF-STEM images of CdSe/CdTe core/crown NPLs having a higher PL-QY are shown in Figures 6.3a, and 6.3b. CdSe/CdTe core/crown NPLs exhibit increased lateral dimension 28.81 ± 4.30 nm and 22.86 ± 3.51 nm with respect to the CdSe core-only NPLs, which supports the growth of CdTe crown region. When compared to HAADF-STEM images of 4 ML thick CdSe NPLs, they exhibit rectangular shape with sharp boundaries, which is not observed for CdSe/CdS core/crown NPLs [20]. Also, the size distribution of CdSe/CdTe core/crown NPLs is found to be increased [17]. In addition, we performed quantitative line EDX analysis for single CdSe/CdTe core/crown NPL confirming the formation core/crown architecture. While a higher amount of tellurium is observed for the outer parts or the crown region of the NPL, a

higher amount of selenium is measured for the inner part or the core region of the NPL (Figures 6.3d and 6.3e).
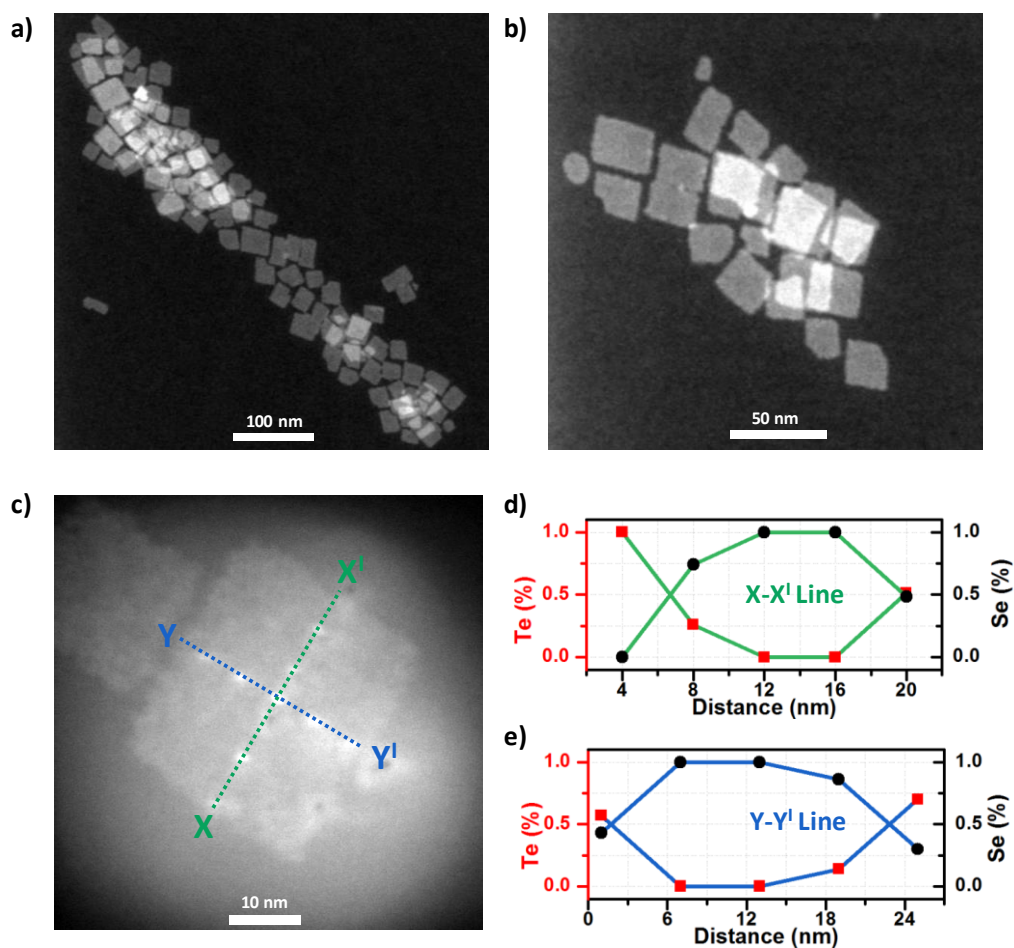
Figure 6.3. Structural characterization of 4 ML thick CdSe/CdTe core/crown NPLs having a higher PL-QY. HAADF-STEM images of CdSe/CdTe core/crown NPLs with a scale bar of (a) 100 and (b) 50 nm. (c) HAADF-STEM image of a single CdSe/CdTe core/crown NPL, with blue (Y−YI) and green lines (X−XI) showing the EDX probe position on CdSe/CdTe core/crown NPL and (d, e) the line EDX analysis reporting the compositions of selenium and tellurium in the CdSe/CdTe core/crown NPL, normalized

to the total anionic composition. Reprinted with permission from [95]. Copyright 2015 American Chemical Society.

In addition, the X-ray diffraction patterns of the CdSe core NPLs and CdSe/CdTe core/crown NPLs are given in Figure 6.4. As shown in Figure 6.4, 4 ML thick CdSe core NPLs exhibit zinc-blende crystal structure with broader diffraction peaks. With the formation of thicker CdTe crown region, the diffraction peaks are shifted to the lower angles, which can be attributed to the formation of strain due to higher lattice mismatch between CdSe and CdTe. In addition, the well-resolved diffraction peaks of the CdSe/CdTe core/crown NPLs with respect to those of the CdSe core NPLs can be attributed to the increased size of NPLs and enhanced crystalline structure.
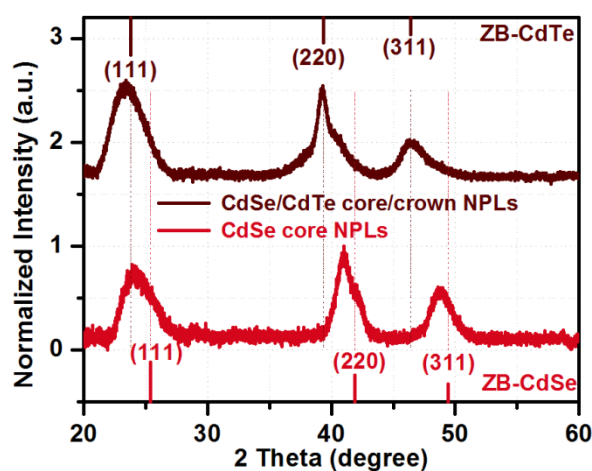
Figure 6.4. X-ray diffraction pattern of 4 ML thick CdSe core NPLs and 4 ML thick CdSe/CdTe core/crown NPLs. Reprinted with permission from [95]. Copyright 2015 American Chemical Society.

One of the most important features of semiconductor nanocrystals having Type-II electronic structure is their characteristic slow fluorescence emission decay kinetics.

When compared to semiconductor nanocrystals with Type-I electronic structure, they exhibit longer radiative lifetime as a result of the spatial separation of electron and hole wave functions, where the electron (hole) wave function is localized in the CdSe core (CdTe crown) region. In order to verify this spatially distinct localization of the electron and hole wave functions and gain more physical insight into the Type-II electronic structure in the CdSe/CdTe core/crown NPLs, we conducted time-resolved fluorescence spectroscopy. TRF measurements were performed by using samples of NPLs in solution with low concentrations and under lower excitation intensities. Excitation pump source was a picosecond semiconductor laser diode at 3.31 eV. Fluorescence decay curves of CdSe/CdTe core/crown NPLs were measured at the emission peak wavelengths, which are presented in Figure 6.5. For a better understanding of emission kinetics, we compare the fluorescence decay curves of CdSe/CdTe core/crown NPLs having a higher PL-QY and lower PL-QY. These decay curves are analyzed by three-exponential decay functions resulting in reduced χ^2 about 1 with uniform residuals.

As compared to 4 ML thick CdSe NPLs, with the growth of CdTe crown region, longer amplitude-averaged fluorescence lifetimes are observed for both samples in the range of 130−190 ns depending on the crown size (Figure 6.5). Also, it was demonstrated that, with the synthesis of NPLs having a gradient core and/or an alloyed crown region, it is possible to tailor the average fluorescence lifetime of CdSe/CdTe NPLs [102]. Lifetime components and their fractional contributions are summarized in Tables 6.1 and 6.2. We find out three lifetime components for both samples: one on the order of 400−500 ns, another on the order of 100 ns, and a fast component on the order of 10 ns. The latter has very small fractional contribution to the emission kinetics (<5%), thus we attribute this fastest lifetime component to either partial coated NPLs or rapid

nonradiative decay channel related to surface related traps in these NPLs. The observed two long fluorescence lifetime components are attributed to the radiative decay of the spatially indirect excitons at the Type-II interface. Previously, two similar decay channels were observed in CdTe/CdSe based colloidal quantum dots [130]. The origin of the coexistence is still under debate; however, these two long lifetime components clearly indicate that there are two distinct exciton states having Type-II properties with varying oscillator strength. A possible explanation might be the emissive mixed hole states (i.e., electron/light-hole and electron/heavy-hole) in these Type-II NPLs as supported by the broadening of the emission.
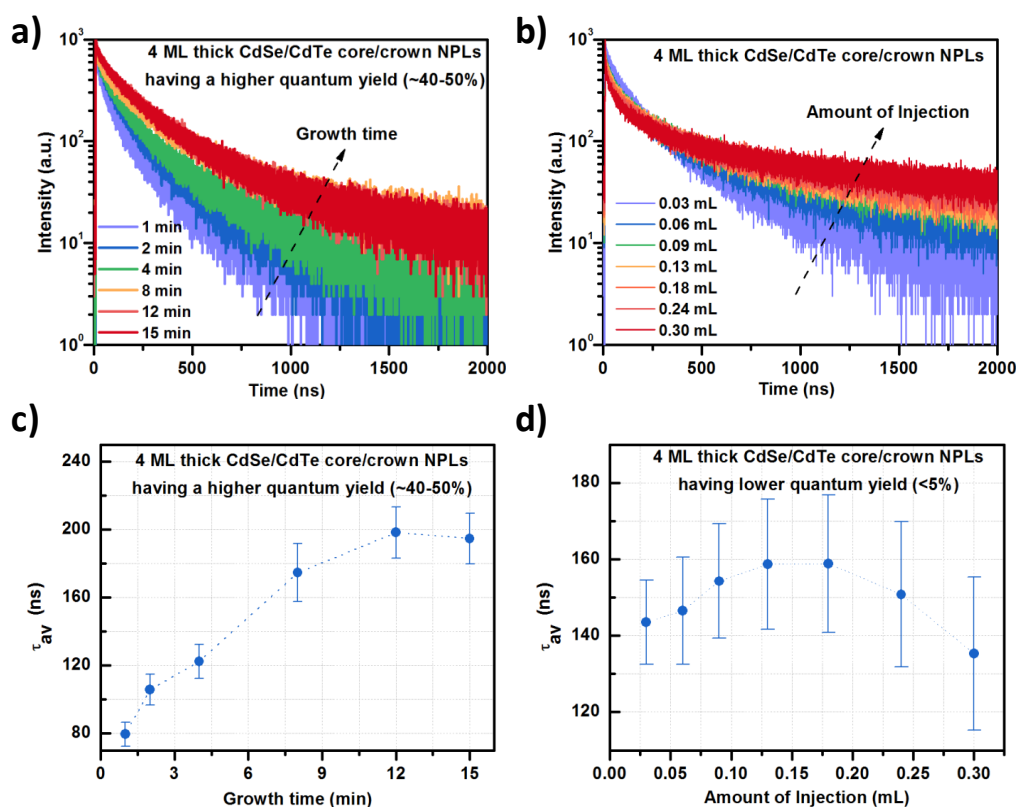
Figure 6.5. Time-resolved fluorescence decay curves of the CdSe/CdTe core/crown NPLs having (a) a higher PL-QY and (b) lower PL-QY with varied crown size. The

127

amplitude-averaged fluorescence lifetimes of CdSe/CdTe core/crown NPLs having (c) a higher PL-QY and (d) lower PL-QY. Reprinted with permission from [95]. Copyright 2015 American Chemical Society.

Table 6.1. Numerical analysis of time-resolved fluorescence from CdSe/CdTe core/crown NPLs having a lower PL-QY with different CdTe crown widths. Reprinted with permission from [95]. Copyright 2015 American Chemical Society.

Injection (mL)	TRF Decay Components					
	τ_1 (ns)	τ_2 (ns)	τ_3 (ns)	A_1	A_2	A_3
0.03	443 ± 12	121 ± 4	26 ± 6	135 ± 5	463 ± 18	253 ± 51
0.06	490 ± 14	111 ± 6	15 ± 4	145 ± 5	324 ± 18	291 ± 64
0.09	558 ± 20	113 ± 7	15 ± 4	143 ± 5	300 ± 18	324 ± 66
0.13	554 ± 17	107 ± 7	13 ± 4	146 ± 5	283 ± 18	294 ± 67
0.18	558 ± 18	102 ± 8	12 ± 4	143 ± 5	257 ± 18	290 ± 69
0.24	590 ± 20	99 ± 9	11 ± 3	127 ± 5	221 ± 18	305 ± 73
0.30	580 ± 24	87 ± 8	7 ± 2	126 ± 5	222 ± 24	350 ± 91

Injection (mL)	Amplitude-average lifetime ($\frac{\sum A_i \times \tau_i}{\sum A_i}$)	Fractional Emission Contribution ($\frac{A_i \times \tau_i}{\sum A_i \times \tau_i}$)		
	τ_{av} (ns)	$A_1 \times \tau_1$ (%)	$A_2 \times \tau_2$ (%)	$A_3 \times \tau_3$ (%)
0.03	144 ± 11	48.79	45.85	5.36
0.06	147 ± 14	63.75	32.39	3.86
0.09	155 ± 15	67.35	28.67	3.98
0.13	159 ± 17	70.25	26.36	3.40
0.18	159 ± 18	72.86	23.92	3.22
0.24	153 ± 19	74.94	21.87	3.20
0.30	136 ± 20	77.00	20.42	2.58

Table 6.2. Numerical analysis of time-resolved fluorescence from CdSe/CdTe core/crown NPLs having a higher PL-QY with different CdTe crown widths. Reprinted with permission from [95]. Copyright 2015 American Chemical Society.

Injection time (min.)	TRF Decay Components					
	τ_1 (ns)	τ_2 (ns)	τ_3 (ns)	A_1	A_2	A_3
1	386 ± 17	93 ± 4	14 ± 3	64 ± 4	359 ± 16	376 ± 61
2	378 ± 15	111 ± 4	20 ± 4	92 ± 5	418 ± 17	320 ± 55
4	411 ± 15	124 ± 5	19 ± 4	110 ± 5	411 ± 16	312 ± 58
8	427 ± 11	126 ± 6	14 ± 6	215 ± 7	363 ± 18	229 ± 70
12	440 ± 10	153 ± 6	25 ± 10	208 ± 7	445 ± 17	174 ± 53
15	457 ± 12	152 ± 5	24 ± 8	198 ± 6	465 ± 17	198 ± 55

Injection time (min.)	Amplitude-average lifetime ($\frac{\sum A_i \times \tau_i}{\sum A_i}$)	Fractional Emission Contribution ($\frac{A_i \times \tau_i}{\sum A_i \times \tau_i}$)		
	τ_{av} (ns)	$A_1 \times \tau_1$ (%)	$A_2 \times \tau_2$ (%)	$A_3 \times \tau_3$ (%)
1	80 ± 7	38.79	52.71	8.50
2	106 ± 9	39.61	53.08	7.30
4	122 ± 10	44.16	50.02	5.82
8	175 ± 17	65.08	32.6	1.32
12	198 ± 15	55.75	41.65	2.61
15	193 ± 15	52.17	44.73	3.10

The trend of fluorescence lifetimes changing over the growth time of CdTe crown region is also summarized in Figures 6.5c and 6.5d. For example, the CdSe/CdTe core/crown NPLs having a higher PL-QY exhibit an amplitude-averaged fluorescence lifetime of ~100 ns in the early stage of CdTe crown growth, and, with the increased size of CdTe crown region, the amplitude-averaged fluorescence lifetime of CdSe/CdTe core/crown NPLs is continuously increased up to ~190 ns. This can be explained with the strong delocalization of holes in the CdTe crown region, which results in the separation of electron and hole wave functions, leading to reduced oscillator strength

and radiative decay rates. On the other hand, the CdSe/CdTe core/crown NPLs synthesized by using an excess amount of TOP in the tellurium precursor and having a lower PL-QY exhibit different behavior. The amplitude-averaged fluorescence lifetime is found to be ∼120 ns in the early stage of CdTe coating, and, with the extension of CdTe crown, the amplitude-averaged fluorescence lifetime of CdSe/CdTe core/crown NPLs is increased to ∼160 ns. However, with the further injection of CdTe crown precursors, although a strong separation of charge carriers in the CdSe/CdTe core/crown NPLs is achieved and an increase in the longer decay component is obtained, a decreased amplitude-averaged fluorescence lifetime (∼130 ns) is observed. This can be explained with the formation of defect sites with the extended CdTe crown region possibly due to nonuniform coating and/or partial coating of CdSe NPLs, making the faster decay component dominant and decreasing the amplitude-averaged fluorescence lifetime of the CdSe/CdTe core/crown NPLs. These findings support the claim that the fast decay component observed for both CdSe/CdTe core/crown NPLs is originating from the formation of defect states and their contribution strongly depends on reaction kinetics and quality of the CdSe/CdTe core/crown NPLs.

Also, we extended the emission kinetics study employing temperature-dependent TRF for a better understanding of the excitonic behavior of the CdSe/CdTe core/crown NPLs with Type-II electronic structure. The CdSe/CdTe core/crown NPLs having the highest PL-QY were used for the temperature-dependent time-resolved fluorescence. For this study, a highly uniform film of CdSe/CdTe core/crown NPLs was prepared by spin-coating on a precleaned quartz substrate. Using closed-cycle He cryostat, the sample temperature was decreased from 297 to 20 K. While the fluorescence lifetime of the NPLs was measured from their spin-coated solid films to be ∼190 ns, the

fluorescence lifetime of ~240 ns was measured from the same NPLs in solution. This is partly attributed to the film effect since the NPLs are placed on the boundary of the quartz having a relatively high refractive index, upon transferring them to the solid phase, which is also common in colloidal nanocrystals [131], [132]. In addition, stacking of the NPLs in solid films can in part affect the decay kinetics [100]. As it can be seen from Figure 6.6, the amplitude-averaged fluorescence lifetime of the CdSe/CdTe core/crown NPLs are slightly decreased from ~190 to ~170 ns with decreasing temperature. Table 6.3 shows the fluorescence lifetime components as a function of the temperature, which were fitted using three exponential decay functions. Each fluorescence lifetime component is observed to grow longer with decreasing temperature. However, the decreased amplitude of the longest decay component (τ_1) led to decreased amplitude-averaged fluorescence lifetimes. The elongation of the radiative fluorescence lifetime components indicates that the electron and hole wave function separation must be increased as a result of the change of the coherence length of the excitons in the core/crown structure as the temperature is decreased. Therefore, excitons formed in the CdSe or CdTe part could be transferred to the interface more slowly. In addition, among the two emissive states (τ_1 and τ_2), the amplitude of the τ_2 component increases with decreasing temperature and becomes dominant at lower temperatures. Increase in the fastest lifetime component might indicate slowing down of the nonradiative processes with decreasing temperatures. The complex decay kinetics should be further investigated, which will be our future work. When compared to Type-I NPLs, Type-II NPLs here exhibit interesting temperature dependency.
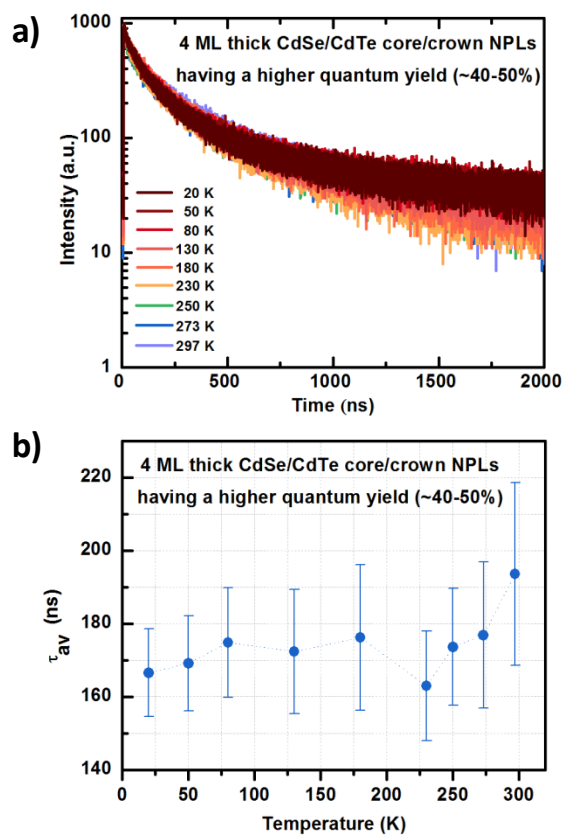
Figure 6.6. (a) Temperature-dependent time-resolved fluorescence decay curves of the CdSe/CdTe core/crown NPLs having a higher PL-QY and (b) their amplitude-averaged fluorescence lifetime. Reprinted with permission from [95]. Copyright 2015 American Chemical Society.

Table 6.3. Numerical analysis of temperature-dependent time-resolved fluorescence from CdSe/CdTe core/crown NPLs having a higher PL-QY. Reprinted with permission from [95]. Copyright 2015 American Chemical Society.

T (K)	TRF Decay Components					
	τ_1 (ns)	τ_2 (ns)	τ_3 (ns)	A_1	A_2	A_3
298	415 ± 9	97 ± 7	8 ± 6	301 ± 8	371 ± 23	166 ± 102
273	411 ± 10	97 ± 7	11 ± 6	252 ± 7	350 ± 22	188 ± 80
250	427 ± 11	103 ± 6	16 ± 6	232 ± 7	352 ± 21	217 ± 66
230	415 ± 11	102 ± 6	18 ± 7	219 ± 7	403 ± 21	212 ± 63
180	391 ± 9	96 ± 5	9 ± 8	282 ± 8	465 ± 24	142 ± 93
130	426 ± 12	107 ± 5	15 ± 8	222 ± 7	454 ± 22	170 ± 72
80	444 ± 14	107 ± 5	21 ± 10	204 ± 7	454 ± 21	159 ± 58
50	464 ± 16	114 ± 5	27 ± 9	176 ± 6	440 ± 20	196 ± 51
20	494 ± 18	123 ± 5	33 ± 8	159 ± 6	444 ± 19	245 ± 46

T (K)	Amplitude-average lifetime ($\frac{\sum A_i \times \tau_i}{\sum A_i}$)	Fractional Emission Contribution ($\frac{A_i \times \tau_i}{\sum A_i \times \tau_i}$)		
	τ_{av} (ns)	$A_1 \times \tau_1$ (%)	$A_2 \times \tau_2$ (%)	$A_3 \times \tau_3$ (%)
298	194 ± 25	76.92	22.30	0.78
273	177 ± 20	74.21	24.26	1.52
250	174 ± 16	71.31	26.17	2.52
230	163 ± 15	66.90	30.31	2.79
180	176 ± 20	70.51	28.65	0.84
130	172 ± 17	64.84	33.41	1.75
80	175 ± 15	63.53	34.13	2.34
50	169 ± 13	59.66	36.46	3.89
20	167 ± 12	55.54	38.71	5.74

In addition to synthesis and characterization of the CdSe/CdTe core/crown NPLs, ligand exchange with 3-mercaptopropionic acid was studied for achieving better properties. Compared to as-synthesized NPLs with long-chain ligands, NPLs with MPA ligands may offer great advantages including enhanced charge extraction thanks to their short-chain ligands and high-quality film formation by using the layer-by-layer (LBL) assembly method, both of which might be highly crucial for a high-performance device.

First, as-synthesized 4 ML thick CdSe NPLs are used for the ligand exchange. The normalized absorption spectra of 4 ML thick CdSe NPLs dissolved in water and hexane are given in Figure 6.7a. After the ligand exchange with MPA, the sharp excitonic transitions corresponding to the electron/light-hole and electron/heavy-hole transitions are red-shifted by ∼14 and ∼18 nm, respectively. As a result of the coating of the surface of CdSe NPLs with a monolayer of sulfur atoms, electrons and holes are delocalized across the whole structure, which results in a decreased oscillator strength and a red-shifted absorption peak. In addition to the delocalization of electrons and holes, broadening of the electron/light-hole and electron/heavy-hole transition peaks are observed, which can be explained with the nonuniform surface coverage of ligands between NPLs. Subsequently, ligand exchange procedure is performed for the CdSe/CdTe core/crown NPLs having a higher PL-QY. The normalized absorption spectra of 4 ML thick CdSe/CdTe core/crown NPLs dissolved in water and hexane are also given in Figure 6.7b.
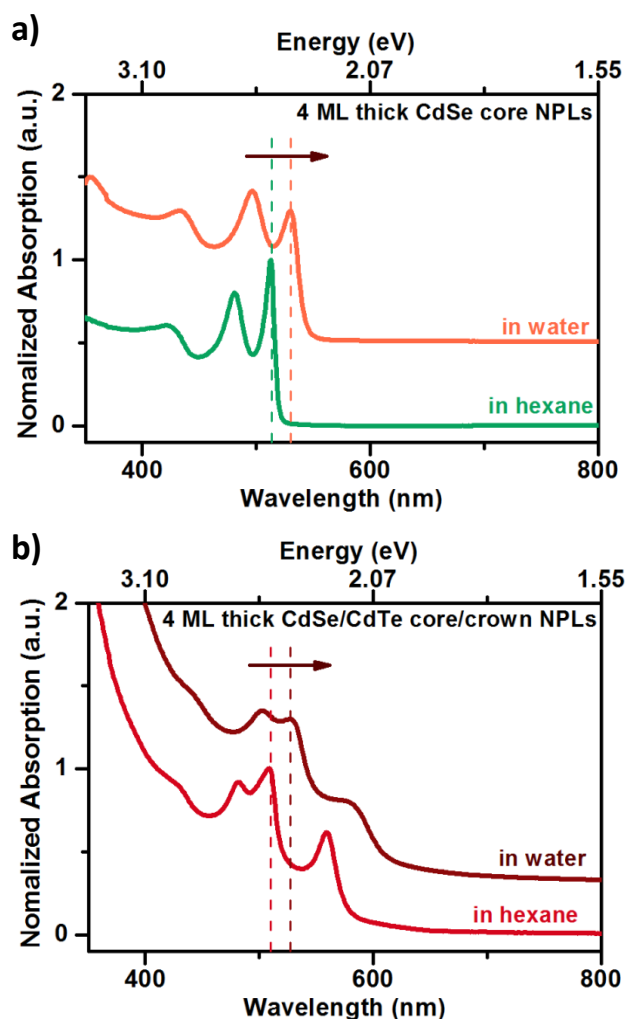
Figure 6.7. Normalized absorption spectra of (a) 4 ML thick CdSe core NPLs and (b) 4 ML thick CdSe/CdTe core/crown NPLs before and after the ligand exchange. Reprinted with permission from [95]. Copyright 2015 American Chemical Society.

Similar to 4 ML thick CdSe NPLs, the same amount of shifting is observed for the electron/light-hole and the electron/heavy-hole transitions of the CdSe core region from the CdSe/CdTe core/crown NPLs. Moreover, similar to CdSe NPLs, the excitonic transition originating from CdTe crown region becomes clear after the ligand exchange with an approximately 30 nm red-shifted and broader peak. The lower intensity of the

absorption tail extending into the lower energy side of spectra with a well-resolved excitonic transition of CdSe core region and CdTe crown region clearly indicates that, after the ligand exchange, the CdSe/CdTe core/crown NPLs are dissolved without any aggregation and/or stacking. However, these ligand-exchanged NPLs exhibit a very low PL-QY (<1%). Owing to the magic-sized thickness and very large surface area of NPLs, they are highly sensitive to surface modifications.

6.4 Summary

In this study, we have demonstrated the synthesis and characterization of CdSe/CdTe core/crown NPLs having Type-II electronic structure. With a suitable crown shell precursor, atomically flat CdSe/CdTe core/crown NPLs are synthesized having well-controlled CdTe crown region widths and higher PL-QY up to 40−50%. By using HAADF-STEM images with quantitative EDX analysis and XRD patterns, uniform and epitaxial growth of CdTe crown region is also confirmed. With increasing width of the CdTe crown region, CdSe/CdTe core/crown NPLs exhibit strongly red-shifted photoluminescence originating from the intermediate transition across the core/crown interface. In addition, they exhibit significantly increased radiative lifetime characteristically for spatially distinct excitons formed at the Type-II interfaces. Finally, we performed ligand exchange with 3-mercaptopropionic acid to reveal the potential of these NPLs as active media in advanced optoelectronic devices. With these promising properties, CdSe/CdTe core/crown NPLs hold great promise for next-generation light-harvesting applications.

Chapter 7

CdSe/CdSe$_{1-x}$Te$_x$ Core/Crown Heteronanoplatelets

This chapter of the thesis is based on the publication "CdSe/CdSe$_{1-x}$Te$_x$ Core/Crown Heteronanoplatelets: Tuning the Excitonic Properties without Changing the Thickness," **Y. Kelestemur**, B. Guzelturk, O. Erdem, M. Olutas, T. Erdem, C. F. Usanmaz, K. Gungor, and H. V. Demir, The Journal of Physical Chemistry C 121 (8), 4650-4658 (2017). Reprinted with permission from [93]. Copyright 2017 American Chemical Society.

7.1 Motivation

Free-standing semiconductor nanoplatelets with magic-sized vertical thickness, also widely known as colloidal quantum wells, have recently emerged as a highly promising class of semiconductor nanocrystals [15], [17], [133]. Owing to tight quantum confinement only in the vertical direction, the NPLs exhibit unique thickness-dependent optical properties. In addition to the core-only NPLs having different vertical thicknesses and chemical compositions [79], [80], [117], [134], different heterostructures of NPLs,

such as core/crown [18], [81], core/shell [19], [82], and core/crown/shell NPLs [94] can be synthesized to further engineer their electronic structure and optical properties. Also, depending on the band alignment between the core and crown or shell materials, either Type-I or Type-II electronic structures can be achieved [50], [51], [53] which results in favorable properties for various optoelectronic applications.

To date, core/crown and core/shell NPLs with Type-I electronic structure, in which electron and hole wave functions are confined in the same region of the NPLs, have been synthesized and studied extensively. In the core/crown and core/shell architectures, the passivation of the periphery and larger surfaces of core-only NPLs has been shown to improve the PL-QY and stability [18], [87]. Also, by growing CdS crown and shell regions, increased absorption cross section and suppressed Auger recombination with reduced blinking have been demonstrated [83], [84]. Moreover, tunable emission behavior has been realized with the synthesis of inverted CdS/CdSe core/crown heterostructure [101]. These appealing properties have led to the demonstrations of low threshold lasing [20], [84], [86], [109] and LEDs with high color purity [21] by using core/crown and core/shell NPLs having Type-I electronic structure. On the other hand, NPLs having Type-II electronic structure have not been studied extensively, despite their significant potential for optical gain and light-harvesting applications.

Several groups, including ours, have reported the synthesis and characterization of CdSe/CdTe core/crown NPLs having Type-II electronic structure with their exciting excitonic properties [95], [102], [135], [136]. In these NPLs, electrons are localized in the CdSe core while holes are confined in the CdTe crown, forming spatially indirect excitons. Therefore, they exhibit strongly red-shifted emission together with

138

significantly increased radiative florescence lifetimes. Also, these NPLs feature remarkably high PL-QY (up to ∼50%) when compared to other classes of semiconductor nanocrystals having Type-II electronic structure [95], [102]. In addition, it has been shown that owing to their large in-plane exciton mobility, ultrafast time scale charge separation at the core/crown interface enables the suppression of nonradiative recombination [136]. However, due to the quantum confinement occurring only in the vertical direction, CdSe/CdTe core/crown NPLs suffer from the limited tunability of their optical properties. Although the emission of CdSe/CdTe core/crown NPLs can be tuned within the range of ∼620−660 nm during the growth of the CdTe crown region, it quickly saturates at ∼660 nm and suffers from the lower PL-QY. Therefore, to further engineer their excitonic properties for advanced optoelectronic applications, novel NPL architectures are desired.

To address this need, here we synthesized $CdSe/CdSe_{1-x}Te_x$ NPLs with precisely tuned crown composition ranging from pure CdTe (x = 1.00) to almost pure CdSe doped with several Te atoms (x = 0.02) for tuning their excitonic properties. With the synthesis of core/crown NPLs having the same vertical thickness together with the same quantum confinement, we showed the systematic evolution of Type-II electronic structure experimentally. Also, by using the transmission electron microscopy, X-ray photoelectron spectroscopy, and X-ray diffraction, we demonstrated the highly monodisperse and uniform growth of $CdSe_{1-x}Te_x$ crown regions with targeted chemical compositions. In addition, we observed that the increase in the Te concentration within the crown region shifts the emission peak wavelength of $CdSe/CdSe_{1-x}Te_x$ NPLs continuously to lower energies with increased radiative fluorescence lifetimes. This behavior is explained by the transition from initial quasi Type-II electronic structure,

where holes are localized around Te atoms and electrons spread over both the core and crown region, to Type-II electronic structure, where holes are confined to the crown region and electrons are localized in the core region [137]. Moreover, $CdSe/CdSe_{1-x}Te_x$ core/crown NPLs exhibit substantially improved PL-QY (up to 95%), which can be attributed to the ultrafast localization of the photogenerated holes around Te atoms and their radiative recombination on the time scale of several tens of nanoseconds instead of nonradiative hole trapping commonly observed in NPLs [103], [136]. With their engineered and promising excitonic properties, $CdSe/CdSe_{1-x}Te_x$ core/crown NPLs are highly promising for high-efficiency light-emitting and -harvesting applications.

7.2 Colloidal Synthesis and Experiments

Chemicals. Cadmium nitrate tetrahydrate ($Cd(NO_3)_2 \cdot 4H_2O$) (99.997% trace metals basis), sodium myristate (>99%), technical-grade 1-octadecene (ODE), selenium (Se) (99.99% trace metals basis), tellurium (Te) (99.99% trace metals basis), cadmium acetate dihydrate ($Cd(OAc)_2 \cdot 2H_2O$) (>98%), technical-grade trioctylphosphine (TOP) (90%), and technical-grade oleic acid (OA) (90%) were purchased from Sigma-Aldrich. Hexane, ethanol, and methanol were purchased from Merck Millipore and used without any further purification.

Preparation of Cadmium Myristate. Cadmium myristate was synthesized by following the protocol reported in the literature [18]. For a typical synthesis, 1.23 g of cadmium nitrate tetrahydrate was mixed with 40 mL of methanol, and 3.13 g of sodium myristate was mixed with 250 mL of methanol. When the cadmium nitrate tetrahydrate and sodium myristate powders were completely dissolved, the solutions were mixed and stirred vigorously for ~1 h. Subsequently, the white cadmium myristate powders were

140

precipitated by using a centrifuge and dissolved in methanol. The cleaning step with methanol was repeated at least three times to remove any unreacted and/or excess precursors. Finally, the precipitated powders of cadmium myristate were kept overnight under vacuum for complete drying.

Synthesis of the 4 ML Thick CdSe NPLs. CdSe core NPLs having 4 ML thickness with an additional layer of Cd atoms were synthesized by using the slightly modified recipe from the literature [18]. For a typical synthesis, 340 mg of cadmium myristate, 24 mg of Se, and 30 mL of ODE were put into a three-neck flask, and the solution was evacuated at 100 °C for 1 h. After the complete removal of oxygen, water, and any other volatile solvents, the temperature of the solution was set to 240 °C under an argon atmosphere. When the color of the solution turned to bright yellowish, 110−120 mg of cadmium acetate dihydrate was injected into the reaction solution. Subsequently, the solution was kept for 10 min at 240 °C for further growth of NPLs. Then, with the injection of 1 mL of OA, the synthesis was stopped and the temperature of the solution was decreased to room temperature. As-synthesized NPLs were precipitated by adding ethanol. Finally, the precipitated NPLs were dissolved in hexane and stored for further crown coating steps.

Preparation of Anisotropic Growth Mixture for CdSe$_{1-x}$Te$_x$ Crown Region. Anisotropic growth mixture was prepared by using the previously published procedure with slight modifications [18]. For the cadmium precursor, 480 mg of cadmium acetate dihydrate, 340 μL of OA, and 2 mL of ODE were put into a three-neck flask. Then, the temperature of the solution was raised to 100 °C under ambient atmosphere and regular sonication. The heating and sonication processes continued alternatingly until the

formation of a homogeneous gel having whitish color. Following that, the cadmium precursor was stored for the successive crown coating. For the Se and Te precursors, 1 M TOP-Se and TOP-Te solutions were prepared inside a glovebox. Then, these solutions were diluted with the addition of ODE to achieve 0.03 M ODE-TOP-Te injection solution for the CdTe crown growth. Depending on the desired composition of the crown region, the concentration of injection solution was adjusted by mixing the 1 M TOP-Se and 1 M TOP−Te solutions.

Synthesis of 4 ML Thick CdSe/CdSe$_{1-x}$Te$_x$ Core/Crown NPLs. By using our previously published procedure, we executed the uniform growth of the CdSe$_{1-x}$Te$_x$ crown region around CdSe core NPLs [95]. For a typical CdTe crown coating, 1 mL of 4 ML thick CdSe NPLs dissolved in hexane (0.1 mL of stock solution dissolved in 3 mL of hexane has an optical density of ∼0.6 at 350 nm), 5 mL of ODE, 400 μL of cadmium precursor, and 50 μL of OA were put into a 50 mL three-neck flask. Then, the solution was evacuated at 100 °C for 1 h. After the complete removal of water, hexane, and any other organic solvents, the temperature of the solution was set to 240 °C under argon flow for the growth of the CdTe crown region. When the temperature reaches 240 °C, a certain amount of ODE-TOP-Te (0.03 M) solution was injected at a rate of 8 mL/h. To control the size of the crown region, the injection amount can be varied between 0.40 and 1.50 mL. After the complete injection of Te precursor, the resulting mixture was further annealed for 5 min at 240 °C. Then, the reaction was stopped and cooled down to room temperature. Owing to their increased lateral size, as-synthesized CdSe/CdTe core/crown NPLs were precipitated by centrifugation without adding any solvents, and they were dissolved in hexane for further characterization steps. For the synthesis of CdSe$_{1-x}$Te$_x$ crown region having different compositions, the same protocol described for

the growth of pure CdTe crown was used. The composition of the crown region can be tuned by simply changing the ratio of Te and Se in the injection precursor.

Preparation of NPL Integrated Light-Emitting Diode. A LED of the NPLs was prepared by embedding them into a two-component silicone (Dow Corning, OE-6630). For this purpose, the solvent from 750 µL of CdSe/CdSe$_{1-x}$Te$_x$ core/crown NPLs (~7.2 mg) was evaporated, and the NPLs were dispersed in 50 µL of hexane followed by the addition of 250 µL of the silicone mixture. To remove the air bubbles and remaining solvent, the mixture was kept under vacuum for 30 min. Subsequently, 200 µL of the NPLs-silicone mixture was placed on a glass substrate and hardened at 75 °C overnight. Finally, the obtained film was transferred onto an Edison near-UV-LED emitting at 400 nm. The optical characterizations of the LED were carried out by measuring the emission intensity using an Ocean Optics integrating sphere and Maya 2000 spectrometer. CIE 1931 color coordinates were calculated using an in-house written MATLAB code.

Photoluminescence Quantum Yield Measurements. The PL-QY measurements were carried out using the methodology reported by de Mello et al [91]. The measurement setup was constructed using a HoribaYvon integrating sphere and Maya 2000 spectrometer.

7.3 Results and Discussion

In this study, we synthesized CdSe/CdSe$_{1-x}$Te$_x$ core/crown NPLs having different crown compositions by employing the core-seeded-growth approach. First, we started with the synthesis of 4 ML thick CdSe core-only NPLs having an additional layer of Cd atoms owing to their well-defined synthesis conditions (see the Experimental Section for

details). Absorption and photoluminescence spectra of CdSe core NPLs are given in Figure 7.1a. Thanks to the synthesis of CdSe core NPLs having magic-sized vertical thickness and atomically-flat surfaces, they exhibit a very narrow emission bandwidth (~9 nm) with moderately high PL-QY (30−40%). From the absorption spectra, splitting of sharp excitonic features, including electron-light hole (~480 nm) and electron-heavy hole transitions (~512 nm), is observed, suggesting the formation of a quantum well like electronic structure. Also, the highly monodisperse and uniform growth of 4 ML thick CdSe core-only NPLs can be clearly seen in the HAADF-STEM images given in Figure 7.1b. They feature almost rectangular shape with lateral dimensions of 16.44 ± 1.72 and 12.60 ± 1.47 nm. These CdSe core-only NPLs were used as a seed for the further synthesis of CdSe/CdSe$_{1-x}$Te$_x$ core/crown NPLs with varied crown compositions.
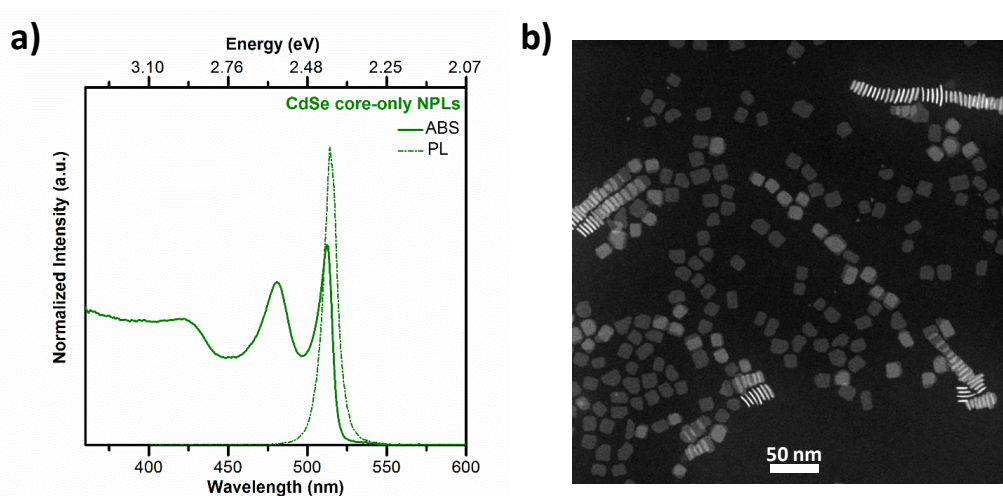
Figure 7.1. (a) Absorption (solid line) and photoluminescence (dotted−dashed line) spectra and (b) HAADF-STEM images of the 4 ML thick CdSe core-only NPLs dissolved in hexane at room temperature, having a lateral size of 16.4 ± 1.7 nm by 12.6

± 1.5 nm. Reprinted with permission from [93]. Copyright 2017 American Chemical Society.

By using freshly synthesized CdSe core-only NPLs as a seed, we grew $CdSe_{1-x}Te_x$ crown region with different crown compositions. First, we determined the optimal crown size by synthesizing core/crown NPLs having pure CdTe crown regions with different lateral sizes. While CdSe/CdTe core/crown NPLs having a smaller CdTe crown exhibit additional lateral confinement [78], [95], [102], CdSe/CdTe core/crown NPLs with a larger CdTe crown suffer from serious stability issues and lower PL-QY (Figure 7.2). Therefore, we preferred the synthesis of core/crown NPLs with medium crown size exhibiting pure vertical confinement together with improved PL-QY and stability. For the synthesis of $CdSe/CdSe_{1-x}Te_x$ core/crown NPLs having a similar crown size to that of the optimized pure CdTe crown region, the same amount of anisotropic growth mixture precursors was injected. In addition, by changing the concentration of Te and Se in the injection solution, the composition of the crown region was tuned and $CdSe/CdSe_{1-x}Te_x$ core/crown NPLs with a specific crown composition ranging from pure CdTe crown to almost pure CdSe crown doped with several Te atoms were synthesized (see Experimental Section for details).
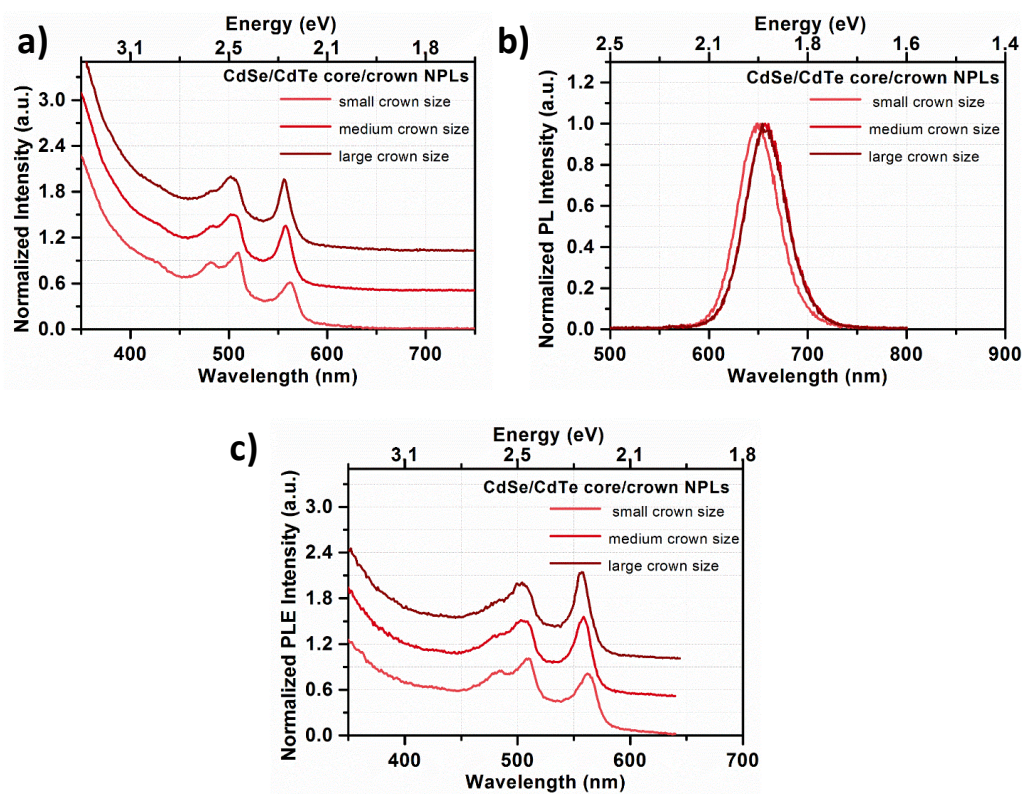
Figure 7.2. (a) Normalized absorption, (b) photoluminescence and (c) photoluminescence excitation spectra of CdSe/CdTe core/crown NPLs having different CdTe crown size. Reprinted with permission from [93]. Copyright 2017 American Chemical Society.

We carried out the structural characterizations of CdSe/CdSe$_{1-x}$Te$_x$ core/crown NPLs, including transmission electron microscopy, X-ray photoelectron spectroscopy, and X-ray diffraction, for a better understanding of the size, shape, and composition of the crown region. HAADF-STEM images of CdSe/CdSe$_{1-x}$Te$_x$ core/crown NPLs having different crown compositions are shown in Figures 7.3 and 7.4. As can be clearly seen from the HAADF-STEM images, the resulting core/crown NPLs having different crown compositions exhibit high monodispersity in size and uniform growth of the crown

region in the lateral direction with sharp boundaries. Owing to the same amount of anisotropic growth mixture injection for the formation of crown regions, the lateral areas of the crown with different crown compositions were found to be similar (Table 7.1). Furthermore, with increasing Se composition in the crown region, the shape of the core/crown NPLs was changed from rectangular to almost square shape, which can be attributed to the variation of the favorable growth direction depending on the composition. For example, while CdSe/CdTe core/crown NPLs (x = 1.00) feature lateral dimensions of 29.11 ± 3.00 and 22.79 ± 2.20 nm, CdSe/CdSe$_{1-x}$Te$_x$ core/crown NPLs (x = 0.02) have lateral dimensions of 25.69 ± 1.61 and 22.97 ± 1.98 nm.
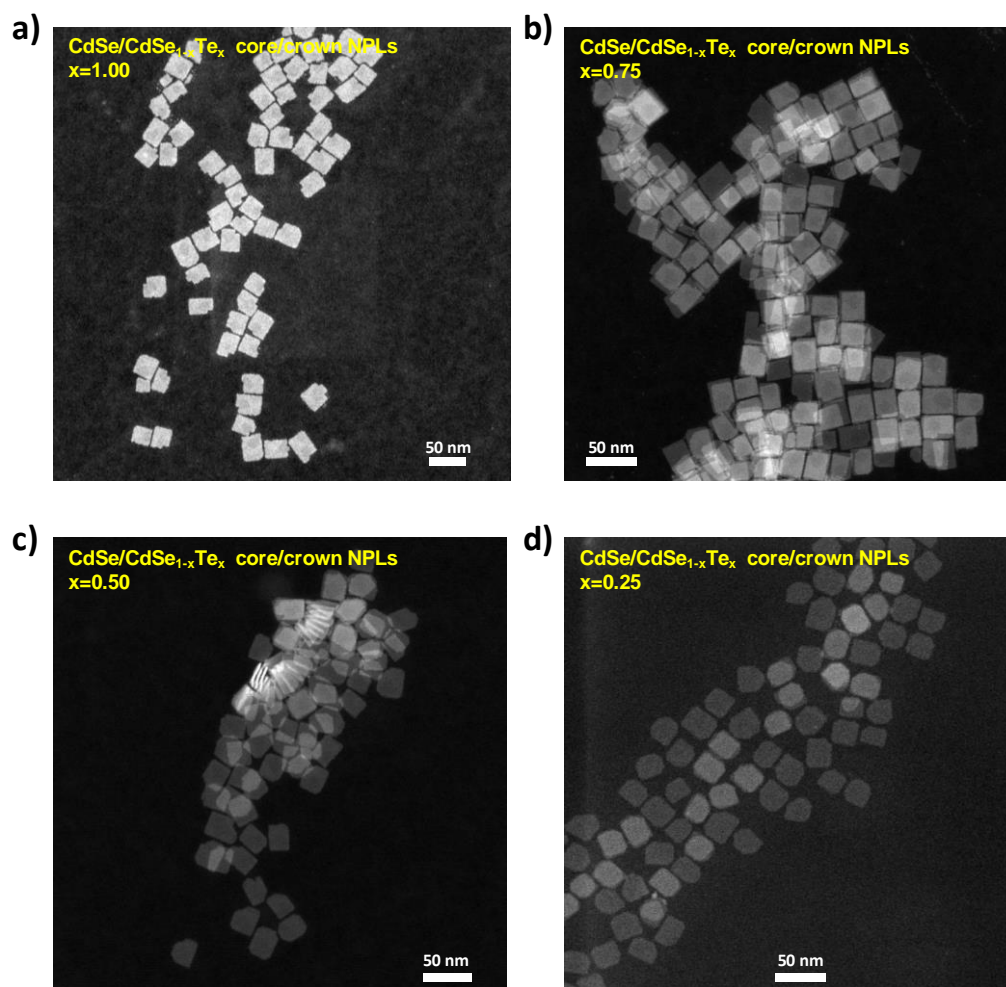
Figure 7.3. HAADF-STEM images of the CdSe/CdSe$_{1-x}$Te$_x$ core/crown NPLs for different Te compositions (a) x = 1.00, (b) x = 0.75, (c) x = 0.50, and (d) x = 0.25 in the crown region. Reprinted with permission from [93]. Copyright 2017 American Chemical Society.
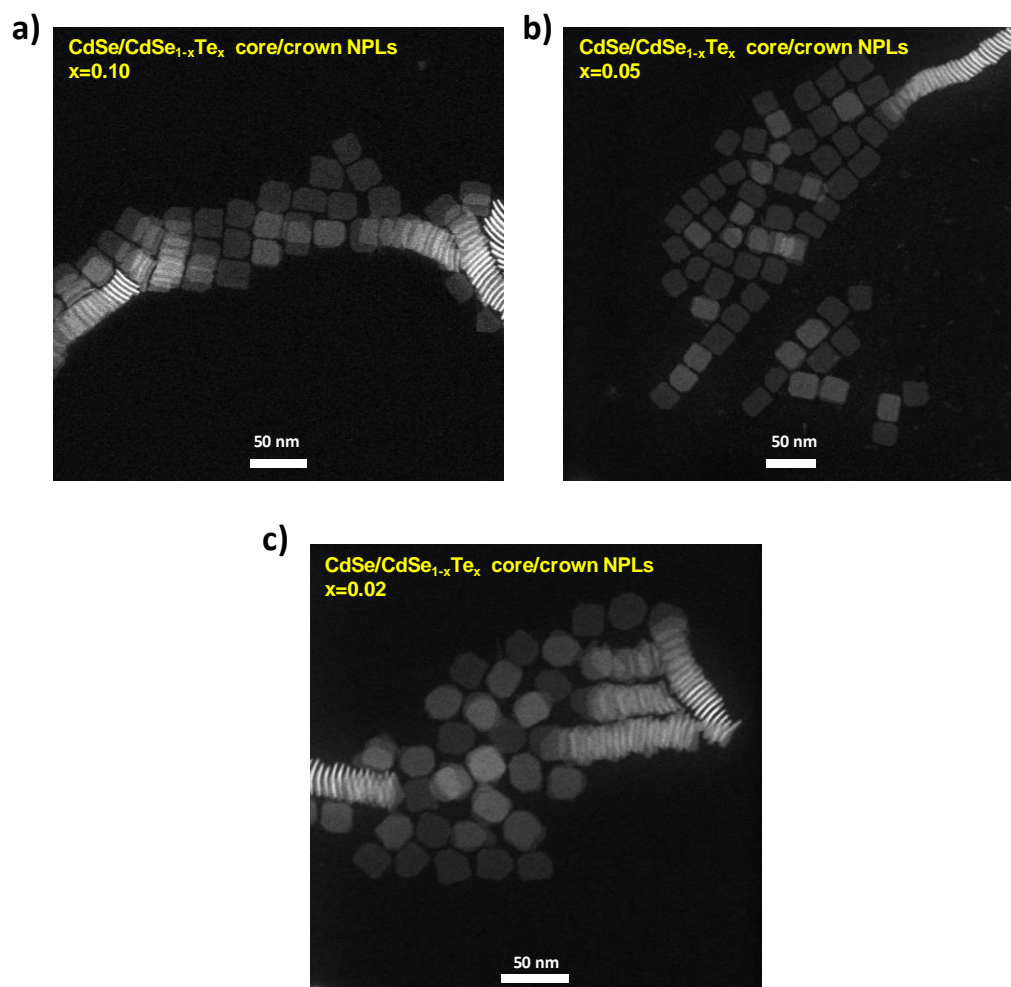
Figure 7.4. HAADF-STEM images of the CdSe/CdSe$_{1-x}$Te$_x$ core/crown NPLs for different Te compositions (a) x = 0.10, (b) x = 0.05, and (c) x = 0.02 in the crown region. Reprinted with permission from [93]. Copyright 2017 American Chemical Society.

Table 7.1. Lateral dimensions of CdSe/CdSe$_{1-x}$Te$_x$ core/crown NPLs having different crown compositions obtained from the HAADF-STEM images. Reprinted with permission from [93]. Copyright 2017 American Chemical Society.

CdSe/CdSe$_{1-x}$Te$_x$ core/crown NPLs	Long axis (nm)	Short axis (nm)
x=1.0	29.11 ± 3.00	22.79 ± 2.20
x=0.75	26.91 ± 2.90	21.07 ± 2.56
x=0.50	28.67 ± 2.80	21.07 ± 1.69
x=0.25	28.06 ± 1.86	21.82 ± 2.17
x=0.10	26.67 ± 2.72	22.13 ± 1.89
x=0.05	25.89 ± 2.45	22.91 ± 1.37
x=0.02	25.69 ± 1.61	22.97 ± 1.98

In addition, we performed energy-dispersive X-ray spectroscopy for single CdSe/CdSe$_{1-x}$Te$_x$ core/crown NPL (x = 1.00, 0.50, and 0.25) to investigate the uniformity of core/crown architecture and chemical compositions (Figure 7.5). The results showed that while the CdSe core region generally located in the inner part of the NPL, it was covered with a laterally extended CdSe$_{1-x}$Te$_x$ crown region. Also, it has been observed that the composition of the CdSe$_{1-x}$Te$_x$ region is almost similar to the concentration of the injection solutions, suggesting that the composition of the crown region can be precisely tuned.
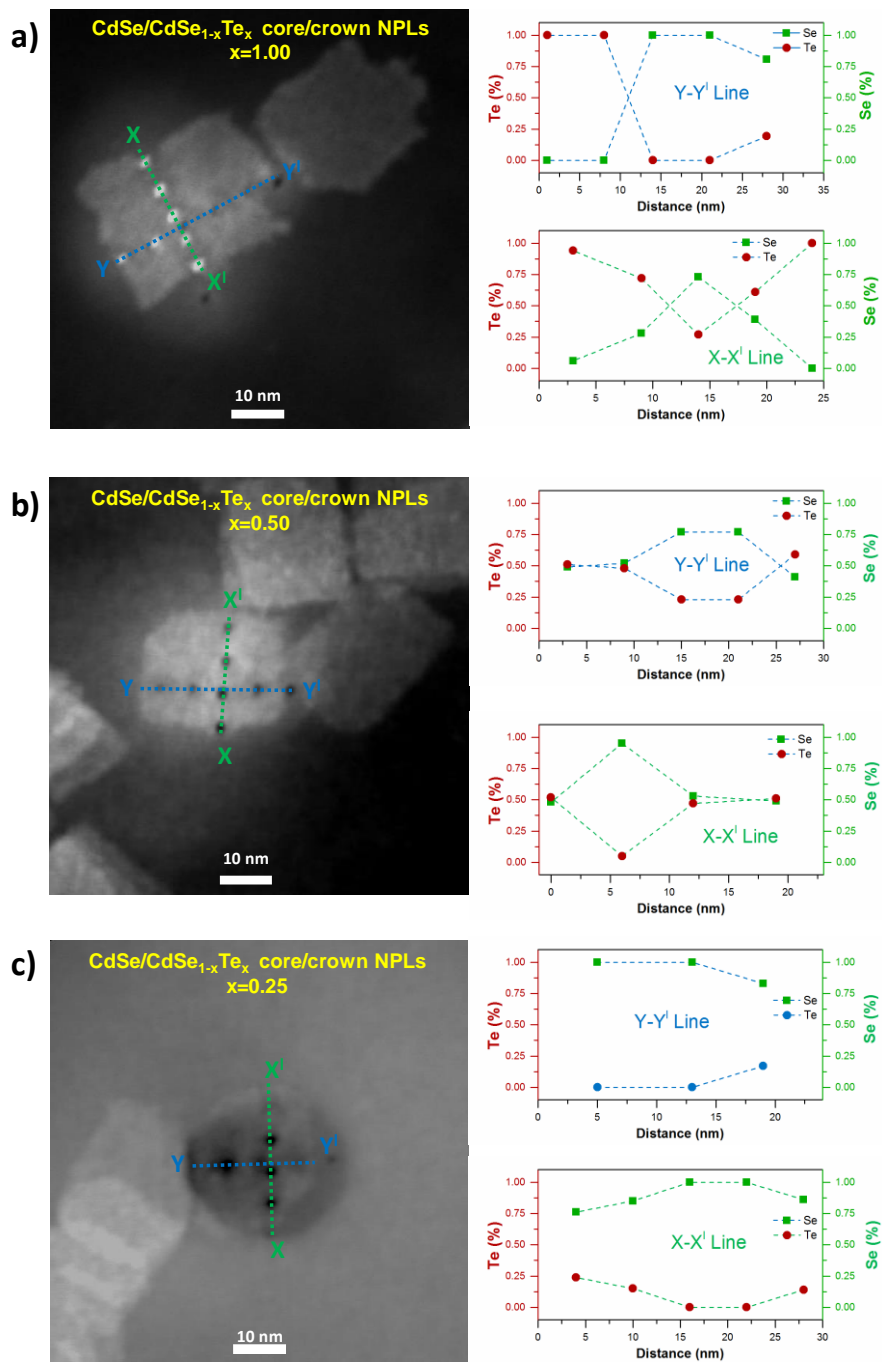
Figure 7.5. HAADF-STEM image of a single CdSe/CdSe$_{1-x}$Te$_x$ core/crown NPL with blue (Y−Yl) and green lines (X−Xl) showing the EDX probe position on core/crown NPL together with their line EDX analysis reporting the compositions of selenium and tellurium in the CdSe/CdSe$_{1-x}$Te$_x$ core/crown NPL, having different crown compositions

(a) x = 1.00, (b) x = 0.50, and (c) x= 0.25. Reprinted with permission from [93]. Copyright 2017 American Chemical Society.

We also analyzed the composition of the $CdSe_{1-x}Te_x$ crown region by using X-ray photoelectron spectroscopy. With the contribution from both the core and crown regions, the concentration of Se was found to be higher than that of Te in the ensemble measurements (except x = 1.00 and 0.75) (Table 7.2). Then, by using the ratio of lateral size between the core and crown obtained from the HAADF-STEM images, the composition of the crown regions was calculated from the ensemble measurements (Table 7.3). The compositions of the crown regions were found to be similar to the concentration of the injection solutions, except the $CdSe/CdSe_{1-x}Te_x$ core/crown NPLs (x = 0.02) having very low Te concentration in the crown region. This can be attributed to the very weak intensity levels collected from the sample, resulting in an overestimated calculation. Thus, the synthesis of $CdSe/CdSe_{1-x}Te_x$ core/crown NPLs having similar crown areas with desired composition strongly suggest the similar reactivities of Te and Se, enabling the achievement of tunable excitonic properties in a controlled way.

Table 7.2. Chemical composition of CdSe/CdSe$_{1-x}$Te$_x$ core/crown NPLs having different crown compositions obtained from the XPS. Reprinted with permission from [93]. Copyright 2017 American Chemical Society.

CdSe/CdSe$_{1-x}$Te$_x$ core/crown NPLs	Chemical compositions (at. %)		
	Cd (%)	Se$_{total}$ (%)	Te$_{total}$ (%)
x = 1.0	50.87	15.31	33.82
x = 0.75	49.86	23.66	26.48
x = 0.50	48.94	32.67	18.39
x = 0.25	47.90	43.77	8.33
x = 0.10	48.97	47.52	3.51
x = 0.05	46.60	51.07	2.34
x = 0.02	46.78	51.26	1.97
x = 0	49.66	50.34	-

Table 7.3. Chemical composition of CdSe$_{1-x}$Te$_x$ crown region obtained from the XPS. Reprinted with permission from [93]. Copyright 2017 American Chemical Society.

Chemical composition of the CdSe$_{1-x}$Te$_x$ crown region from XPS	
Injected	XPS
x = 1.00	x = 1.00
x = 0.75	x = 0.64
x = 0.50	x = 0.46
x = 0.25	x = 0.22
x = 0.10	x = 0.10
x = 0.05	x = 0.07
x = 0.02	x = 0.06

We also studied the crystal structure of CdSe/CdSe$_{1-x}$Te$_x$ core/crown NPLs having different crown compositions with powder X-ray diffraction. The powder diffraction patterns of CdSe/CdSe$_{1-x}$Te$_x$ core/crown NPLs are presented in Figure 7.6. CdSe core-only NPLs exhibit zinc blende crystal structure with broader diffraction peaks owing to

their finite crystal size. Furthermore, the relative intensities of diffraction peaks were observed to be different when compared to those of their bulk counterparts, suggesting the growth of an anisotropic shape with a preferred growth direction. In addition, as the crown regions having different compositions were grown, the initial zinc blende crystal structure was preserved. However, increasing the concentration of Te in the crown region continuously shifts the diffraction peaks to lower angles, which further suggests the formation of an alloyed crown region. Moreover, by applying Vegard's law for the (022) plane, we roughly estimated the composition of the crown region, which is tabulated in Table 7.4. However, due to contribution from both the CdSe core and $CdSe_{1-x}Te_x$ crown regions in the diffraction patterns with their broader diffraction peaks, the compositions estimated from the powder diffraction patterns exhibit slight deviations.
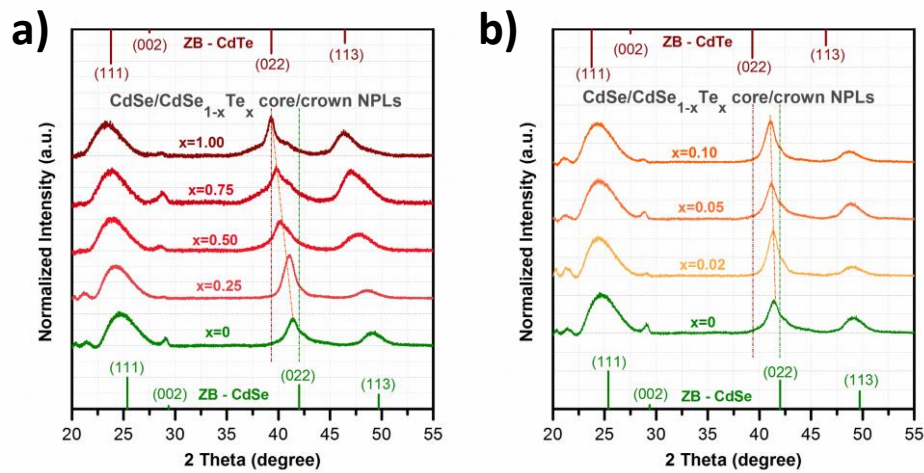
Figure 7.6. X-ray diffraction patterns of the 4 ML thick CdSe core-only NPLs and the $CdSe/CdSe_{1-x}Te_x$ core/crown NPLs having different crown compositions. The green (on the bottom) and the brown bars (on the top) show the diffraction peaks of the bulk CdSe

154

and bulk CdTe having zinc blende (ZB) structure, respectively. Reprinted with permission from [93]. Copyright 2017 American Chemical Society.

Table 7.4. Chemical composition of $CdSe_{1-x}Te_x$ crown region obtained from the XRD. Reprinted with permission from [93]. Copyright 2017 American Chemical Society.

Chemical composition of the $CdSe_{1-x}Te_x$ crown region from XRD	
Injected	Vegard's Law for (022) plane
x = 1.00	x = 1.00
x = 0.75	x = 0.76
x = 0.50	x = 0.58
x = 0.25	x = 0.17
x = 0.10	x = 0.14
x = 0.05	x = 0.08
x = 0.02	x = 0.03

After the complete analysis of the structural characterization, including the size, shape, and composition of the crown region, we systematically studied the resulting optical properties of $CdSe/CdSe_{1-x}Te_x$ core/crown NPLs. Their absorption and PL spectra are presented in Figure 7.7a. With the formation of a pure CdTe crown region, a new peak emerges around ~556 nm and makes a strong contribution to the absorption of the core/crown NPLs in the lower-energy side of the spectrum. Since the crown region was grown only in the lateral dimensions, the excitonic features of CdSe core NPLs remained almost in the same spectral positions. However, owing to formation and recombination of spatially indirect excitons at the core/crown interface, where electrons are localized in the CdSe core region and holes are confined to the CdTe crown region, they exhibit significantly red-shifted emission (~656 nm) with a broadened spectrum. In addition, when compared to other classes of semiconductor nanocrystals having Type-II electronic structure and CdSe core-only NPLs, they exhibit relatively high PL-QY

(∼30−50%). However, owing to the pure vertical confinement in this material system, their emission wavelengths remain almost in the same spectral position upon changing the size of the CdTe crown region and suffer from the limited tunability.
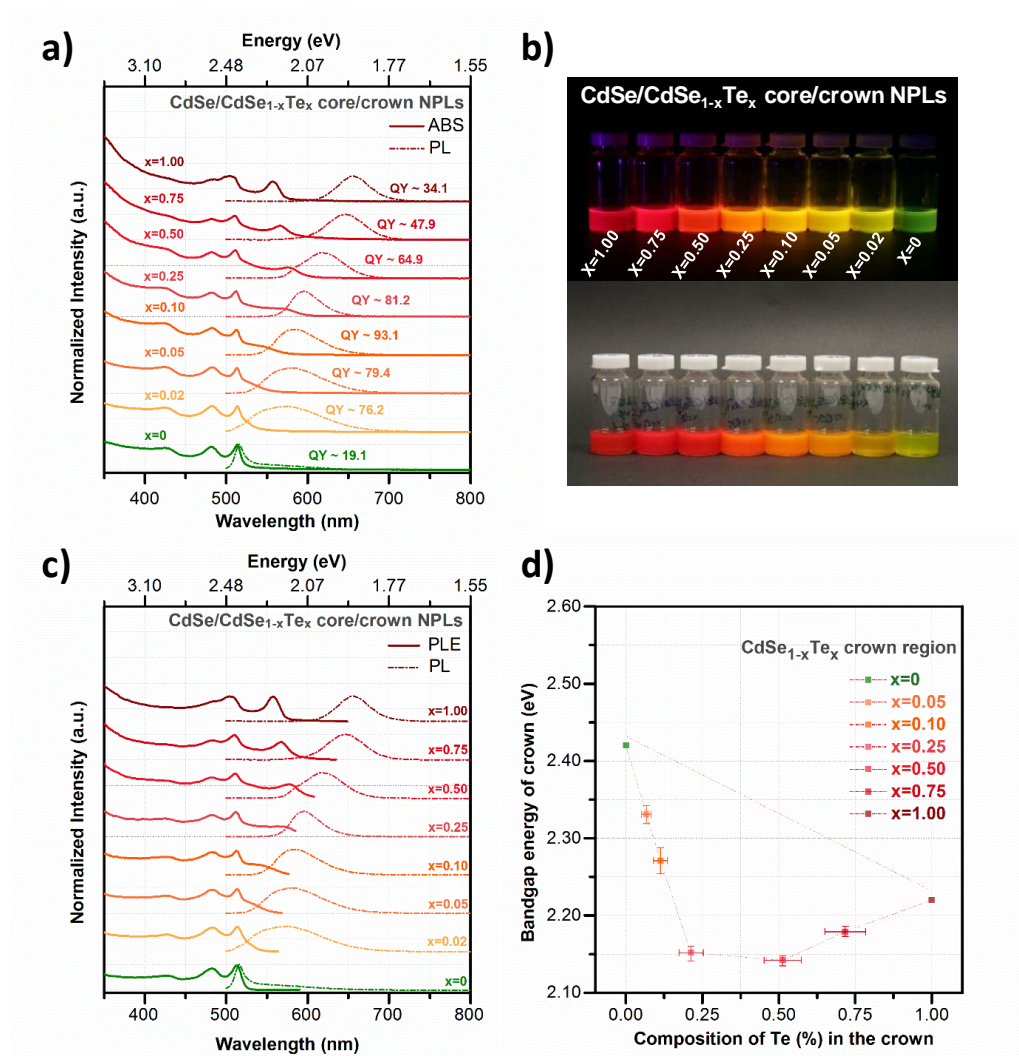
Figure 7.7. (a) Evolution of the absorption and photoluminescence spectra along with PL-QY as a function of the $CdSe_{1-x}Te_x$ crown region composition. (b) The real color images of $CdSe/CdSe_{1-x}Te_x$ core/crown NPLs having different crown compositions dissolved in hexane under UV light (top) and ambient light (bottom). (c) Photoluminescence excitation spectra of the $CdSe/CdSe_{1-x}Te_x$ core/crown NPLs

together with their photoluminescence and (d) extracted band gap energy of the crown region as a function of the composition of the Te in the crown. Reprinted with permission from [93]. Copyright 2017 American Chemical Society.

To realize tunable excitonic properties without changing the vertical thickness of the NPLs, we engineered the band gap of the crown region by adjusting the composition. As can be seen from Figure 7.7a, increasing the concentration of Se in the crown region allowed for continuously tuning the emission of core/crown NPLs from ~660 nm (for $CdSe_{1-x}Te_x$ crown with x = 1.00) to ~570 nm (for $CdSe_{1-x}Te_x$ crown with x = 0.02). The continuous shift of the emission spectrum can be explained by the decrease in the hole energy levels by tailoring the composition of the crown region, which can be clearly seen from the extracted relative band offsets of the $CdSe/CdSe_{1-x}Te_x$ core/crown NPLs having different compositions (Figures 7.7a, and 7.7b) [137]. Thus, the recombination energy of the electrons localized in the CdSe core region and the holes confined in the $CdSe_{1-x}Te_x$ crown region increases and results in a continuous blue-shifting in the emission spectrum. Also, $CdSe/CdSe_{1-x}Te_x$ core/crown NPL exhibit significantly broadened emission spectrum as compared to the CdSe core-only NPLs (~40 meV). This is a common feature of colloidal semiconductor nanocrystals having Type-II electronic structure and can be explained by the spatially indirect exciton recombination [51], [102]. In addition, the same excitonic features observed from the PLE spectra of $CdSe/CdSe_{1-x}Te_x$ core/crown NPLs taken at different emission wavelengths have ruled out the possibility of inhomogeneous broadening due to the composition variation in the crown region and suggested the formation of a crown region with well-defined and homogeneous compositions (Figure 7.8).
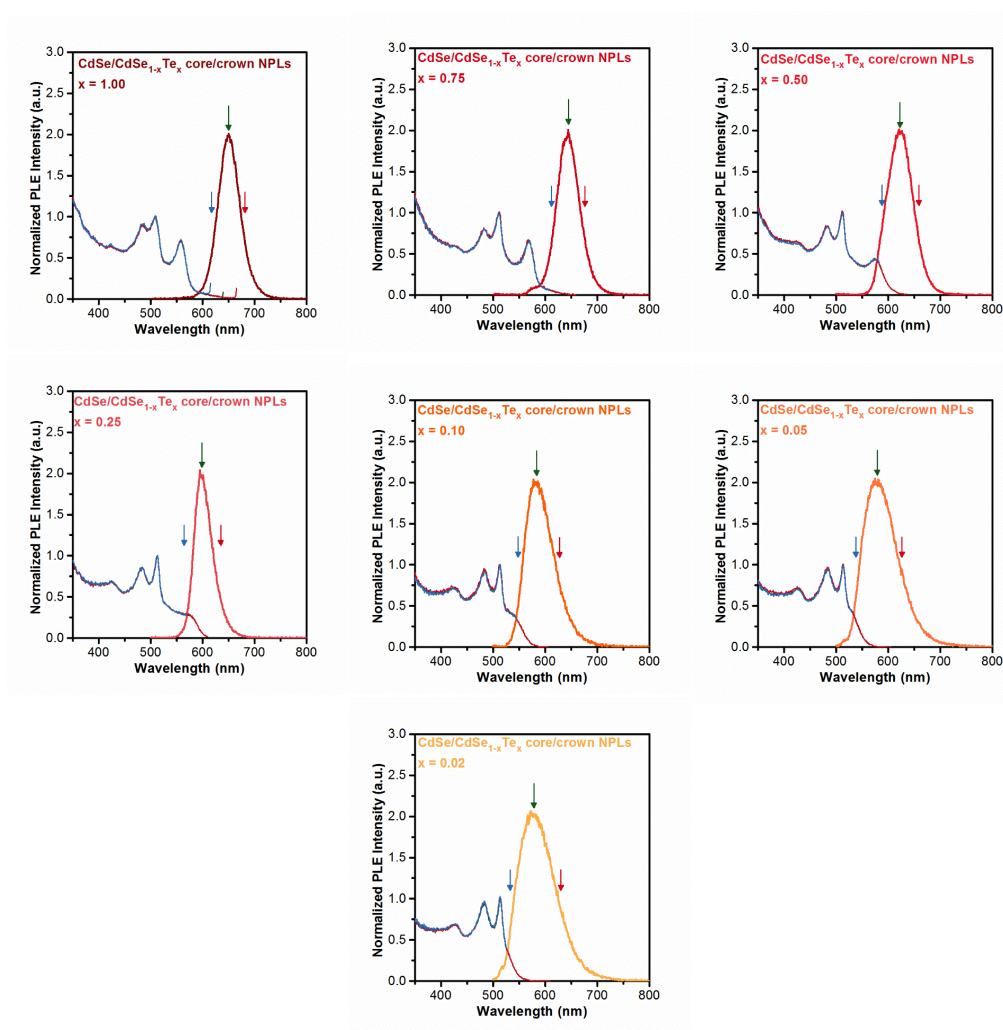
Figure 7.8. Photoluminescence excitation spectra of CdSe/CdSe$_{1-x}$Te$_x$ core/crown NPLs having different crown composition taken at different emission wavelength. Reprinted with permission from [93]. Copyright 2017 American Chemical Society.

It is also important to note that while CdSe/CdSe$_{1-x}$Te$_x$ core/crown NPLs (x ≥ 0.25) feature broadened emission spectra (∼140−190 meV) with respect to CdSe core-only NPLs, CdSe/CdSe$_{1-x}$Te$_x$ core/crown NPLs (x ≤ 0.10) exhibit further broadened emission (up to ∼360 meV) with increasing Se concentration in the crown region. This behavior can be explained by the transition from Type-II electronic structure (for x ≥ 0.25), where

spatially indirect excitons recombine at the core/crown interface, to quasi Type-II electronic structure (for $x \leq 0.10$), where Te atoms act as deep hole-trap sites. In previous studies, similar behavior was also observed for Te-doped CdSe quantum dots and attributed to the size distribution of quantum dots, resulting in different quantum confinement among the quantum dots within the ensemble solution [138], [139]. However, because of the pure vertical quantum confinement in our NPLs, the further broadened emission behavior cannot be explained by the difference in the quantum confinement. Therefore, together with the homogeneous broadening, the fluctuation of the Te composition and variation of Te location within the NPLs should be responsible for the further broadening.

We also measured the PL-QY of $CdSe/CdSe_{1-x}Te_x$ core/crown NPLs. With the laterally extended $CdSe_{1-x}Te_x$ crown region, $CdSe/CdSe_{1-x}Te_x$ core/crown NPLs exhibit substantially improved PL-QY (up to $\sim$95%) as compared to that having a pure CdTe or CdSe crown region. The relatively high PL-QY of $CdSe/CdSe_{1-x}Te_x$ core/crown NPLs with respect to other classes of semiconductor nanocrystals having Type-II electronic structure can be explained by several factors. First, with increasing Se concentration in the crown region, the overlap of electron and hole wave functions in the $CdSe/CdSe_{1-x}Te_x$ core/crown NPLs is significantly increased when compared to $CdSe/CdSe_{1-x}Te_x$ core/crown NPLs having a pure CdTe crown region ($x = 1.00$), resulting in the enhanced PL-QY. Second, the substitution of Te atoms with Se atoms in the crown region decreases the lattice mismatch between the core and crown region. Thus, the possibility of strain and/or defect formation, which act as trap sites, is reduced. Finally, the localization of the photogenerated holes in the $CdSe_{1-x}Te_x$ crown region and/or around Te atoms, which is followed by radiative recombination, competed with

the nonradiative hole trapping commonly observed in NPLs owing to absence of proper surface passivation. In other words, the localization of the holes in the engineered $CdSe_{1-x}Te_x$ crown and/or around Te atoms, instead of being captured by surface trap sites, and their radiative recombination on the time scale of several tens of nanoseconds contributed to the improved the PL-QY. Also, the observation of both the ultrafast exciton localization ($\sim$0.65 ps) at the core/crown interface in CdSe/CdTe core/crown NPLs and ultrafast hole trapping around Te atoms on a sub-picosecond time scale in Te-doped CdSe quantum dots further supports this hypothesis [136], [140]. The dramatically improved PL-QY of CdSe core NPLs from $\sim$19.1% to 76.2% upon replacing several Se atoms by Te atoms in the CdSe crown region (x = 0.02) shows the efficient localization of photogenerated holes around Te atoms instead of their capture by the surface trap sites.

In addition to the tunable emission behavior of $CdSe/CdSe_{1-x}Te_x$ core/crown NPLs with significantly improved PL-QY, these NPLs show interesting absorption behavior. Owing to the growth of the crown regions only in the lateral direction, excitonic absorption features of CdSe core NPLs preserved their spectral positions for all different crown compositions. On the other hand, the excitonic absorption features of the $CdSe_{1-x}Te_x$ crown region exhibit a nonlinear relationship between the compositions (Figure 7.6d). From the absorption spectra of the core/crown NPLs, we extracted the band gap energies of the crown regions having different compositions. It is observed that the band gap energies of the crown region do not change linearly with the composition as predicted by Vegard's law and exhibit a strongly nonlinear effect, which is called as "optical bowing". This kind of behavior has already been observed for alloyed

nanocrystal quantum dots and attributed to structural and electronic factors, including different atomic radii and the electronegativity of the ions [141].

For a deeper understanding of the excitonic properties of CdSe/CdSe$_{1-x}$Te$_x$ core/crown NPLs depending on the composition of the crown region, we performed time-resolved fluorescence spectroscopy. TRF measurements were carried out under low excitation intensities to avoid multiexciton generation by using core/crown NPL solutions having low concentrations. Fluorescence decay curves of CdSe core and CdSe/CdSe$_{1-x}$Te$_x$ core/crown NPLs (for x = 1.00, 0.50, and 0.10) and their amplitude-averaged fluorescence lifetimes (τ_{av}) are presented in Figures 7.9c and 7.9d. Owing to the complex emission kinetics of NPLs, the decay curves were fitted by using four-exponential decay functions so that the reduced χ^2 values remain about 1 with uniform residuals. As can be seen from Figure 7.9b, with increasing Te concentration in the crown region, we observed continuously increased τ_{av} from ∼1.5 ns (for CdSe core-only NPLs) to ∼326.2 ns (for CdSe/CdSe$_{1-x}$Te$_x$ core/crown NPLs with x = 1.00). Also, while CdSe/CdSe$_{1-x}$Te$_x$ core/crown NPLs (x = 0.02) had a τ_{av} of ∼49.2 ns, CdSe/CdSe$_{1-x}$Te$_x$ core/crown NPLs (x = 1.00) having a pure CdTe crown region exhibit a strongly elongated τ_{av} of ∼326.2 ns. This can be explained by transitioning from a quasi Type-II electronic structure to a Type-II electronic structure. With the substitution of several Se atoms with Te in the crown region, CdSe/CdSe$_{1-x}$Te$_x$ core/crown NPLs (x ≤0.10) possess quasi Type-II structure, where Te atoms acts as deep hole trap sites and holes are localized around Te atoms (Figure 7.9b). Our findings are also strongly consistent with the recent study of Tenne et al., who reported that the fluorescence lifetime of Te-doped CdSe NPLs was dominated by the lifetime component of ∼50 ns [142]. On the other hand, CdSe/CdSe$_{1-x}$Te$_x$ core/crown NPLs having a higher Te concentration (x ≥ 0.25)

exhibit Type-II electronic structure, where holes are localized around the crown region and electrons are confined to the core. This increased separation of electron and hole wave functions results in increased fluorescence lifetimes in $CdSe/CdSe_{1-x}Te_x$ core/crown NPLs. Therefore, this series of observations demonstrate the evolution of the band alignment from quasi Type-II to Type-II experimentally.
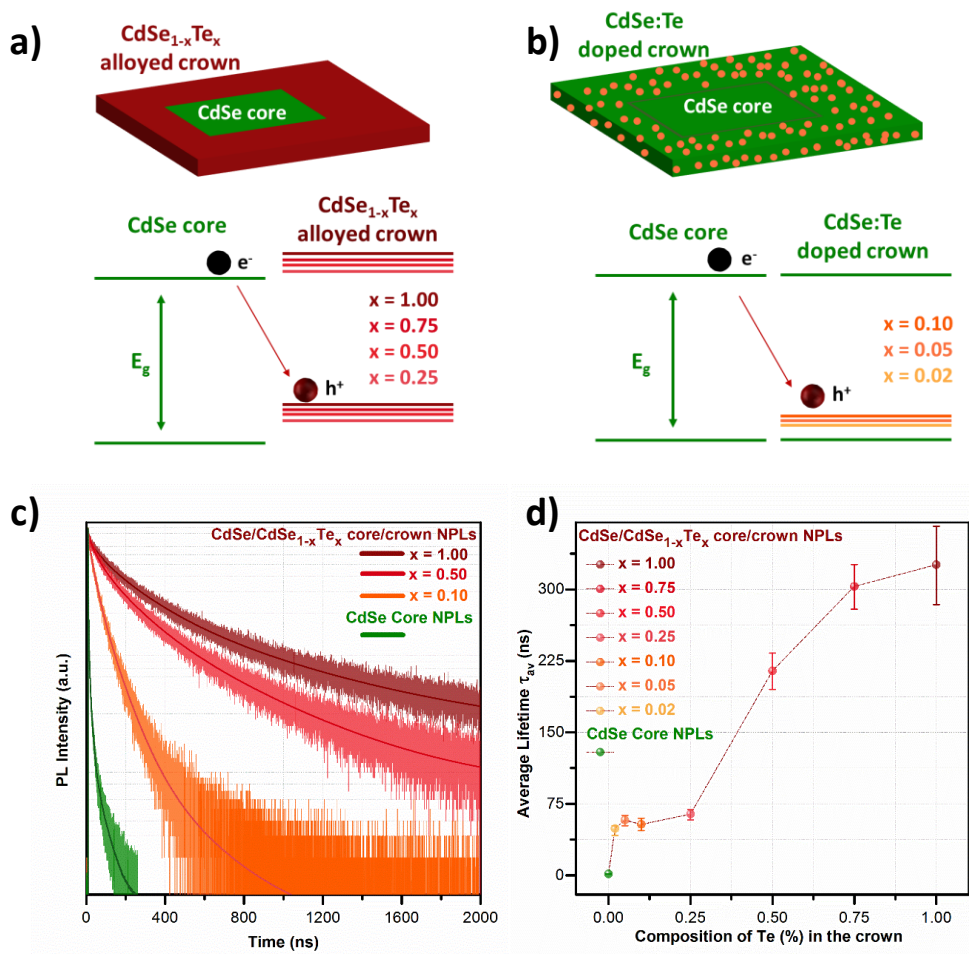
Figure 7.9. Schematic demonstration of band diagrams of the $CdSe/CdSe_{1-x}Te_x$ core/crown NPLs (a) for $x \geq 0.25$, and (b) for $x \leq 0.10$. (c) Time-resolved fluorescence decay curves of the CdSe core and $CdSe/CdSe_{1-x}Te_x$ core/crown NPLs for different crown region compositions (e.g., x = 1.00, 0.50, and 0.10). The solid lines on the decay

curves represent the four-exponential fitting curves. (d) Amplitude-averaged fluorescence lifetimes of the CdSe/CdSe$_{1-x}$Te$_x$ core/crown NPLs with tuned crown compositions. Reprinted with permission from [93]. Copyright 2017 American Chemical Society.

Finally, we demonstrated a proof-of-concept color-converting LED employing CdSe/CdSe$_{1-x}$Te$_x$ core/crown NPLs. For this purpose, we prepared a film of NPLs (x = 0.05) in a commercially available silicone and integrated it onto a near-UV-LED emitting at 400 nm. The spectrum of the obtained LED is presented in Figure 7.10, along with the chromaticity coordinates and luminous efficiency (LE) in the insets. We observe that the emitted yellowish color corresponds to around (0.48, 0.33) on the CIE 1931 chromaticity diagram and its LE takes values up to 9.5 lm/W$_{elect}$.
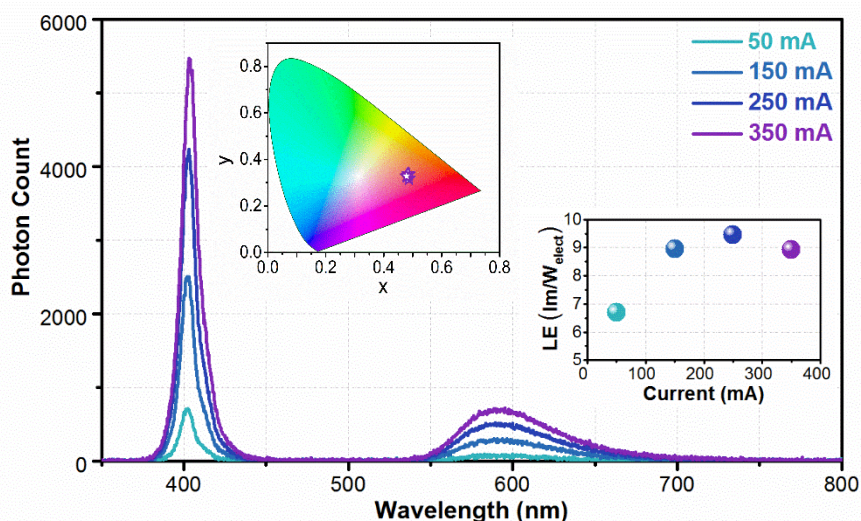
Figure 7.10. Emission spectra of the NPL-integrated LED at varying currents along with luminous efficiency (LE) (inset, right) and CIE 1931 color coordinates (inset, left). Reprinted with permission from [93]. Copyright 2017 American Chemical Society.

7.4 Summary

In summary, we have demonstrated the synthesis of CdSe/CdSe$_{1-x}$Te$_x$ core/crown NPLs with precisely tuned crown composition from pure CdTe to almost pure CdSe doped with several Te atoms. Thanks to the same vertical quantum confinement in the core/crown architectures, we have shown experimentally the evolution of Type-II electronic structure. Also, with engineering the band gap of the crown region, we have successfully tuned the excitonic properties of the NPLs without changing their thickness. Moreover, by the substitution of several Se atoms with Te in the crown region, we have substantially improved the PL-QY (up to 95%), which can be attributed to the suppressed nonradiative hole trap sites. When compared to previously synthesized doped semiconductor nanocrystals having lower PL-QY, the near unity PL-QY of CdSe/CdSe$_{1-x}$Te$_x$ core/crown NPLs can be attributed to the large in-plane exciton mobility and higher exciton binding energies observed in these atomically-flat semiconductor NPLs. Considering these appealing and tunable excitonic properties, CdSe/CdSe$_{1-x}$Te$_x$ core/crown NPLs have become highly attractive for advanced optoelectronic applications. With their large Stoke-shifted emission and near unity PL-QY, CdSe/CdSe$_{1-x}$Te$_x$ core/crown NPLs have become highly promising candidates for highly efficient luminescent solar concentrators and low threshold optical gain.

Chapter 8

Conclusion

In this chapter, we summarize our thesis with concluding remarks and future outlook about the colloidal quantum wells. Subsequently, we present our contribution to the literature.

8.1 Concluding Remarks

Within the scope of our thesis, we demonstrated the synthesis and characterization of novel heterostructured NPLs to further exploit the benefits of these solution-processed nanocrystals for the utilization of next-generation optoelectronic devices.

These two-dimensional semiconductor NPLs with their atomically-flat surfaces and magic-sized vertical thicknesses exhibit fascinating excitonic properties including narrower emission linewidths, giant oscillator strength, ultrafast fluorescence lifetimes and larger absorption cross-section. Also, the colloidal synthesis of heterostructured NPLs such as core/crown and core/shell architectures has led to the realization of the

improved optical properties as compared to core-only NPLs. However, these previously demonstrated heterostructured NPLs suffer from serious stability issues due to lack of proper passivation on their larger lateral surfaces and/or the formation of trap sites during the shell growth. To address these problems, in Chapter 4, we demonstrated the successful synthesis of CdSe/CdS@CdS core/crown@shell NPLs with a novel three-dimensional architecture resembling a platelet-in-box structure and systematically studied their resulting excitonic properties. We uncovered the critical importance of sidewall passivation of the inner core region with the laterally extending crown layer before the vertical shell growth, which enable favorable excitonic properties essential to low-threshold gain including increased PL-QY, enhanced absorption cross-section and eliminated trap sites. As a result, here we also showed the lowest gain threshold (~ 20 $\mu J/cm^2$) enabled by this proposed core/crown@shell heterostructure among different architectures of NPLs. This study has shown the importance of sidewall passivation in these two-dimensional colloidal NPLs and inspired our community for the synthesis of highly efficient and stable heterostructured NPLs.

Although these solution-processed NPLs has shown exciting excitonic properties, they have suffered from the discrete emission and absorption behaviors due to the pure vertical quantum confinement observed in these NPLs. To overcome this barrier, in Chapter 5, we have designed and synthesized alloyed heterostructures of $CdSe_xS_{1-x}$ NPLs using CdS coating in the lateral and vertical direction. By precisely tuning the composition of $CdSe_xS_{1-x}$ NPLs, we have achieved highly tunable optical properties with these atomically-flat nanocrystals. Also, with these $CdSe_xS_{1-x}$ alloyed NPLs offering reduced re-absorption and spectrally tunable optical gain range, we obtained highly tunable amplified spontaneous emission performance with low gain thresholds down to

~53 µJ/cm^2. This study has suggested the significant potential of alloyed heterostructures of CdSe$_x$S$_{1-x}$ NPLs for the utilization of the next-generation colloidal laser technology covering visible spectrum by using these solution-processed NPLs. Also, this highly effective alloying approach can be extended to the different material combinations for the achievement of further tunable excitonic properties, which is one of the major concern of colloidal NPLs.

In addition to the colloidal NPLs having Type-I electronic structure, colloidal NPLs having Type-II electronic structures have been also appealing with their unique excitonic features. To explore these exciting features, in Chapter 6, we have synthesized and characterized CdSe/CdTe core/crown NPLs having Type-II electronic structure. With the formation of spatially indirect excitons and their radiative recombination at the core/crown interface, we observed strongly red-shifted emission behaviors (up to ~150 nm) and 2 orders of magnitude longer radiative lifetimes (up to ~350 ns). With these core/crown architectures enabling enhanced charge extraction efficiency, CdSe/CdTe core/crown NPLs have become highly promising for the light-harvesting applications.

Like core-only NPLs, the CdSe/CdTe core/crown NPLs have also suffered from the limited tunability of their excitonic features, which is strongly related with the thickness of the starting CdSe core. For example, 4 ML thick CdSe/CdTe core/crown NPLs exhibit discrete emission peak at ~650 nm. To extend their spectral tunability, in Chapter 7, we have successfully synthesized CdSe/CdSe$_{1-x}$Te$_x$ core/crown NPLs by precisely tuning the composition of crown region from pure CdTe (x=1.00) to almost pure CdSe (x=0.02) and systematically studied their resulting excitonic properties. By tailoring the composition of the crown region, we achieved highly tunable excitonic properties

without changing the thickness of NPL and uncovered the evolution of Type-II electronic structure experimentally. Also, these CdSe/CdSe$_{1-x}$Te$_x$ core/crown NPLs have shown the highest PL-QY (up to ~95%) among various heterostructures of colloidal NPLs, which can be attributed to the suppression of nonradiative hole traps with the ultrafast localization of holes around CdSe$_{1-x}$Te$_x$ crown region and/or Te atoms. In addition, their large stokes shifted emission with near-unity PL-QY has shown the great potential of CdSe/CdSe$_{1-x}$Te$_x$ core/crown NPLs for the development of highly efficient luminescent solar concentrators.

In conclusion, we believe that our thesis studies have provided an important guideline for the synthesis of highly efficient and crystalline colloidal NPLs with engineered heterostructures and made great contribution to the development of high-performance colloidal optoelectronic devices.

8.2 Future Outlook

There are still various challenges for employing these colloidal quantum wells in the next-generation optoelectronic devices. One of the difficulties associated with these solution-processed NPLs is the lower PL-QY and stability of core/shell NPLs. For the synthesis of core/shell NPLs, colloidal atomic layer deposition (c-ALD) technique has been widely used, offering atomically precise shell thickness control and uniform shell growth. However, owing to room temperature coating of the shell, it is unavoidable to prevent the formation of trap sites, decreasing their PL-QY and stability. Therefore, new synthesis approaches should be developed for the uniform growth of shell, enabling the achievement of highly efficient and crystalline NPLs with uniform chemical compositions.

Also, it has been already shown that core/shell nanocrystals having smooth interface have led to suppression of nonradiative Auger recombination, limiting the optical gain and lasing performance of these tiny nanocrystals. Thus, colloidal synthesis of core/shell NPLs having smooth interfaces with composition gradient and/or alloyed heterostructures have been strongly desired to further push their performances.

Another difficulty related with the usage of colloidal NPLs is their heavy metal content causing serious health and environmental problems. To date, Cd-based colloidal NPLs together with their core/crown and core/shell heterostructures have been widely studied to explore and understand the unique excitonic properties of these atomically-flat nanocrystals. These knowledges and experiences obtained with the Cd-based NPLs should be extended to the colloidal synthesis of Cd-free semiconductor nanoplatelets to overcome these serious problems.

We strongly believe that with addressing these difficulties, solution-processed colloidal NPLs have shown great potential to revolutionize the optoelectronic technology with the fabrication of large-area, ultra-flexible and functional devices with cost-effective methods.

8.3 Contributions to the Literature

In this part, we list our contributions to the literature during the graduate studies at Bilkent University.

SCI Journal Publications:

(1)   **Kelestemur, Y.**; Dede, D.; Gungor, K.; Usanmaz, C. F.; Erdem, O.; Demir, H. V. Alloyed Heterostructures of $CdSe_xS_{1-x}$ Nanoplatelets with Highly Tunable Optical Gain Performance. Chem. Mater. 2017, (DOI: 10.1021/acs.chemmater.7b00829).

(2)   **Kelestemur, Y.**; Guzelturk, B.; Erdem, O.; Olutas, M.; Erdem, T.; Usanmaz, C. F.; Gungor, K.; Demir, H. V. $CdSe/CdSe_{1-x}Te_X$ Core/Crown Heteronanoplatelets: Tuning the Excitonic Properties without Changing the Thickness. J. Phys. Chem. C 2017, 121 (8), 4650–4658.

(3)   **Kelestemur, Y.**; Guzelturk, B.; Erdem, O.; Olutas, M.; Gungor, K.; Demir, H. V. Platelet-in-Box Colloidal Quantum Wells: CdSe/CdS@CdS Core/Crown@Shell Heteronanoplatelets. Adv. Funct. Mater. 2016, 26 (21), 3570–3579.

(4)   Olutas, M.; Guzelturk, B.; **Kelestemur, Y.**; Gungor, K.; Demir, H. V. Highly Efficient Nonradiative Energy Transfer from Colloidal Semiconductor Quantum Dots to Wells for Sensitive Noncontact Temperature Probing. Adv. Funct. Mater. 2016, 26 (17), 2891–2899.

(5)   Erdem, O.; Olutas, M.; Guzelturk, B.; **Kelestemur, Y.**; Demir, H. V. Temperature-Dependent Emission Kinetics of Colloidal Semiconductor Nanoplatelets Strongly Modified by Stacking. J. Phys. Chem. Lett. 2016, 7 (3), 548–554.

(6)   Sharma, V. K.; Alipour, A.; Soran-Erdem, Z.; **Kelestemur, Y.**; Aykut, Z. G.; Demir, H. V. Fluorescent Heterodoped Nanotetrapods as Synergistically Enhancing

Positive and Negative Magnetic Resonance Imaging Contrast Agents. ACS Appl. Mater. Interfaces 2016, 8 (19), 12352–12359.

(7)   Frohleiks, J.; Wepfer, S.; **Kelestemur, Y.**; Demir, H. V.; Bacher, G.; Nannen, E. Quantum Dot/Light-Emitting Electrochemical Cell Hybrid Device and Mechanism of Its Operation. ACS Appl. Mater. Interfaces 2016, 8 (37), 24692–24698.

(8)   Guzelturk, B.; Menk, F.; Philipps, K.; **Kelestemur, Y.**; Olutas, M.; Zentel, R.; Demir, H. V. Colloidal Nanoplatelet/Conducting Polymer Hybrids: Excitonic and Material Properties. J. Phys. Chem. C 2016, 120 (6), 3573–3582.

(9)   Erdem, T.; Soran-Erdem, Z.; **Kelestemur, Y.**; Gaponik, N.; Demir, H. V. Excitonic Improvement of Colloidal Nanocrystals in Salt Powder Matrix for Quality Lighting and Color Enrichment. Opt. Express 2016, 24 (2), A74.

(10)   **Kelestemur, Y.**; Olutas, M.; Delikanli, S.; Guzelturk, B.; Akgul, M. Z.; Demir, H. V. Type-II Colloidal Quantum Wells: CdSe/CdTe Core/Crown Heteronanoplatelets. J. Phys. Chem. C 2015, 119 (4), 2177–2185.

(11)   Guzelturk, B.; **Kelestemur, Y.**; Gungor, K.; Yeltik, A.; Akgul, M. Z.; Wang, Y.; Chen, R.; Dang, C.; Sun, H.; Demir, H. V. Stable and Low-Threshold Optical Gain in CdSe/CdS Quantum Dots: An All-Colloidal Frequency Up-Converted Laser. Adv. Mater. 2015, 27 (17), 2741–2746.

(12)   Olutas, M.; Guzelturk, B.; **Kelestemur, Y**.; Yeltik, A.; Delikanli, S.; Demir, H. V. Lateral Size-Dependent Spontaneous and Stimulated Emission Properties in Colloidal CdSe Nanoplatelets. ACS Nano 2015, 9 (5), 5041–5050.

(13) Delikanli, S.; Guzelturk, B.; Hernández-Martínez, P. L.; Erdem, T.; **Kelestemur, Y.**; Olutas, M.; Akgul, M. Z.; Demir, H. V. Continuously Tunable Emission in Inverted Type-I CdS/CdSe Core/Crown Semiconductor Nanoplatelets. Adv. Funct. Mater. 2015, 25 (27), 4282–4289.

(14) Guzelturk, B.; Olutas, M.; Delikanli, S.; **Kelestemur, Y.**; Erdem, O.; Demir, H. V. Nonradiative Energy Transfer in Colloidal CdSe Nanoplatelet Films. Nanoscale 2015, 7 (6), 2545–2551.

(15) Erdem, T.; Soran-Erdem, Z.; Sharma, V. K.; **Kelestemur, Y.**; Adam, M.; Gaponik, N.; Demir, H. V. Stable and Efficient Colour Enrichment Powders of Nonpolar Nanocrystals in LiCl. Nanoscale 2015, 7 (42), 17611–17616.

(16) Akhavan, S.; Uran, C.; Bozok, B.; Gungor, K.; **Kelestemur, Y.**; Lesnyak, V.; Gaponik, N.; Eychmüller, A.; Demir, H. V. Flexible and Fragmentable Tandem Photosensitive Nanocrystal Skins. Nanoscale 2015, 8 (8), 4495–4503.

(17) Yeltik, A.; Delikanli, S.; Olutas, M.; **Kelestemur, Y.**; Guzelturk, B.; Demir, H. V. Experimental Determination of the Absorption Cross-Section and Molar Extinction Coefficient of Colloidal CdSe Nanoplatelets. J. Phys. Chem. C 2015, 119 (47), 26768–26775.

(18) Wolff, S.; Jansen, D.; Terlinden, H.; **Kelestemur, Y.**; Mertin, W.; Demir, H. V.; Bacher, G.; Nannen, E. Implementation of Graphene Multilayer Electrodes in Quantum Dot Light-Emitting Devices. Appl. Phys. A Mater. Sci. Process. 2015, 120 (3), 1197–1203.

(19) **Kelestemur, Y.**; Cihan, A. F.; Guzelturk, B.; Demir, H. V. Type-Tunable Amplified Spontaneous Emission from Core-Seeded CdSe/CdS Nanorods Controlled by Exciton–exciton Interaction. Nanoscale 2014, 6 (15), 8509.

(20) Guzelturk, B.*; **Kelestemur, Y.***; Olutas, M.; Delikanli, S.; Demir, H. V. Amplified Spontaneous Emission and Lasing in Colloidal Nanoplatelets. ACS Nano 2014, 8 (7), 6599–6605 (* equal contribution).

(21) Guzelturk, B.; Erdem, O.; Olutas, M.; **Kelestemur, Y.**; Demir, H. V. Stacking in Colloidal Nanoplatelets: Tuning Excitonic Properties. ACS Nano 2014, 8 (12), 12524–12533.

(22) Guzelturk, B.*; **Kelestemur, Y.***; Akgul, M. Z.; Sharma, V. K.; Demir, H. V. Ultralow Threshold One-Photon- and Two-Photon-Pumped Optical Gain Media of Blue-Emitting Colloidal Quantum Dot Films. J. Phys. Chem. Lett. 2014, 5 (13), 2214–2218. (* equal contribution).

(23) Sharma, V. K.; Gokyar, S.; **Kelestemur, Y.**; Erdem, T.; Unal, E.; Demir, H. V. Manganese Doped Fluorescent Paramagnetic Nanocrystals for Dual-Modal Imaging. Small 2014, 10 (23), 4961–4966.

(24) Sharma, V. K.; Guzelturk, B.; Erdem, T.; **Kelestemur, Y.**; Demir, H. V. Tunable White-Light-Emitting Mn-Doped ZnSe Nanocrystals. ACS Appl. Mater. Interfaces 2014, 6 (5), 3654–3660.

(25)   Erdem, T.; **Kelestemur, Y.**; Soran-Erdem, Z.; Ji, Y.; Demir, H. V. Energy-Saving Quality Road Lighting with Colloidal Quantum Dot Nanophosphors. Nanophotonics 2014, 3 (6), 373–381.

(26)   Cihan, A. F.*; **Kelestemur, Y.***; Guzelturk, B.; Yerli, O.; Kurum, U.; Yaglioglu, H. G.; Elmali, A.; Demir, H. V. Attractive versus Repulsive Excitonic Interactions of Colloidal Quantum Dots Control Blue- to Red-Shifting (and Non-Shifting) Amplified Spontaneous Emission. J. Phys. Chem. Lett. 2013, 4 (23), 4146–4152 (* equal contribution).

(27)   Cihan, A. F.; Hernandez Martinez, P. L.; **Kelestemur, Y.**; Mutlugun, E.; Demir, H. V. Observation of Biexcitons in Nanocrystal Solids in the Presence of Photocharging. ACS Nano 2013, 7 (6), 4799–4809.

(28)   Yeltik, A.; Kucukayan-Dogu, G.; Guzelturk, B.; Fardindoost, S.; **Kelestemur, Y.**; Demir, H. V. Evidence for Nonradiative Energy Transfer in Graphene-Oxide-Based Hybrid Structures. J. Phys. Chem. C 2013, 117 (48), 25298–25304.

Bibliography

[1]   A. P. Alivisatos, "Semiconductor Clusters, Nanocrystals, and Quantum Dots," *Science*, vol. 271, no. 5251, pp. 933–937, 1996.

[2]   A. P. Alivisatos, "Perspectives on the Physical Chemistry of Semiconductor Nanocrystals," *J. Phys. Chem.*, vol. 100, no. 31, pp. 13226–13239, 1996.

[3]   D. V. Talapin, J.-S. Lee, M. V. Kovalenko, and E. V. Shevchenko, "Prospects of Colloidal Nanocrystals for Electronic and Optoelectronic Applications," *Chem. Rev.*, vol. 110, no. 1, pp. 389–458, 2010.

[4]   C. B. Murray, D. J. Norris, and M. G. Bawendi, "Synthesis and characterization of nearly monodisperse CdE (E= sulfur, selenium, tellurium) semiconductor nanocrystallites," *J. Am. Chem. Soc.*, vol. 115, no. 4, pp. 8706–8715, 1993.

[5]   C. de M. Donegá, "Synthesis and properties of colloidal heteronanocrystals," *Chem. Soc. Rev.*, vol. 40, no. 3, pp. 1512–1546, 2011.

[6]   J. M. Pietryga, Y.-S. Park, J. Lim, A. F. Fidler, W. K. Bae, S. Brovelli, and V. I. Klimov, "Spectroscopic and Device Aspects of Nanocrystal Quantum Dots," *Chem. Rev.*, vol. 116, no. 18, pp. 10513–10622, 2016.

[7]   C. R. Kagan, E. Lifshitz, E. H. Sargent, and D. V. Talapin, "Building devices from colloidal quantum dots," *Science*, vol. 353, no. 6302, p. aac5523-aac5523, 2016.

[8]   K. Bourzac, "Quantum dots go on display," *Nature*, vol. 493, no. 7432, pp. 283–283, 2013.

[9]   "Nanocrystals in their prime," *Nat. Nanotechnol.*, vol. 9, no. 5, pp. 325–325, 2014.

[10]   S. Coe, W.-K. Woo, M. Bawendi, V. Bulović, and V. Bulović, "Electroluminescence from single monolayers of nanocrystals in molecular organic devices," *Nature*, vol. 420, no. 6917, pp. 800–803, 2002.

[11]   V. I. Klimov, A. A. Mikhailovsky, S. Xu, A. Malko, J. A. Hollingsworth, C. A. Leatherdale, H.-J. Eisler, and M. G. Bawendi, "Optical Gain and Stimulated Emission in Nanocrystal Quantum Dots," *Science*, vol. 290, no. 5490, pp. 314–317, 2000.

[12]   W. U. Huynh, J. J. Dittmer, and A. P. Alivisatos, "Hybrid nanorod-polymer solar cells.," *Science*, vol. 295, no. 5564, pp. 2425–7, 2002.

[13]   S. A. McDonald, G. Konstantatos, S. Zhang, P. W. Cyr, E. J. D. Klem, L. Levina, and E. H. Sargent, "Solution-processed PbS quantum dot infrared photodetectors

and photovoltaics," *Nat. Mater.*, vol. 4, no. 2, pp. 138–142, 2005.

[14]   F. Meinardi, A. Colombo, K. A. Velizhanin, R. Simonutti, M. Lorenzon, L. Beverina, R. Viswanatha, V. I. Klimov, and S. Brovelli, "Large-area luminescent solar concentrators based on 'Stokes-shift-engineered' nanocrystals in a mass-polymerized PMMA matrix," *Nat. Photonics*, vol. 8, no. 5, pp. 392–399, 2014.

[15]   S. Ithurria and B. Dubertret, "Quasi 2D Colloidal CdSe Platelets with Thicknesses Controlled at the Atomic Level," *J. Am. Chem. Soc.*, vol. 130, no. 49, pp. 16504–16505, 2008.

[16]   M. Nasilowski, B. Mahler, E. Lhuillier, S. Ithurria, and B. Dubertret, "Two-Dimensional Colloidal Nanocrystals," *Chem. Rev.*, vol. 116, no. 18, pp. 10934–10982, 2016.

[17]   S. Ithurria, M. D. Tessier, B. Mahler, R. P. S. M. Lobo, B. Dubertret, and A. L. Efros, "Colloidal nanoplatelets with two-dimensional electronic structure," *Nat. Mater.*, vol. 10, no. 12, pp. 936–941, 2011.

[18]   M. D. Tessier, P. Spinicelli, D. Dupont, G. Patriarche, S. Ithurria, and B. Dubertret, "Efficient Exciton Concentrators Built from Colloidal Core/Crown CdSe/CdS Semiconductor Nanoplatelets," *Nano Lett.*, vol. 14, no. 1, pp. 207–213, 2014.

[19]   B. Mahler, B. Nadal, C. Bouet, G. Patriarche, and B. Dubertret, "Core/Shell Colloidal Semiconductor Nanoplatelets," *J. Am. Chem. Soc.*, vol. 134, no. 45, pp. 18591–18598, 2012.

[20]   B. Guzelturk, Y. Kelestemur, M. Olutas, S. Delikanli, and H. V. Demir, "Amplified Spontaneous Emission and Lasing in Colloidal Nanoplatelets," *ACS Nano*, vol. 8, no. 7, pp. 6599–6605, 2014.

[21]   Z. Chen, B. Nadal, B. Mahler, H. Aubin, and B. Dubertret, "Quasi-2D Colloidal Semiconductor Nanoplatelets for Narrow Electroluminescence," *Adv. Funct. Mater.*, vol. 24, no. 3, pp. 295–302, 2014.

[22]   L. E. Brus, "Electron–electron and electron-hole interactions in small semiconductor crystallites: The size dependence of the lowest excited electronic state," *J. Chem. Phys.*, vol. 80, no. 9, pp. 4403–4409, 1984.

[23]   I. L. IL Medintz, H. T. Uyeda, E. R. E. Goldman, and H. Mattoussi, "Quantum dot bioconjugates for imaging, labelling and sensing," *Nat. Mater.*, vol. 4, no. 6, pp. 435–446, 2005.

[24]   J. Yang, M. K. Choi, D. H. Kim, and T. Hyeon, "Designed Assembly and Integration of Colloidal Nanocrystals for Device Applications," *Adv. Mater.*, vol. 28, no. 6, pp. 1176–1207, 2016.

[25]   A. I. Ekimov and A. A. Onushchenko, "Quantum size effect in three-dimensional

microscopic semiconductor crystals," *J. Exp. Theor. Phys. Lett.*, vol. 34, no. 6, pp. 345–348, 1981.

[26]   L. Brus, "Electronic wave functions in semiconductor clusters: experiment and theory," *J. Phys. Chem.*, vol. 90, no. 12, pp. 2555–2560, 1986.

[27]   C. B. Murray, C. R. Kagan, and M. G. Bawendi, "Synthesis and Characterization of Monodisperse Nanocrystals and Close-Packed Nanocrystal Assemblies," *Annu. Rev. Mater. Sci.*, vol. 30, no. 1, pp. 545–610, 2000.

[28]   S. Abe, R. K. Capek, B. De Geyter, and Z. Hens, "Reaction Chemistry/Nanocrystal Property Relations in the Hot Injection Synthesis, the Role of the Solute Solubility," *ACS Nano*, vol. 7, no. 2, pp. 943–949, 2013.

[29]   Z. A. Peng and X. Peng, "Nearly Monodisperse and Shape-Controlled CdSe Nanocrystals via Alternative Routes: Nucleation and Growth," *J. Am. Chem. Soc.*, vol. 124, no. 13, pp. 3343–3353, 2002.

[30]   W. W. Yu and X. Peng, "Formation of High-Quality CdS and Other II-VI Semiconductor Nanocrystals in Noncoordinating Solvents: Tunable Reactivity of Monomers," *Angew. Chemie Int. Ed.*, vol. 41, no. 13, pp. 2368–2371, 2002.

[31]   N. Pradhan, D. Reifsnyder, R. Xie, J. Aldana, and X. Peng, "Surface ligand dynamics in growth of nanocrystals," *J. Am. Chem. Soc.*, vol. 129, no. 30, pp. 9500–9509, 2007.

[32]   Z. A. Peng and X. Peng, "Mechanisms of the Shape Evolution of CdSe Nanocrystals," *J. Am. Chem. Soc.*, vol. 123, no. 7, pp. 1389–1395, 2001.

[33]   S. Kumar and T. Nann, "Shape Control of II–VI Semiconductor Nanomaterials," *Small*, vol. 2, no. 3, pp. 316–329, 2006.

[34]   X. Wang, J. Zhuang, Q. Peng, and Y. Li, "A general strategy for nanocrystal synthesis," *Nature*, vol. 437, no. 7055, pp. 121–124, 2005.

[35]   V. K. LaMer and R. H. Dinegar, "Theory, Production and Mechanism of Formation of Monodispersed Hydrosols," *J. Am. Chem. Soc.*, vol. 72, no. 11, pp. 4847–4854, 1950.

[36]   X. Peng, J. Wickham, and A. P. Alivisatos, "Kinetics of II-VI and III-V Colloidal Semiconductor Nanocrystal Growth: 'Focusing' of Size Distributions," *J. Am. Chem. Soc.*, vol. 120, no. 21, pp. 5343–5344, 1998.

[37]   B. A. Kairdolf, A. M. Smith, and S. Nie, "One-pot synthesis, encapsulation, and solubilization of size-tuned quantum dots with amphiphilic multidentate ligands," *J. Am. Chem. Soc.*, vol. 130, no. 39, pp. 12866–12867, 2008.

[38]   A. A. Guzelian, J. E. B. Katari, A. V. Kadavanich, U. Banin, K. Hamad, E. Juban, A. P. Alivisatos, R. H. Wolters, C. C. Arnold, and J. R. Heath, "Synthesis of Size-

Selected, Surface-Passivated InP Nanocrystals," *J. Phys. Chem.*, vol. 100, no. 17, pp. 7212–7219, 1996.

[39]   D. Battaglia and X. Peng, "Formation of High Quality InP and InAs Nanocrystals in a Noncoordinating Solvent," *Nano Lett.*, vol. 2, no. 9, pp. 1027–1030, 2002.

[40]   M. A. Hines and G. D. Scholes, "Colloidal PbS Nanocrystals with Size-Tunable Near-Infrared Emission: Observation of Post-Synthesis Self-Narrowing of the Particle Size Distribution," *Adv. Mater.*, vol. 15, no. 21, pp. 1844–1849, 2003.

[41]   W. W. Yu, J. C. Falkner, B. S. Shih, and V. L. Colvin, "Preparation and Characterization of Monodisperse PbSe Semiconductor Nanocrystals in a Noncoordinating Solvent," *Chem. Mater.*, vol. 16, no. 17, pp. 3318–3322, 2004.

[42]   J. E. Murphy, M. C. Beard, A. G. Norman, S. P. Ahrenkiel, J. C. Johnson, P. Yu, O. I. Mićić, R. J. Ellingson, and A. J. Nozik, "PbTe Colloidal Nanocrystals: Synthesis, Characterization, and Multiple Exciton Generation," *J. Am. Chem. Soc.*, vol. 128, no. 10, pp. 3241–3247, 2006.

[43]   X. Peng, "Mechanisms for the Shape-Control and Shape-Evolution of Colloidal Semiconductor Nanocrystals," *Adv. Mater.*, vol. 15, no. 5, pp. 459–463, 2003.

[44]   D. J. Milliron, S. M. Hughes, Y. Cui, L. Manna, J. Li, L.-W. Wang, and A. Paul Alivisatos, "Colloidal nanocrystal heterostructures with linear and branched topology," *Nature*, vol. 430, no. 6996, pp. 190–195, 2004.

[45]   L. Manna, E. C. Scher, and A. P. Alivisatos, "Synthesis of soluble and processable rod-, arrow-, teardrop-, and tetrapod-shaped CdSe nanocrystals," *J. Am. Chem. Soc.*, vol. 122, no. 51, pp. 12700–12706, 2000.

[46]   L. Carbone, C. Nobile, M. De Giorgi, F. Della Sala, G. Morello, P. Pompa, M. Hytch, E. Snoeck, A. Fiore, I. R. Franchini, M. Nadasan, A. F. Silvestre, L. Chiodo, S. Kudera, R. Cingolani, R. Krahne, and L. Manna, "Synthesis and Micrometer-Scale Assembly of Colloidal CdSe/CdS Nanorods Prepared by a Seeded Growth Approach," *Nano Lett.*, vol. 7, no. 10, pp. 2942–50, 2007.

[47]   D. V Talapin, R. Koeppe, S. Götzinger, A. Kornowski, J. M. Lupton, A. L. Rogach, O. Benson, J. Feldmann, and H. Weller, "Highly Emissive Colloidal CdSe/CdS Heterostructures of Mixed Dimensionality," *Nano Lett.*, vol. 3, no. 12, pp. 1677–1681, 2003.

[48]   P. Reiss, M. Protière, and L. Li, "Core/Shell Semiconductor Nanocrystals," *Small*, vol. 5, no. 2, pp. 154–168, 2009.

[49]   A. M. Smith and S. Nie, "Semiconductor Nanocrystals: Structure, Properties, and Band Gap Engineering," *Acc. Chem. Res.*, vol. 43, no. 2, pp. 190–200, 2010.

[50]   M. A. Hines and P. Guyot-Sionnest, "Synthesis and Characterization of Strongly Luminescing ZnS-Capped CdSe Nanocrystals," *J. Phys. Chem.*, vol. 100, no. 2,

pp. 468–471, 1996.

[51] S. Kim, B. Fisher, H.-J. Eisler, and M. Bawendi, "Type-II Quantum Dots: CdTe/CdSe(Core/Shell) and CdSe/ZnTe(Core/Shell) Heterostructures," *J. Am. Chem. Soc.*, vol. 125, no. 38, pp. 11466–11467, 2003.

[52] B. O. Dabbousi, J. Rodriguez-Viejo, F. V. Mikulec, J. R. Heine, H. Mattoussi, R. Ober, K. F. Jensen, and M. G. Bawendi, "(CdSe)ZnS Core−Shell Quantum Dots: Synthesis and Characterization of a Size Series of Highly Luminescent Nanocrystallites," *J. Phys. Chem. B*, vol. 101, no. 46, pp. 9463–9475, 1997.

[53] X. Peng, M. C. Schlamp, A. V. Kadavanich, and A. P. Alivisatos, "Epitaxial Growth of Highly Luminescent CdSe/CdS Core/Shell Nanocrystals with Photostability and Electronic Accessibility," *J. Am. Chem. Soc.*, vol. 119, no. 30, pp. 7019–7029, 1997.

[54] J. J. Li, Y. A. Wang, W. Guo, J. C. Keay, T. D. Mishima, M. B. Johnson, and X. Peng, "Large-Scale Synthesis of Nearly Monodisperse CdSe/CdS Core/Shell Nanocrystals Using Air-Stable Reagents via Successive Ion Layer Adsorption and Reaction," *J. Am. Chem. Soc.*, vol. 125, no. 41, pp. 12567–75, 2003.

[55] D. V Talapin, I. Mekis, S. Götzinger, A. Kornowski, O. Benson, and H. Weller, "CdSe/CdS/ZnS and CdSe/ZnSe/ZnS Core−Shell−Shell Nanocrystals," *J. Phys. Chem. B*, vol. 108, no. 49, pp. 18826–18831, 2004.

[56] R. Xie, U. Kolb, J. Li, T. Basché, and A. Mews, "Synthesis and Characterization of Highly Luminescent CdSe−Core CdS/Zn 0.5 Cd 0.5 S/ZnS Multishell Nanocrystals," *J. Am. Chem. Soc.*, vol. 127, no. 20, pp. 7480–7488, 2005.

[57] W. K. Bae, K. Char, H. Hur, and S. Lee, "Single-Step Synthesis of Quantum Dots with Chemical Composition Gradients," *Chem. Mater.*, vol. 20, no. 2, pp. 531–539, 2008.

[58] W. K. Bae, M. K. Nam, K. Char, and S. Lee, "Gram-Scale One-Pot Synthesis of Highly Luminescent Blue Emitting Cd1− x Znx S/ZnS Nanocrystals," *Chem. Mater.*, vol. 20, no. 16, pp. 5307–5313, 2008.

[59] E. Jang, S. Jun, H. Jang, J. Lim, B. Kim, and Y. Kim, "White-light-emitting diodes with quantum dot color converters for display backlights.," *Adv. Mater.*, vol. 22, no. 28, pp. 3076–80, 2010.

[60] L. Li and P. Reiss, "One-pot Synthesis of Highly Luminescent InP/ZnS Nanocrystals without Precursor Injection," *J. Am. Chem. Soc.*, vol. 130, no. 35, pp. 11588–11589, 2008.

[61] Y. Altıntas, M. Y. Talpur, M. Ünlü, and E. Mutlugün, "Highly Efficient Cd-Free Alloyed Core/Shell Quantum Dots with Optimized Precursor Concentrations," *J. Phys. Chem. C*, vol. 120, no. 14, pp. 7885–7892, 2016.

[62]   L. Li, T. J. Daou, I. Texier, T. T. Kim Chi, N. Q. Liem, and P. Reiss, "Highly Luminescent CuInS 2 /ZnS Core/Shell Nanocrystals: Cadmium-Free Quantum Dots for In Vivo Imaging," *Chem. Mater.*, vol. 21, no. 12, pp. 2422–2429, 2009.

[63]   H. Zang, H. Li, N. S. Makarov, K. A. Velizhanin, K. Wu, Y.-S. Park, and V. I. Klimov, "Thick-Shell CuInS 2 /ZnS Quantum Dots with Suppressed 'Blinking' and Narrow Single-Particle Emission Line Widths," *Nano Lett.*, vol. 17, no. 3, pp. 1787–1795, 2017.

[64]   S. S. Lo, T. Mirkovic, C.-H. Chuang, C. Burda, and G. D. Scholes, "Emergent Properties Resulting from Type-II Band Alignment in Semiconductor Nanoheterostructures," *Adv. Mater.*, vol. 23, no. 2, pp. 180–197, 2011.

[65]   S. A. Ivanov, A. Piryatinski, J. Nanda, S. Tretiak, K. R. Zavadil, W. O. Wallace, D. Werder, and V. I. Klimov, "Type-II Core/Shell CdS/ZnSe Nanocrystals: Synthesis, Electronic Structures, and Spectroscopic Properties," *J. Am. Chem. Soc.*, vol. 129, no. 38, pp. 11708–11719, 2007.

[66]   J. Bang, J. Park, J. H. Lee, N. Won, J. Nam, J. Lim, B. Y. Chang, H. J. Lee, B. Chon, J. Shin, J. B. Park, J. H. Choi, K. Cho, S. M. Park, T. Joo, and S. Kim, "ZnTe/ZnSe (Core/Shell) Type-II Quantum Dots: Their Optical and Photovoltaic Properties," *Chem. Mater.*, vol. 22, no. 1, pp. 233–240, 2010.

[67]   Y. Chen, J. Vela, H. Htoon, J. L. Casson, D. J. Werder, D. A. Bussian, V. I. Klimov, and J. A. Hollingsworth, "'Giant' Multishell CdSe Nanocrystal Quantum Dots with Suppressed Blinking," *J. Am. Chem. Soc.*, vol. 130, no. 15, pp. 5026–5027, 2008.

[68]   Y. Ghosh, B. D. Mangum, J. L. Casson, D. J. Williams, H. Htoon, and J. A. Hollingsworth, "New Insights into the Complexities of Shell Growth and the Strong Influence of Particle Volume in Nonblinking 'Giant' Core/Shell Nanocrystal Quantum Dots," *J. Am. Chem. Soc.*, vol. 134, no. 23, pp. 9634–9643, 2012.

[69]   C. Galland, Y. Ghosh, A. Steinbrück, J. A. Hollingsworth, H. Htoon, and V. I. Klimov, "Lifetime blinking in nonblinking nanocrystal quantum dots," *Nat. Commun.*, vol. 3, no. May, p. 908, 2012.

[70]   B. N. Pal, Y. Ghosh, S. Brovelli, R. Laocharoensuk, V. I. Klimov, J. A. Hollingsworth, and H. Htoon, 'Giant' CdSe/CdS Core/Shell Nanocrystal Quantum Dots As Efficient Electroluminescent Materials: Strong Influence of Shell Thickness on Light-Emitting Diode Performance," *Nano Lett.*, vol. 12, no. 1, pp. 331–336, 2012.

[71]   F. García-Santamaría, Y. Chen, J. Vela, R. D. Schaller, J. A. Hollingsworth, and V. I. Klimov, "Suppressed Auger Recombination in 'Giant' Nanocrystals Boosts Optical Gain Performance," *Nano Lett.*, vol. 9, no. 10, pp. 3482–3488, 2009.

[72] O. Chen, J. Zhao, V. P. Chauhan, J. Cui, C. Wong, D. K. Harris, H. Wei, H.-S. Han, D. Fukumura, R. K. Jain, and M. G. Bawendi, "Compact high-quality CdSe–CdS core–shell nanocrystals with narrow emission linewidths and suppressed blinking," *Nat. Mater.*, vol. 12, no. 5, pp. 445–451, 2013.

[73] B. Guzelturk, Y. Kelestemur, K. Gungor, A. Yeltik, M. Z. Akgul, Y. Wang, R. Chen, C. Dang, H. Sun, and H. V. Demir, "Stable and Low-Threshold Optical Gain in CdSe/CdS Quantum Dots: An All-Colloidal Frequency Up-Converted Laser," *Adv. Mater.*, vol. 27, no. 17, pp. 2741–2746, 2015.

[74] A. Riedinger, F. D. Ott, A. Mule, S. Mazzotti, P. N. Knüsel, S. J. P. Kress, F. Prins, S. C. Erwin, and D. J. Norris, "An intrinsic growth instability in isotropic materials leads to quasi-two-dimensional nanoplatelets," *Nat. Mater.*, no. April, 2017.

[75] M. D. Tessier, C. Javaux, I. Maksimovic, V. Loriette, and B. Dubertret, "Spectroscopy of Single CdSe Nanoplatelets," *ACS Nano*, vol. 6, no. 8, pp. 6751–6758, 2012.

[76] M. Olutas, B. Guzelturk, Y. Kelestemur, A. Yeltik, S. Delikanli, and H. V. Demir, "Lateral Size-Dependent Spontaneous and Stimulated Emission Properties in Colloidal CdSe Nanoplatelets," *ACS Nano*, vol. 9, no. 5, pp. 5041–5050, 2015.

[77] A. Yeltik, S. Delikanli, M. Olutas, Y. Kelestemur, B. Guzelturk, and H. V. Demir, "Experimental Determination of the Absorption Cross-Section and Molar Extinction Coefficient of Colloidal CdSe Nanoplatelets," *J. Phys. Chem. C*, vol. 119, no. 47, pp. 26768–26775, 2015.

[78] S. Ithurria, G. Bousquet, and B. Dubertret, "Continuous Transition from 3D to 1D Confinement Observed during the Formation of CdSe Nanoplatelets," *J. Am. Chem. Soc.*, vol. 133, no. 9, pp. 3070–3077, 2011.

[79] Z. Li, H. Qin, D. Guzun, M. Benamara, G. Salamo, and X. Peng, "Uniform thickness and colloidal-stable CdS quantum disks with tunable thickness: Synthesis and properties," *Nano Res.*, vol. 5, no. 5, pp. 337–351, 2012.

[80] S. Pedetti, B. Nadal, E. Lhuillier, B. Mahler, C. Bouet, B. Abécassis, X. Xu, and B. Dubertret, "Optimized Synthesis of CdTe Nanoplatelets and Photoresponse of CdTe Nanoplatelets Films," *Chem. Mater.*, vol. 25, no. 12, pp. 2455–2462, 2013.

[81] A. Prudnikau, A. Chuvilin, and M. Artemyev, "CdSe–CdS Nanoheteroplatelets with Efficient Photoexcitation of Central CdSe Region through Epitaxially Grown CdS Wings," *J. Am. Chem. Soc.*, vol. 135, no. 39, pp. 14476–14479, 2013.

[82] S. Ithurria and D. V. Talapin, "Colloidal atomic layer deposition (c-ALD) using self-limiting reactions at nanocrystal surface coupled to phase transfer between polar and nonpolar media," *J. Am. Chem. Soc.*, vol. 134, no. 45, pp. 18585–18590, 2012.

[83]   L. T. Kunneman, M. D. Tessier, H. Heuclin, B. Dubertret, Y. V. Aulin, F. C. Grozema, J. M. Schins, and L. D. A. Siebbeles, "Bimolecular Auger Recombination of Electron–Hole Pairs in Two-Dimensional CdSe and CdSe/CdZnS Core/Shell Nanoplatelets," *J. Phys. Chem. Lett.*, vol. 4, no. 21, pp. 3574–3578, 2013.

[84]   C. She, I. Fedin, D. S. Dolzhnikov, P. D. Dahlberg, G. S. Engel, R. D. Schaller, and D. V Talapin, "Red, Yellow, Green, and Blue Amplified Spontaneous Emission and Lasing Using Colloidal CdSe Nanoplatelets," *ACS Nano*, vol. 9, no. 10, pp. 9475–9485, 2015.

[85]   B. Guzelturk, Y. Kelestemur, M. Z. Akgul, V. K. Sharma, and H. V. Demir, "Ultralow Threshold One-Photon- and Two-Photon-Pumped Optical Gain Media of Blue-Emitting Colloidal Quantum Dot Films," *J. Phys. Chem. Lett.*, vol. 5, no. 13, pp. 2214–2218, 2014.

[86]   C. She, I. Fedin, D. S. Dolzhnikov, A. Demortière, R. D. Schaller, M. Pelton, and D. V Talapin, "Low-Threshold Stimulated Emission Using Colloidal Quantum Wells," *Nano Lett.*, vol. 14, no. 5, pp. 2772–2777, 2014.

[87]   M. D. Tessier, B. Mahler, B. Nadal, H. Heuclin, S. Pedetti, and B. Dubertret, "Spectroscopy of Colloidal Semiconductor Core/Shell Nanoplatelets with High Quantum Yield," *Nano Lett.*, vol. 13, no. 7, pp. 3321–3328, 2013.

[88]   J. McBride, J. Treadway, L. C. Feldman, S. J. Pennycook, and S. J. Rosenthal, "Structural basis for near unity quantum yield core/shell nanostructures.," *Nano Lett.*, vol. 6, no. 7, pp. 1496–501, 2006.

[89]   N. J. Orfield, J. R. McBride, F. Wang, M. R. Buck, J. D. Keene, K. R. Reid, H. Htoon, J. A. Hollingsworth, and S. J. Rosenthal, "Quantum Yield Heterogeneity among Single Nonblinking Quantum Dots Revealed by Atomic Structure-Quantum Optics Correlation," *ACS Nano*, vol. 10, no. 2, pp. 1960–1968, 2016.

[90]   M. Grabolle, M. Spieles, V. Lesnyak, N. Gaponik, A. Eychmüller, and U. Resch-Genger, "Determination of the Fluorescence Quantum Yield of Quantum Dots: Suitable Procedures and Achievable Uncertainties," *Anal. Chem.*, vol. 81, no. 15, pp. 6285–6294, 2009.

[91]   J. C. de Mello, H. F. Wittmann, and R. H. Friend, "An improved experimental determination of external photoluminescence quantum efficiency," *Adv. Mater.*, vol. 9, no. 3, pp. 230–232, 1997.

[92]   T. Erdem, Z. Soran-Erdem, V. K. Sharma, Y. Kelestemur, M. Adam, N. Gaponik, and H. V. Demir, "Stable and efficient colour enrichment powders of nonpolar nanocrystals in LiCl," *Nanoscale*, vol. 7, no. 42, pp. 17611–17616, 2015.

[93]   Y. Kelestemur, B. Guzelturk, O. Erdem, M. Olutas, T. Erdem, C. F. Usanmaz, K. Gungor, and H. V. Demir, "CdSe/CdSe $1-x$ Te x Core/Crown

182

Heteronanoplatelets: Tuning the Excitonic Properties without Changing the Thickness," *J. Phys. Chem. C*, vol. 121, no. 8, pp. 4650–4658, 2017.

[94]   Y. Kelestemur, B. Guzelturk, O. Erdem, M. Olutas, K. Gungor, and H. V. Demir, "Platelet-in-Box Colloidal Quantum Wells: CdSe/CdS@CdS Core/Crown@Shell Heteronanoplatelets," *Adv. Funct. Mater.*, vol. 26, no. 21, pp. 3570–3579, 2016.

[95]   Y. Kelestemur, M. Olutas, S. Delikanli, B. Guzelturk, M. Z. Akgul, and H. V. Demir, "Type-II Colloidal Quantum Wells: CdSe/CdTe Core/Crown Heteronanoplatelets," *J. Phys. Chem. C*, vol. 119, no. 4, pp. 2177–2185, 2015.

[96]   D. D. Sarma, P. K. Santra, S. Mukherjee, and A. Nag, "X-ray Photoelectron Spectroscopy: A Unique Tool To Determine the Internal Heterostructure of Nanoparticles," *Chem. Mater.*, vol. 25, no. 8, pp. 1222–1232, 2013.

[97]   D. V. Talapin, J. H. Nelson, E. V. Shevchenko, S. Aloni, B. Sadtler, and A. P. Alivisatos, "Seeded Growth of Highly Luminescent CdSe/CdS Nanoheterostructures with Rod and Tetrapod Morphologies," *Nano Lett.*, vol. 7, no. 10, pp. 2951–2959, 2007.

[98]   S. Jana, T. N. T. Phan, C. Bouet, M. D. Tessier, P. Davidson, B. Dubertret, and B. Abécassis, "Stacking and Colloidal Stability of CdSe Nanoplatelets," *Langmuir*, vol. 31, no. 38, pp. 10532–10539, 2015.

[99]   B. Abécassis, M. D. Tessier, P. Davidson, and B. Dubertret, "Self-Assembly of CdSe Nanoplatelets into Giant Micrometer-Scale Needles Emitting Polarized Light," *Nano Lett.*, vol. 14, no. 2, pp. 710–715, 2014.

[100]   B. Guzelturk, O. Erdem, M. Olutas, Y. Kelestemur, and H. V. Demir, "Stacking in Colloidal Nanoplatelets: Tuning Excitonic Properties," *ACS Nano*, vol. 8, no. 12, pp. 12524–12533, 2014.

[101]   S. Delikanli, B. Guzelturk, P. L. Hernández-Martínez, T. Erdem, Y. Kelestemur, M. Olutas, M. Z. Akgul, and H. V Demir, "Continuously Tunable Emission in Inverted Type-I CdS/CdSe Core/Crown Semiconductor Nanoplatelets," *Adv. Funct. Mater.*, vol. 25, no. 27, pp. 4282–4289, 2015.

[102]   S. Pedetti, S. Ithurria, H. Heuclin, G. Patriarche, and B. Dubertret, "Type-II CdSe/CdTe Core/Crown Semiconductor Nanoplatelets," *J. Am. Chem. Soc.*, vol. 136, no. 46, pp. 16430–16438, 2014.

[103]   L. T. Kunneman, J. M. Schins, S. Pedetti, H. Heuclin, F. C. Grozema, A. J. Houtepen, B. Dubertret, and L. D. A. Siebbeles, "Nature and Decay Pathways of Photoexcited States in CdSe and CdSe/CdS Nanoplatelets," *Nano Lett.*, vol. 14, no. 12, pp. 7039–7045, 2014.

[104]   K. E. Knowles, E. A. McArthur, and E. A. Weiss, "A Multi-Timescale Map of

Radiative and Nonradiative Decay Pathways for Excitons in CdSe Quantum Dots," *ACS Nano*, vol. 5, no. 3, pp. 2026–2035, 2011.

[105] P. Jing, J. Zheng, M. Ikezawa, X. Liu, S. Lv, X. Kong, J. Zhao, and Y. Masumoto, "Temperature-Dependent Photoluminescence of CdSe-Core CdS/CdZnS/ZnS-Multishell Quantum Dots," *J. Phys. Chem. C*, vol. 113, no. 31, pp. 13545–13550, 2009.

[106] J. Li, K. B. Nam, J. Y. Lin, and H. X. Jiang, "Optical and electrical properties of Al-rich AlGaN alloys," *Appl. Phys. Lett.*, vol. 79, no. 20, pp. 3245–3247, 2001.

[107] L. Grenouillet, C. Bru-Chevallier, G. Guillot, P. Gilet, P. Duvaut, C. Vannuffel, A. Million, and A. Chenevas-Paule, "Evidence of strong carrier localization below 100 K in a GaInNAs/GaAs single quantum well," *Appl. Phys. Lett.*, vol. 76, no. 16, pp. 2241–2243, 2000.

[108] J. Munguía, J.-M. Bluet, O. Marty, G. Bremond, M. Mermoux, and D. Rouchon, "Temperature dependence of the indirect bandgap in ultrathin strained silicon on insulator layer," *Appl. Phys. Lett.*, vol. 100, no. 10, p. 102107, 2012.

[109] J. Q. Grim, S. Christodoulou, F. Di Stasio, R. Krahne, R. Cingolani, L. Manna, and I. Moreels, "Continuous-wave biexciton lasing at room temperature using solution-processed quantum wells," *Nat. Nanotechnol.*, vol. 9, no. 11, pp. 891–895, 2014.

[110] Y. Kelestemur, A. F. Cihan, B. Guzelturk, and H. V. Demir, "Type-tunable amplified spontaneous emission from core-seeded CdSe/CdS nanorods controlled by exciton–exciton interaction," *Nanoscale*, vol. 6, no. 15, p. 8509, 2014.

[111] A. F. Cihan, Y. Kelestemur, B. Guzelturk, O. Yerli, U. Kurum, H. G. Yaglioglu, A. Elmali, and H. V. Demir, "Attractive versus Repulsive Excitonic Interactions of Colloidal Quantum Dots Control Blue- to Red-Shifting (and Non-shifting) Amplified Spontaneous Emission," *J. Phys. Chem. Lett.*, vol. 4, no. 23, pp. 4146–4152, 2013.

[112] Y. Kelestemur, D. Dede, K. Gungor, C. F. Usanmaz, O. Erdem, and H. V. Demir, "Alloyed Heterostructures of CdSe x S 1– x Nanoplatelets with Highly Tunable Optical Gain Performance," *Chem. Mater.*, vol. 29, no. 11, pp. 4857–4865, 2017.

[113] B. T. Diroll, D. V. Talapin, and R. D. Schaller, "Violet-to-Blue Gain and Lasing from Colloidal CdS Nanoplatelets: Low-Threshold Stimulated Emission Despite Low Photoluminescence Quantum Yield," *ACS Photonics*, vol. 4, no. 3, pp. 576–583, 2017.

[114] M. Li, M. Zhi, H. Zhu, W.-Y. Wu, Q.-H. Xu, M. H. Jhon, and Y. Chan, "Ultralow-threshold Multiphoton-pumped Lasing from Colloidal Nanoplatelets in Solution," *Nat. Commun.*, vol. 6, p. 8513, 2015.

[115] P. S. Maiti, L. Houben, and M. Bar-Sadan, "Growth Schemes of Tunable Ultrathin CdS x Se 1– x Alloyed Nanostructures at Low Temperatures," *J. Phys. Chem. C*, vol. 119, no. 19, pp. 10734–10739, 2015.

[116] P. S. Maiti and M. Bar Sadan, "Tuning the surface properties of alloyed CdS x Se 1−x 2D nanosheets," *RSC Adv.*, vol. 5, no. 122, pp. 100834–100837, 2015.

[117] F. Fan, P. Kanjanaboos, M. Saravanapavanantham, E. Beauregard, G. Ingram, E. Yassitepe, M. M. Adachi, O. Voznyy, A. K. Johnston, G. Walters, G.-H. Kim, Z.-H. Lu, and E. H. Sargent, "Colloidal CdSe 1– x S x Nanoplatelets with Narrow and Continuously-Tunable Electroluminescence," *Nano Lett.*, vol. 15, no. 7, pp. 4611–4615, 2015.

[118] F. T. Rabouw, J. C. van der Bok, P. Spinicelli, B. Mahler, M. Nasilowski, S. Pedetti, B. Dubertret, and D. Vanmaekelbergh, "Temporary Charge Carrier Separation Dominates the Photoluminescence Decay Dynamics of Colloidal CdSe Nanoplatelets," *Nano Lett.*, vol. 16, no. 3, pp. 2047–2053, 2016.

[119] V. I. Klimov, S. A. Ivanov, J. Nanda, M. Achermann, I. Bezel, J. A. McGuire, and A. Piryatinski, "Single-exciton optical gain in semiconductor nanocrystals," *Nature*, vol. 447, no. 7143, pp. 441–446, 2007.

[120] A. B. Greytak, P. M. Allen, W. Liu, J. Zhao, E. R. Young, Z. Popović, B. J. Walker, D. G. Nocera, and M. G. Bawendi, "Alternating layer addition approach to CdSe/CdS core/shell quantum dots with near-unity quantum yield and high on-time fractions," *Chem. Sci.*, vol. 3, no. 6, p. 2028, 2012.

[121] B. S. Mashford, M. Stevenson, Z. Popovic, C. Hamilton, Z. Zhou, C. Breen, J. Steckel, V. Bulovic, M. Bawendi, S. Coe-Sullivan, and P. T. Kazlas, "High-efficiency quantum-dot light-emitting devices with enhanced charge injection," *Nat. Photonics*, vol. 7, no. 5, pp. 407–412, 2013.

[122] C. Dang, J. Lee, C. Breen, J. S. Steckel, S. Coe-Sullivan, and A. Nurmikko, "Red, green and blue lasing enabled by single-exciton gain in colloidal quantum dot films," *Nat. Nanotechnol.*, vol. 7, no. 5, pp. 335–339, 2012.

[123] D. Oron, M. Kazes, and U. Banin, "Multiexcitons in type-II colloidal semiconductor quantum dots," *Phys. Rev. B*, vol. 75, no. 3, p. 35330, 2007.

[124] H. Zhu, N. Song, and T. Lian, "Wave Function Engineering for Ultrafast Charge Separation and Slow Charge Recombination in Type II Core/Shell Quantum Dots," *J. Am. Chem. Soc.*, vol. 133, no. 22, pp. 8762–8771, 2011.

[125] S. Kumar, M. Jones, S. S. Lo, and G. D. Scholes, "Nanorod Heterostructures Showing Photoinduced Charge Separation," *Small*, vol. 3, no. 9, pp. 1633–1639, 2007.

[126] A. E. Saunders, B. Koo, X. Wang, C.-K. Shih, and B. A. Korgel, "Structural

Characterization and Temperature-Dependent Photoluminescence of Linear CdTe/CdSe/CdTe Heterostructure Nanorods," *ChemPhysChem*, vol. 9, no. 8, pp. 1158–1163, 2008.

[127] J. E. Halpert, V. J. Porter, J. P. Zimmer, and M. G. Bawendi, "Synthesis of CdSe/CdTe Nanobarbells," *J. Am. Chem. Soc.*, vol. 128, no. 39, pp. 12590–12591, 2006.

[128] M. Kirsanova, A. Nemchinov, N. N. Hewa-Kasakarage, N. Schmall, and M. Zamkov, "Synthesis of ZnSe/CdS/ZnSe Nanobarbells Showing Photoinduced Charge Separation," *Chem. Mater.*, vol. 21, no. 18, pp. 4305–4309, 2009.

[129] K. Boldt, K. N. Schwarz, N. Kirkwood, T. A. Smith, and P. Mulvaney, "Electronic Structure Engineering in ZnSe/CdS Type-II Nanoparticles by Interface Alloying," *J. Phys. Chem. C*, vol. 118, no. 24, pp. 13276–13284, 2014.

[130] C. de Mello Donegá, "Formation of nanoscale spatially indirect excitons: Evolution of the type-II optical character of CdTe/CdSe heteronanocrystals," *Phys. Rev. B*, vol. 81, no. 16, p. 165303, 2010.

[131] B. Guzelturk, P. L. H. Martinez, Q. Zhang, Q. Xiong, H. Sun, X. W. Sun, A. O. Govorov, and H. V. Demir, "Excitonics of semiconductor quantum dots and wires for lighting and displays," *Laser Photon. Rev.*, vol. 8, no. 1, pp. 73–93, 2014.

[132] A. Yeltik, B. Guzelturk, P. L. Hernandez-Martinez, A. O. Govorov, and H. V. Demir, "Phonon-Assisted Exciton Transfer into Silicon Using Nanoemitters: The Role of Phonons and Temperature Effects in Förster Resonance Energy Transfer," *ACS Nano*, vol. 7, no. 12, pp. 10492–10501, 2013.

[133] E. Lhuillier, S. Pedetti, S. Ithurria, B. Nadal, H. Heuclin, and B. Dubertret, "Two-Dimensional Colloidal Metal Chalcogenides Semiconductors: Synthesis, Spectroscopy, and Applications," *Acc. Chem. Res.*, vol. 48, no. 1, pp. 22–30, 2015.

[134] G. B. Bhandari, K. Subedi, Y. He, Z. Jiang, M. Leopold, N. Reilly, H. P. Lu, A. T. Zayak, and L. Sun, "Thickness-Controlled Synthesis of Colloidal PbS Nanosheets and Their Thickness-Dependent Energy Gaps," *Chem. Mater.*, vol. 26, no. 19, pp. 5433–5436, 2014.

[135] A. V. Antanovich, A. V. Prudnikau, D. Melnikau, Y. P. Rakovich, A. Chuvilin, U. Woggon, A. W. Achtstein, and M. V. Artemyev, "Colloidal synthesis and optical properties of type-II CdSe–CdTe and inverted CdTe–CdSe core–wing heteronanoplatelets," *Nanoscale*, vol. 7, no. 17, pp. 8084–8092, 2015.

[136] K. Wu, Q. Li, Y. Jia, J. R. McBride, Z.-X. Xie, and T. Lian, "Efficient and Ultrafast Formation of Long-Lived Charge-Transfer Exciton State in Atomically Thin Cadmium Selenide/Cadmium Telluride Type-II Heteronanosheets," *ACS*

Nano, vol. 9, no. 1, pp. 961–968, 2015.

[137] L. Zhang, Z. Lin, J.-W. Luo, and A. Franceschetti, "The birth of a type-II nanostructure: carrier localization and optical properties of isoelectronically doped CdSe:Te nanocrystals.," *ACS Nano*, vol. 6, no. 9, pp. 8325–34, 2012.

[138] A. Avidan and D. Oron, "Large blue shift of the biexciton state in tellurium doped CdSe colloidal quantum dots.," *Nano Lett.*, vol. 8, no. 8, pp. 2384–7, 2008.

[139] T. Franzl, J. Müller, T. A. Klar, A. L. Rogach, J. Feldmann, D. V. Talapin, and H. Weller, "CdSe:Te Nanocrystals: Band-Edge versus Te-Related Emission," *J. Phys. Chem. C*, vol. 111, no. 7, pp. 2974–2979, 2007.

[140] A. Avidan, I. Pinkas, and D. Oron, "How Quickly Does a Hole Relax into an Engineered Defect State in CdSe Quantum Dots," *ACS Nano*, vol. 6, no. 4, pp. 3063–3069, 2012.

[141] R. E. Bailey and S. Nie, "Alloyed semiconductor quantum dots: tuning the optical properties without changing the particle size.," *J. Am. Chem. Soc.*, vol. 125, no. 23, pp. 7100–6, 2003.

[142] R. Tenne, S. Pedetti, M. Kazes, S. Ithurria, L. Houben, B. Nadal, D. Oron, and B. Dubertret, "From dilute isovalent substitution to alloying in CdSeTe nanoplatelets," *Phys. Chem. Chem. Phys.*, vol. 18, no. 22, pp. 15295–15303, 2016.